Fall 2021

A Novel Model to Study Adipose-Derived Stem Cell Differentiation

Austin N. Worden

A Novel Model to Study Adipose-Derived Stem Cell Differentiation

by

Austin N. Worden

Bachelor of Science
University of South Carolina-Aiken, 2016

Master of Science
University of South Carolina, 2019

Submitted in Partial Fulfillment of the Requirements

For the Degree of Doctor of Philosophy in

Biomedical Science

School of Medicine

University of South Carolina

2022

Accepted by:

Jay D. Potts, Major Professor

John Eberth, Committee Member

Robert L. Price, Committee Member

Ioulia Chatzistamou, Committee Member

Mark J. Uline, Committee Member

Tracey L. Weldon, Interim Vice Provost and Dean of the Graduate School

ACKNOWLEDGEMENTS

I would like to thank my supervisor, Dr. Jay Potts, for his invaluable advice, continuous support, and patience during my time at UofSC SOM. I am eternally grateful for Dr. Bill Jackson at UofSC Aiken for steering me down this path so many years ago. Thank you to the members of my committee, Drs. Price, Chatzistamou, Uline, and Eberth, for all of your guidance throughout my dissertation. I am extremely thankful for my parents, my sister Alysha, and my soon-to-be wife Meg. I could not have completed this degree or dissertation without all of your love and support. Finally, I would like to thank my best friends, Mary, Kaleb, Steph, and Kendell, who have kept me sane throughout the years by providing stimulating conversation, happy distractions, and new hobbies to mentally recover outside of research.

ABSTRACT

The use of three-dimensional (3D) culture systems (hydrogels) and adipose-derived stem cells (ADSCs) in regenerative medicine to advance early-stage investigation and modeling of the mechanisms of diseases, treatments, targets, etc. has recently increased. ADSCs, specifically, are utilized due to their innate programming during embryogenesis and in adult tissues in addition to their ability to differentiate into mesodermal, endodermal, and ectodermal cell-specific lineages. Of importance is that these advancements do not involve a model specimen (i.e. mice or rats) and simulate the numerous conflicting signals a migrating cell is exposed to in vivo such as chemokines, extracellular matrix (ECM), growth factors, and physical forces. However, our understanding of the cellular integration of these signals is lacking. We previously developed a novel self-organizing cellularized collagen hydrogel model that is adaptable, tunable, reproducible, and capable of mimicking the multitude of stimuli that cells experience. Our model formed toroids of cells around 24h, while data we present suggests initial migration as early as 3hr after seeding. Toroid formation appears to be a near universal process with the exception being the cancer cell lines we have tried (<4). Interestingly, when cells are seeded inside the hydrogel, there is contraction of the gel, but no toroid is formed. We observed differences in the cell-cell and cell-ECM interactions in response to a changing microenvironment. Moreover, using rheology, collagen binding peptides, and scanning electron

microscope (SEM), we found variation in the remodeling of hydrogels when comparing toroid gels to gels with cells embedded. Lastly, we sought to define the underlying signaling pathways that regulate ADSC directed migration and toroid formation by dissecting the CXCL12-CXCR4 pathway. This work will begin to establish toroid formation as a novel, 3D model for high-throughput investigation of diverse molecular mechanisms and disease progression.

TABLE OF CONTENTS

LIST OF FIGURES

LIST OF ABBREVIATIONS

ABC..... Amphiphilic block copolymers

ADSC..... Adipose-derived stem cell

Akt..... Protein kinase B

AmphoB..... Amphotericin B

ASC..... Adult stem cell

BMSC..... Bone-marrow stem cell

BSA..... Bovine serum albumin

Cdc42..... Cell division control protein 42 homolog

CHP..... Collagen hybridizing peptide

CXCL12..... C-X-C motif chemokine 12

CXCR4/7..... C-X-C chemokine receptor type 4/7

DAPI..... 4′,6-diamidino-2-phenylindole

DMEM..... Dulbecco's Modified Eagle Medium

EDTA..... Ethylenediaminetetraacetic acid

EPC..... Embryonic progenitor cell

ERK..... Extracellular signal-regulated kinase

ESC..... Embryonic stem cell

FAK..... Focal adhesion kinase

FBS..... Fetal Bovine Serum

HEPES.....4-(2-hydroxyethyl)-1-piperazineethanesulfonic acid

iPSC.....Induced pluripotent stem cell

JAK .....Janus kinases

MAPK.....Mitogen-activated protein kinase

MEM.....Minimum Essential Media

MMP..... Matrix metalloprotease

NHF..... Neonatal heart fibroblast

PBS.....Phosphate Buffered Saline (pH 7.4)

PEG .....Polyethylene glycol

PFA..... Paraformaldehyde

PI3K .....Phosphoinositide 3-kinase

PLA ..... Polylactide

P/S .....Penicillin Strip

Raf ..... Rapidly accelerated fibrosarcoma

Ras.....Rat sarcomas virus

Rho .....Ras homologous

RPM..... Revolutions Per Minute

ROCK..... Rho-associated protein kinase

SDF-1.....Stromal cell-derived factor 1

SHG .....Second harmonic generation

STAT.....Signal transducer and activator of transcription proteins

TAE ..... Tris-Acetate-EDTA

CHAPTER 1

INTRODUCTION

1.1 Background

There has been a progressive shift away from two-dimensional (2D) cell culture techniques over the last few decades. This was initiated by the technical advances of three-dimensional (3D) cell culture, such as hydrogels. These new-aged methods provide a more consistent extracellular matrix (ECM) and a more accurate physiological response in differentiation, proliferation, tissue development, and protein expression (van Duinen et al, 2015). While 3D techniques are constantly progressing, the basic science understanding of the matrix environment and cellular interactions within this ECM must be improved.

1.11 Hydrogels

With any new method or technique, there is a trial period filled with as many failures as there are successes. Attempts with solvent casting, molten substance molding, and freeze drying, eventually all gave way to the more successful hydrogels (Mir and Nakamura, 2017). Hydrogels are a group of hydrophilic, polymeric structures that can hold a large amount of water while maintaining their chemical and physical structure of cross-linked polymer chains (Ahmed, 2015; Bahram et al, 2016). Their unique structure can undergo a phase transition, from liquid to solid, in response to certain external stimuli. The stimulant needed for

transition classifies the hydrogel into one of three main categories: physical, chemical, or biochemical. Physical hydrogels respond to change in temperature or pH. Chemical hydrogels react to two or more components being mixed and have an increased mechanical integrity and resistance to degradation due to covalent bonds. Biochemical hydrogels contain enzymes and amino acids that aid in gelation under key conditions (Bahram et al, 2016).

There are two main types of hydrogels, each with its own advantages and disadvantages. *Naturally derived* hydrogels (ex. collagen, alginate, and fibrin) are extracted from natural sources (ex. Bovine placenta) and can be purified or manipulated in the laboratory. The physical properties are less adaptable, but the innate bioactivity supporting cell:tissue integration and biocompatibility is difficult to replicate (Bajaj et al, 2014; Guillemot et al, 2010; Pashuck and Stevens, 2012; Seol et al, 2014). Recently, natural hydrogels have begun to be replaced by laboratory-formed *synthetic hydrogels* due to their longer service life, higher water absorption capacity, and increased gel strength. One example is VitroGel3D (TheWell Bioscience) which is animal free and carbohydrate based. Synthetic hydrogels maintain the advantage of having well-defined structures with modifiable mechanical, chemical, and physical properties by fine-tuning the molecular weights, molecular distributions, and crosslinking densities. However, they lack the naturally occurring bioactivity important to integration and biocompatibility, thus requiring additional chemical modifications (Bahram et al, 2016; Rutz et al, 2015).

In order for the cells to interact with the biomaterials in hydrogels, they must interpret and decode specific signals as biochemical signals. These signals are

received from a plethora of topographical, chemical, and physical properties within the hydrogel. It has previously been shown that cells sense and adhere to the scale and shape of their topography, thus surface topography and chemical composition are key influences on cellular migration, adhesion, proliferation, and differentiation (Kumari et al, 2010; Curtis et al, 2001; den Braber et al, 1996; Flemming et al, 1999). Likewise, the possibly for scaffold morphology (i.e., pore-size and interconnectivity of biomaterial) to mimic surrounding tissue is crucial for cell:ECM interactions thus enabling cell attachment, migration, and transfer of nutrients and biochemical stimuli (Yuan et al, 1999). Cells also respond to the mechanical (Discher et al, 2005; Engler et al, 2006), electrostrictive (Smela, 2003), and electrical (Wang et al, 2003) properties within these biomaterials.

Not only are hydrogels more accurate in simulating the physiology of native tissues than other models, but they are widely tunable structures that can simulate the complex *in* vivo cell:cell and cell:ECM interactions. They have been used in a wide variety of studies including high-throughput drug screening and delivery, pH- and bio- sensors, 3D printing bioinks, and scaffolds for tissue engineering and modeling (Bahram et al, 2016). Hydrogels have increasingly been used in the field of regenerative medicine due to their ability to be prefabricated and implanted for *in vivo* degradation and remodeling or *in vitro* creation of tissue constructs (Lee and Dai, 2016). Tissue-engineered constructs composed of collagen are well tolerated immunologically when implanted in the body (Hunt and Grove, 2010; Badylak et al, 2009; deCastro Bras es al, 2010). Moreover, gels placed in living tissues are remodeled over time by enzymes such as matrix metalloproteases

(MMP)s, enhancing the potential for integration of implants with surrounding tissue (Macleod et al, 2005; Pedraza et al, 2020). We have used these collagen hydrogels in a number of studies and are expert in the use of these gels (Gourdie et al, 2012; Worden et al, 2022).

In fact, recent studies have focused on developing technology that allow simultaneous deposition of hydrogels with live cells to form 3D tissue structures (Bajaj et al, 2014). These new 3D printing technologies employ hydrogels as a scaffolding material for the direct assembly of cells and ECM to form 3D tissue models that are functional in many of the aforementioned uses. For example, the animal models exploited in various scientific fields, like cancer biology, are expensive and have a long discovery process. While these models are important, the differences between human and mouse immunology and cancer biology are significant, i.e., many drugs that work on mice are ineffective in humans. Therefore, the development of a 3D human tumor model using a hydrogel offers the opportunity to advance the field quicker and with lower cost (Lee and Dai, 2016). For example, Zhao et al (2014) recently created an *in vitro* cervical tumor hydrogel model that appears more reproducible than in mice. Other areas where these 3D printed scaffolds are being used are in bone (Li et al, 2015; Strobel et al, 2014), cartilage (Cui et al, 2014; Gao et al, 2014), skin (Binder et al, 2010; Killat et al, 2013; Lee et al, 2009), vascular system (Bertassoni et al, 2015; Lee et al, 2014; Lee et al, 2010), cardiac tissue (Gaetani et al, 2012), cardiac valves (Duan et al, 2014), and other clinical applications (Binder et al, 2010; Ozbolat, 2015; Weinand et al, 2009).

Inconsistent drug release from hydrophobic polymer matrices has led to a need for non-collagen materials that lack host inflammatory stimulants and can be used for long-term release of bioactive molecules for therapies. Most common for drug delivery applications, staples, and sutures, this non-collagen alternative belongs to a family of amphiphilic block copolymers (ABCs) made up of two chemically different homopolymer blocks. One block is the hydrophilic polyethylene glycol (PEG) while the other is the hydrophobic polylactide (PLA). PEG hydrogels tend to be more biocompatible, temperature responsive, water soluble, and resist protein absorption. However, they are not biodegradable (Nuttleman et al, 2006; Benoit et al, 2007; Lin and Anseth, 2009; Metter et al, 2000).

PLA, on the other hand, is a highly degradable material that can be combined with PEG and tuned for a faster degradation by increasing the number of PLA repeats (Hoffman et al, 2014). In 1997, Jeong et al. prepared the first PLA-PEG copolymer to release fluorescein isothiocyanate labeled dextrin against bioactive macromolecules. Since its first synthesis, PEG-PLA copolymerization has become a means to form new polymeric materials that consist of newly adaptable, biological, chemical, and physical properties for specific uses (Li et al, 1996; Sawhney et al, 1993). Recent efforts exhibited an enhanced degradation, with a half-life of approximately 4 days *in vivo*, for an siRNA release leading to improved fracture healing (Shu et al, 2013). Several studies have shown their usefulness for limiting postsurgical adhesion formation (Hill-West et al, 1994), preventing vascular injury-related thrombosis and vessel narrowing (Hill West et

al, 1994), and for temporary regrowth scaffolds for cartilage and bone (Anseth et al, 1999). While microstructural networks are still unknown, PEG-PLA degradation dynamics are advantageous for a number of applications.

Ultimately, developments in regenerative medicine and tissue engineering strive to generate functional tissue and organs. To date, many impressive advancements have been made through the exploitation of hydrogel tunability allowing for a model to facilitate *in vivo* spatial distribution and organization. Gilbert et al (2010) provided evidence that adult muscle stem cells mimic *in vivo* elastic and regenerative properties when cultured on soft hydrogels. Subbaiah and Thomas (2011) have advanced clinical bone replacement using mesenchymal stem cells. Lastly, Worden et al (2022) developed a novel collagen model that is adaptable and capable of mimicking the multitude of stimuli that cells experience. The future of regenerative medicine will be based on the fabrication of these biomaterials and the study of stem cell interaction within the hydrogel.

1.12 Stem Cells

Recent advances in tissue-engineered treatment options for wound healing can be linked to stem cell therapy (Hassan et al, 2014; Han et al, 2015; De Francesco et al, 2015). Found in both embryonic and adult organisms, stem cells are the undifferentiated beginning of cell lineages characterized by self-renewal and multipotential differentiation (Atala & Lanza, 2012). Within their niche (i.e., their microenvironment), stem cells are maintained by a constant balancing of quiescent and active cells (Carlesso & Cardoso, 2010). Stem cells are reactive to the chemical milieu of their niche, leading to variability in their behavior and regulatory

processes such as morphology, adhesion, proliferation, differentiation, motility, and survival (McNamara et al, 2010). These processes are largely influenced by the complex mixture of chemokines, cytokines, growth factors, and receptor ligands in the ECM (Abbott, 2003; Nili et al, 2003; Santra et al, 2002). Thus, there is a natural, mutualistic relationship with the ECM which moderates behavior (Behonick & Werb, 2003). One essential biological process that is highly dependent on the ECM is motility and migration. Different types of active and spontaneous motion (crawling, gliding, swarming, and swimming) are linked to development, morphology, tissue repair, and wound healing (Scarpa & Mayor, 2016; Satoshi & Kashina, 2008; Franz et al, 2002; Li et al, 2013). Likewise, any issue leading to abnormal migration can result in developmental disorders and cancer metastasis (Hatten, 1993; Friedl et al, 2012).

There are many types and subtypes of stem cells currently known and utilized. Embryonic stem cells (ESCs) are pluripotent stem cells that are derived from the inner cell mass of a blastocyst (Richards et al, 2004; Trounson, 2006). Although their mechanisms are not yet fully understood, ESCs can differentiate into more than 200 adult cell types depending on their external stimulation (Thomson et al, 1998). Induced pluripotent stem cells (iPSC) are adult stem cells that have been genetically engineered with transcription factors to behave like ESCs (Takahashi & Yamanaka, 2006; Belay et al, 2010). Adult (also called tissue-specific or somatic) stem cells (ASCs) are multipotent, lineage-specific cells that are named for their tissue origins such as mesenchymal, hematopoietic, and adipose-derived (Jiang et al, 2002; Coughlin et al, 2017). While typically they are

used to maintain and repair their local tissues, ASCs can be transplanted into a separate host tissue where they can maintain their regenerative ability by recognizing and responding to novel signals (Cossu & Bianco, 2003; Lee and Park, 2009).

Induced pluripotent stem cells (iPSCs) were first introduced in 2006 by Shinya Yamanaka's lab. By introducing the Myc, Oct3/4, Sox2, and Klf4 genes, Yamanaka found that somatic cells could be converted to pluripotent stem cells (Takahashi and Yamanaka, 2006). Their significance lies in the fact that they can propagate indefinitely and differentiate into any bodily cell type such as cardiomyocytes, neuronal, and hepatocytes (Mahla, 2016). In addition, they circumvent the controversial use of ESCs and the need for embryos because they are derived directly from patient-matched, adult tissue. This also aids in preventing immune rejection, personalized drug discovery, and treatment of patient-specific diseases (Hockemeyer and Jaenisch, 2016). While there are certainly advantages to iPSCs, there exist a number of risks including low efficiency of iPSC conversion (Takahashi and Yamanaka, 2006), genomic mutations (Selvaraj et al, 2010), increased tumorigenicity (Marion et al, 2009), and incomplete reprogramming (Zhao et al, 2009).

Mesenchymal stem cells (MSCs) are essential for regenerative medicine research due to their ease of isolation as well as the high yield and plasticity necessary for cell growth, differentiation, and regeneration. MSCs are multipotential cells found in the stroma of adult tissues where they typically function as structural support (Zomer et al, 2015). In adult tissues, they appear specifically

in the mesodermal layer and differentiate into cell lineages such as adipocytes, osteocytes, and chondrocytes. However, in early embryonic development, they are active in the ecto- and endodermal layers as well (Caplan, 1991). Adipose tissue has become a major source of stem cells due to their ease of collection and the various ECM components useful for wound healing (Paulos et al, 2010; Karastergiou & Mohammed Ali, 2010). Adipose-derived stem cells (ADSCs) are mesenchymal stem cells that maintain the ability to differentiate into mesodermic, endodermic, and ectodermic cell-specific lineages (Vermette et al, 2007). Upon transplantation into a damaged site, they interact with the microenvironment to generate new progenitors and cells. Conventional regenerative therapies based on MSCs introduce cells randomly into the diseased organ without a way to track their status (Rennert et al, 2012). They aid in tissue regeneration and function by secreting exosomes filled with growth factors, cytokines, chemokines, and micro-RNA (Othmani et al, 2019), however there is a lack of depth in the knowledge pertaining to the molecular mechanisms that drive their behavior.

These cells are governed by molecular mechanisms that lead to angiogenesis, immunomodulation, and cell proliferation and differentiation. Across the multitude of stem cells, a few specific regulatory elements have been identified. Wnt ligands, Notch signaling, and a number of growth factors and cytokines are active in stem cell self-renewal, differentiation, and neural development (Angers & Moon, 2009; Michel et al, 2009; De Felici et al, 2009). Distinct microRNAs regulate differentiation across different cell populations (Yi & Fuchs, 2011; Guo et al, 2011). Lastly, numerous transcription factors generate the networks of signaling

cascades modulating the coordinated action of gene expression (Amann et al, 2011). One signaling pathway, the CXCL12-CXCR4/7 pathway, has been significantly implicated in the regulation of stem cells.

1.13 CXCL12-CXCR4/7 Pathway

CXCL12, also known as SDF-1, is a chemokine protein that is expressed throughout many cell types (including immune, endothelial, stem, and cancer cells) and tissues (including brain, heart, lung, kidney, and bone marrow) (Schrader et al, 2002; Guo et al, 2016). During embryogenesis, CXCL12 plays a direct role in hematopoietic stem cells honing to the bone marrow as well as large blood vessel formation. In adults, it acts in a chemotactic manner for lymphocytes and mesenchymal stem cells, regulates B cell expression of CD20, mediates the suppression of osteoclastogenesis, and drives angiogenesis by inducing endothelial progenitor cell (EPC) migration through the binding of its cognate receptors, CXCR4 and CXCR7 (Bleul et al, 1996; Askari et al, 2003; Takano et al, 2014; Zheng et al, 2007). Of importance is the fact that chemokines must bind to one of their specific G-coupled transmembrane receptors to be activated (Balkwill, 2004; Viola and Luster, 2008; Lagerstrom and Schioth, 2008). Figure 1.4 shows a diagram of the CXCL12-CXCR4 pathway. This pathway has been evaluated as a therapeutic target in cardiovascular disease due to its cardioprotective role in progenitor cell honing to myocardial ischemia locations (Ma et al, 1998; Doring et al, 2014). The upregulation of this pathway in wound healing has suggested increased stem cell migration to the site of injury and enhanced healing, repair, and regeneration (Ji et al, 2004). In addition, the CXCL12-CXCR4 pathway has

been implicated in several negative effects on the body including tissue damage from heart infarct, excessive bleeding, limb ischemia, and directly in diseases such as HIV, cardiovascular disease, and cancer (Chang et al, 2020; Greenbaum et al, 2013; Ara et al, 2003; Li et al, 2009). Since CXCR4 mediates stem cell recruitment for the survival and regeneration of cardiomyocytes, issues with this process can lead to improper embryonic heart development. Likewise, a mouse CXCR4 knockout model was shown to produce a lethal phenotype in embryos (Nagasawa et al, 1998; Tachibana et al, 1998).

In cancer, however, it is not the downregulation of this pathway that creates problems. Instead, it is the exploitation of chemokine receptor signaling that allows cancer to survive, proliferate, and metastasize. Since CXCL12-CXCR4 regulates a large number of downstream effector molecules, it is a well-established source for the many pathobiological effects of cancer. While the extent of this pathway's control over these various molecules is currently unknown in cancer, it has been found that CXCL12 is highly expressed in human breast (Kang et al, 2005), bladder (Yang et al, 2015), gastric (Ishigami et al, 2007), prostate (Zhang et al, 2008), lung (Imai et al, 2016), and other cancers (Ghanem et al, 2014; Sakai et al, 2012; Teng et al, 2016).

Breast cancer, the second most common type of cancer behind skin cancer, is found predominantly in women and sporadically in men (Weigelt et al, 2005; American Cancer Society, 2021). In relevance to breast cancer metastasis, there is no correlation to blood flow patterns like in other types of cancer, suggesting a preferential honing and proliferation of cancer cells in specific tissues and organs

which have shown the highest CXCL12 expression (Luker and Luker, 2005; Muller et al, 2001). Breast cancer metastasis requires several steps including intravasation into blood vessels and cancer cells must survive circulation, migration and adhesion to secondary targets, and proliferation (Chamber et al, 2002). These steps are all potentially governed by effector molecules activated by CXCL12-CXCR4. For example, AKT is active in the proliferation and chemotactic migration towards CXCL12 expression (Kayali et al, 2003; Curnock et al, 2003; Peng et al, 2005); MAP kinases increase gene expression driving proliferation and survival by phosphorylating transcription factors (Chang and Karin, 2001; Vara et al, 2004); JAK/STAT enhances motility and invasion of cancer cells (Soriano et al, 2003); MMP secretion is increased by CXCR4 activation leading to ECM degradation thus enhancing invasion and metastasis (Kang et al, 2005); and CXCR4 directly regulates the angiogenesis key to formation and growth of metastatic tumors (Folkman, 2002).

While there is still a gap in the knowledge surrounding how the CXCL12-CXCR4 pathway is reactive in the many types of cancer, recent work has suggested a way to utilize CXCR4 overexpression as prognostic biomarkers or even diagnostic markers by identifying organ-specific, protein networks (Sanz-Pamplona et al, 2012). There has also been some success in blocking CXCR4 expression using RNA interference (RNAi), limiting spontaneous lung metastases (Smith et al, 2004; Liang et al, 2005). In fact, Smith et al. (2004) was able to utilize RNAi to reduce this expression in the 4T1 mouse breast cancer cell line. Likewise, neutralizing antibodies and compounds, such as AMD3100, reduces proliferation

and angiogenesis and increases apoptosis in different cancer models (Rubin et al, 2003; Darash-Yahana et al, 2004). Thus, the use of CXCR4 as a target for cancer diagnostics and therapeutics is becoming increasingly more valid.

1.2 Previous Studies

Our work has focused on the phenomenon that occurs when studying stem cell interactions within a hydrogel and the molecular mechanisms that are involved. Hydrogels provide the ECM framework necessary to meet morphogenic and necessary demands of developing tissues. With their potential, we have created a new culture model exploiting the nuances of ECM-mechanical stress to study the regulation of multicellular organization dynamics in development and disease. Our laboratory observed a unique morphological phenomenon when using collagen hydrogels to examine the self-organizing structure of cells called toroids (Gourdie et al, 2012). By culturing cells *on the surface of matrices* a “donut-like”, self-organizing structure toroid forms (Figure 1.1a). Of importance is that when cells were mixed into the collagen hydrogel, a contraction of the scaffold was observed but no toroid was formed (Figure 1.1b). Interestingly, the toroids adhere to the size and shape of the well in which they are cultured (Figure 1.2).

To date, we have cultured 10 different cell types in this model including stem cells (adipose and bone marrow derived), cardiac fibroblasts, microvascular endothelial cells, and four cancer cells lines (such as 4T1 breast cancer). We have determined that regardless of cell type used, the toroids are universally formed (Gourdie and Potts, 2014). The exception to this tenet is that the *cancer cells do*

*not form toroids (*Figure 1.3*)*. This may be a result of a measure of plasticity as it does not appear to relate to anchorage-independent proliferation of cancer cells.

The work described in the following pages will study the fundamental need for a model system to reproduce native tissue ECM, thus creating a universal, tunable model that can be utilized for early-stage investigation and modeling mechanisms pertaining to diseases, treatments, targets, etc. without having to involve a live animal model. We will 1) investigate how a variable ECM affects cellular behavior, 2) assess the effect cells have on the microenvironment in which they are placed, and 3) define the underlying signaling pathways that regulate adipose-derived stem cell (ADSC) toroid formation in this changing microenvironment.

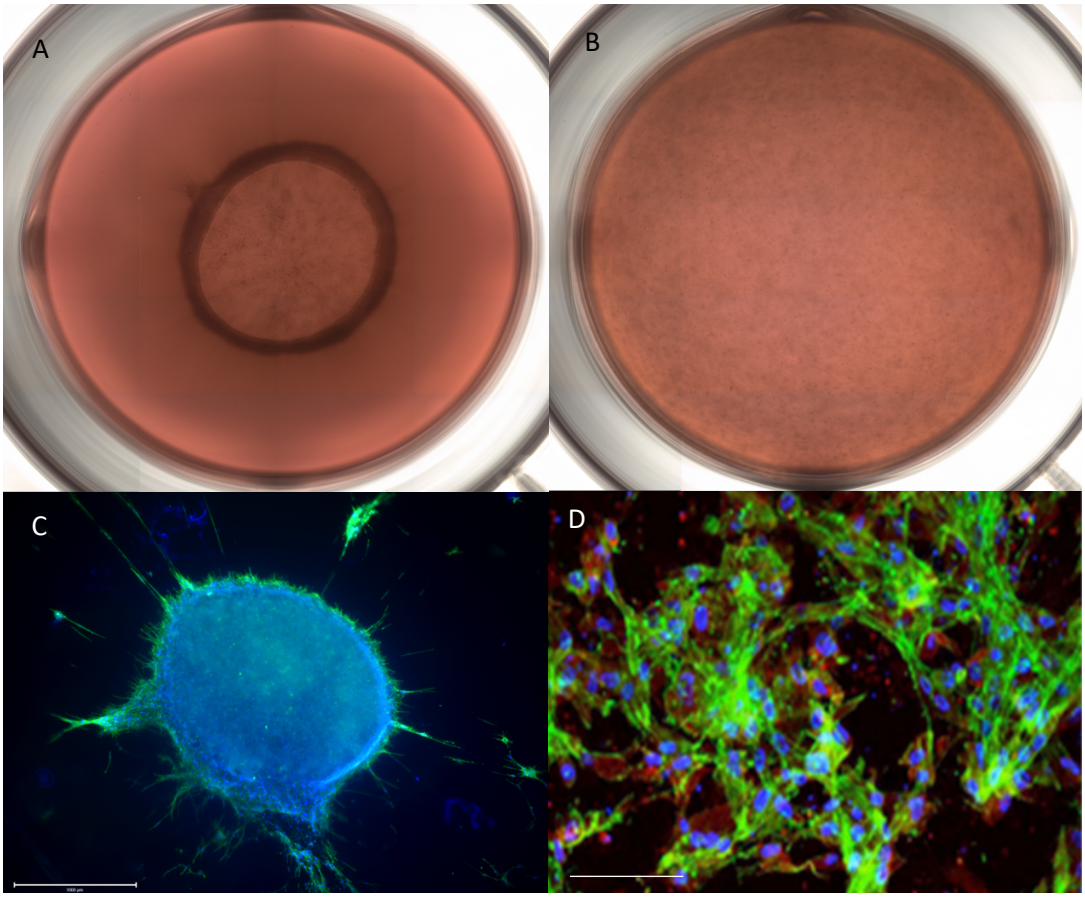

Figure 1.1 On top vs mixed-in hydrogels. In a 96-well plate, 25,000 ADSCs were seeded A) on top of a PureCol collagen I hydrogel and B) inside of a collagen I hydrogel. Of importance is that cells seeded on top form a toroid while cells mixed into a hydrogel stay spread throughout the gel and do not form a toroid. C) Fluorescence image of toroid. D) Fluorescence image of mixed in cells. Blue- DAPI; Green- Phalloidin; Red- SMA; Scale Bars= 100μM (C) and 100μM (D).

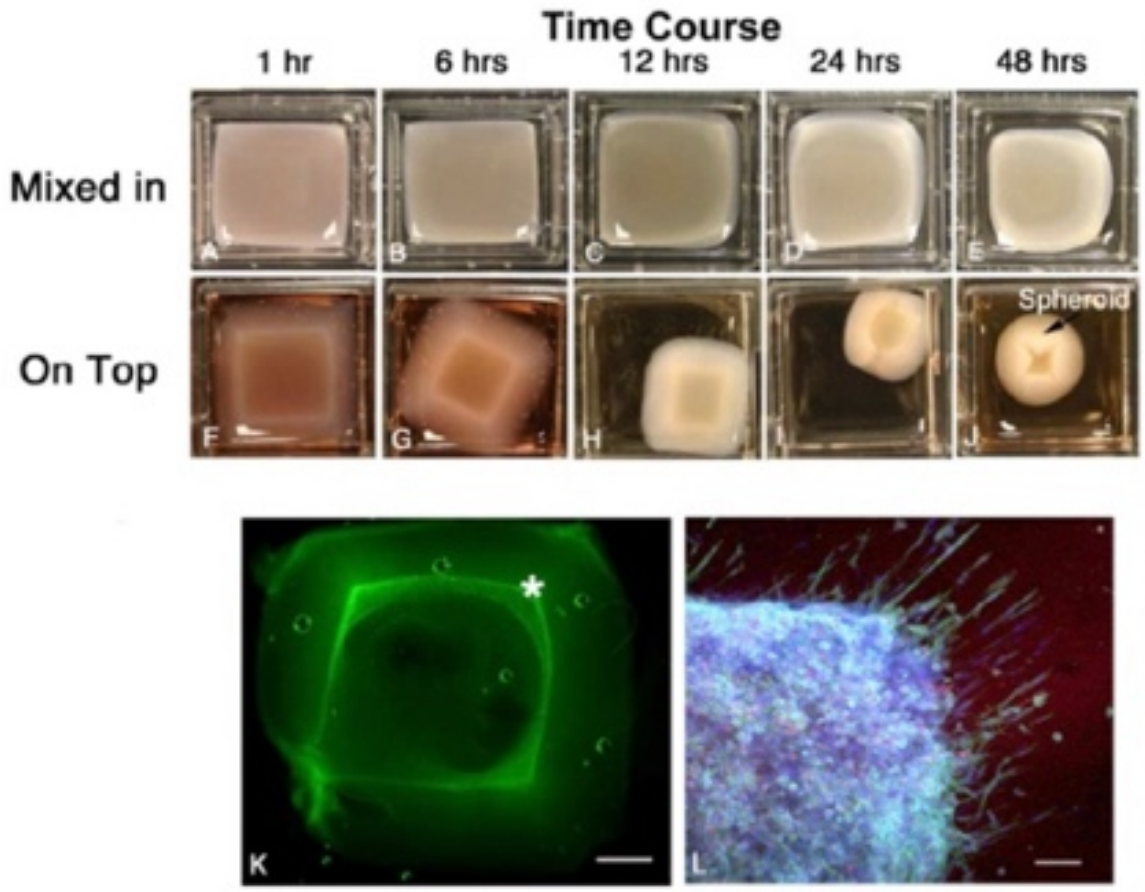

Figure 1.2. **Toroids adhere to the shape of the well in which they are formed.** Twenty-five thousand ADSCs were seeded under toroid forming and non-forming conditions on collagen I hydrogels prepared in a square well. A-E) Under non-forming conditions, the mixed in cells do not form toroids, but there is a slight contraction of the hydrogel away from the well wall. F-I) Over our standard 24 hr period, the cells adhere to the shape of the gel on which they are seeded (i.e. square). Confocal images show the square toroid (K) and higher mag insert (L) shows the cells streaming into the corner of the toroid. Green-Phalloidin; Blue- DAPI; Scale Bars= 100um.

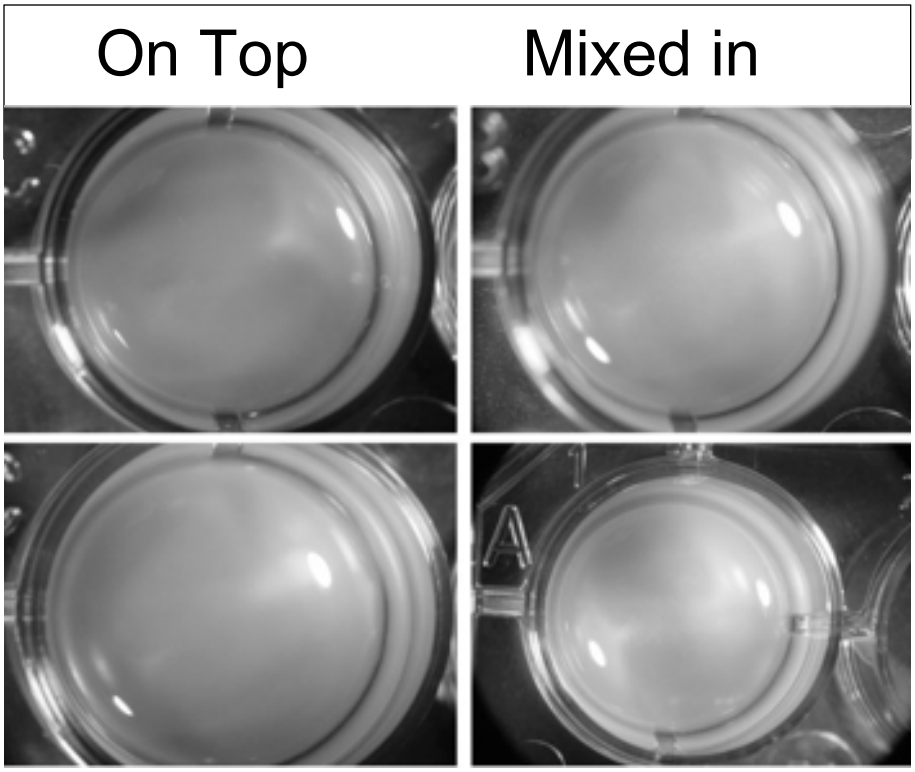

Figure 1.3. Breast cancer cell lines DO NOT produce toroids. Top panel are E07771cells, and lower panel is 4T1-Luc cancer cells.

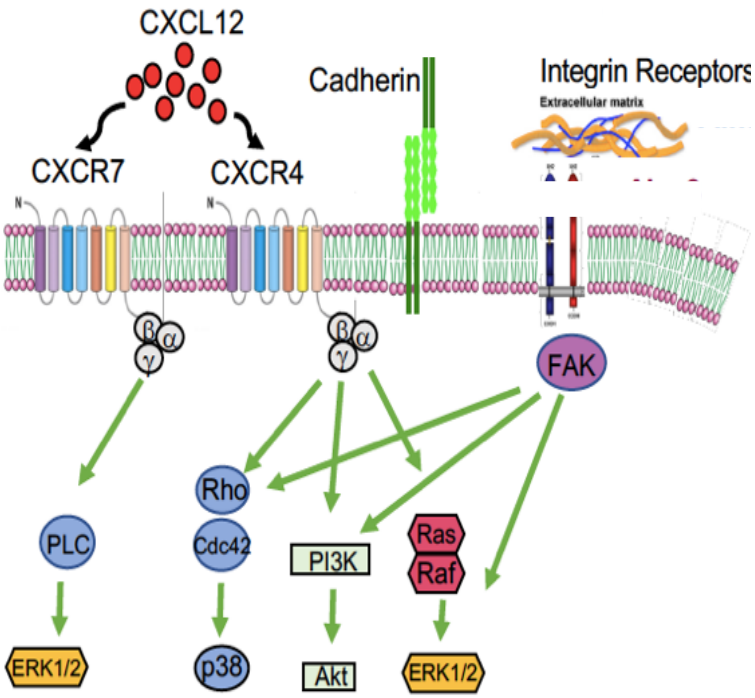

Figure 1.4. CXCL12-CXCR4 pathway. The CXCL12-CXCR4 pathway causes a signaling cascade that plays a major role in cell survival, migration, differentiation, and proliferation.

CHAPTER 2

SELF-ASSEMBLING TOROIDAL CELL CONSTRUCTS FOR TISSUE ENGINEERING APPLICATIONS[1]

[1] Worden A, Uline MJ, Shazly T, Stern M, and Potts JD. *Microscopy and Microanalysis*, 1-10. Reprinted here with permission of the publisher.

2.1 Abstract

Developing tissues have intricate, three-dimensional (3D) organizations of cells and ECM that provide the framework necessary to meet morphogenic and physiological demands. Migrating cells, *in vivo*, are exposed to numerous conflicting signals: chemokines, ECM, growth factors and physical forces. While most of these have been studied individually *in vivo* or *in vitro*, our understanding of how cells integrate these various signals is lacking. We previously developed a novel self-organizing cellularized collagen hydrogel model that is adaptable, tunable, reproducible, and capable of mimicking the multitude of stimuli that cells experience. Our model produced self-assembled ***toroids*** of cells that were formed by 24 hr. Data we present here show toroids initially form as early as 3 hr after seeding. Additionally, toroids formed when cells were seeded on various collagen subtypes and were sensitive to the composition of the hydrogel. Moreover, we found differences in remodeling in toroid gels compared to gels with cells embedded in them using both a collagen binding peptide and rheology. Using scanning electron microscopy (SEM), we observed that toroids form a crater like structure compared to whole gel contractions in mixed in gels. Finally, when multiple cells were mixed prior to seeding, heterogenous toroids formed with some containing clusters of cells.

Keywords: Collagen, Tissue Engineering, Self-Organizing, Hydrogels, Stem Cells

2.2 Introduction

Tissue formation through cellular self-assembly and cellular aggregate fusion is a common phenomenon during embryonic development and

morphogenesis, in which tissues and organs are formed by living cells through a myriad of cell-cell and cell-extracellular matrix (ECM) interactions (Gourdie et al., 2012; Rennert et al.,2012; Sun & Wang, 2013). Hydrogels composed of collagen are frequently used as three-dimensional (3D) scaffolds for cultured cells, with the goal of promoting tissue formation *in vitro* (Huynh et al., 1999; Cen et al., 2008; Glowacki & Mizuno, 2008; Pang & Greisler, 2010; Pedraza et al., 2010). Collagen is the most widely used biopolymer, and in mammals, is the most abundant protein in major structural components of almost all organs and tissues thus providing a ubiquitous framework for cell attachment and growth (Badylak et al., 2009).

Collagen scaffolds are also amenable to experimental screens of cell migration, proliferation, death, angiogenesis and tissue differentiation (Tonnesen et al., 2000; Hansen et al., 2006; Mercado-Pimentel & Runyan, 2007), and can be used in a wide variety of ways including as implantable scaffolds for tissue repair, as well coatings for cell culture, as drug delivery vehicles, and as controllable matrices for modeling and imaging (Macleod et al., 2005; Vu et al., 2015; Xing et al., 2019).

Collagen constructs are well tolerated immunologically when implanted in the body (Badylak et al., 2009; deCastro Brás et al., 2010; Hunt & Grover, 2010). Once placed in living tissues, these hydrogels are remodeled over time by enzymes such as matrix metalloproteases (MMPs), enhancing the potential for integration with surrounding tissue. Due to their biocompatibility and widely tunable structure, they have been shown to simulate the ECM in physical structure to a point that promotes cell proliferation and regeneration of tissues (Li et al., 2009). Accordingly,

collagen hydrogels are of significant interest in the field of regenerative medicine (Patino et al., 2002; Hunt and Grover, 2002; Badylak et al., 2009) in which material and cellular components are integrated and appropriated for a wide range of applications.

Tissue-engineered approaches for wound healing attempt to promote regenerative and scar-free healing. In this regard, stem cells are increasingly being utilized as part of regenerative therapies. To date, conventional regenerative therapies based on stem cells involve the introduction of dispersed cells into a diseased organ with little regard for the status of these randomly introduced cells. Current therapies often show marginal, variable, or even controversial capability to promote regenerative and scar-free healing. As such, improvements to available compositions and methods would be beneficial. Tissue repair and regeneration are thought to involve resident cell proliferation as well as the selective recruitment of circulating stem and progenitor cell populations (Rennert et al., 2012).

Numerous tissue engineering approaches attempt to recapitulate the process of stem cell organization to provide the basis for studying *in vivo* interactions *ex vivo*. This allows for the early stages of investigation and modeling mechanisms pertaining to diseases, treatments, targets, etc. without having to involve a specimen. Stem cells are affected by the stiffness of the matrix that they are being cultured in. Depending on the stiffness of the gel, stem cells produce a certain phenotype. This was reported in a seminal paper by Engler et al. (2006) showing MSCs cultured on a stiff gel produce more osteogenic markers. In contrast, a softer matrix induced neurogenic markers. Moreover, substrate

stiffness and tissue geometry influence cardiac myocyte size, shape, and alignment. (Ribeiro et al., 2015, Gaetani et al., 2020, Bian et al., 2014).

Our laboratory observed a unique morphological phenomenon when using collagen hydrogels where groups of cells self-organized into structures called toroids (Gourdie et al., 2012). When lens epithelial cells were initially placed on top of the hydrogel, a toroid ring of cells was formed. These toroids or “self-organizing tissue structures” initially take the shape of the well-plates in which they are prepared. Cells forming toroids appeared long and thin as they migrated from the outer region of the gel to the inner gel toroid structure (Gourdie et al., 2012). In contrast, when the cells were mixed inside the hydrogel, contraction of the scaffold was observed but no toroid was formed, with the cells remaining spread throughout. While those studies are the origin for current studies, there remains a lack of understanding as to the molecular mechanisms underlying cellular migration and toroid formation, as well as the reaction to multi-cell environments (i.e., within a human body).

Our current study provides detailed timing of toroid formation using this 3D microenvironment with both single- and multi-cell contribution using two different types of stem cells, to support the evidence that toroid formation is a near universal event. We analyzed and quantified the ability of different collagen concentrations to affect cellular migration and formation of toroid structures. Subsequently we analyzed the ability of cells to remodel their matrices during toroid formation using a collagen binding peptide and rheology analysis of the remodeled matrix. Finally,

we determined the outcome of allowing multiple cell types to interact during toroid formation.

2.3 Materials and Methods

2.31 Cell Culture

Neonatal heart fibroblasts (NHF) and adipose-derived stem cells (ADSC) were extracted from adult mice and cultured in Dulbecco's Modified Eagle Medium (DMEM) supplemented with 10% Fetal Bovine Serum (FBS), Penicillin-Streptomycin (10mL/L), and Amphotericin B (2.5mg/L). Cells were grown until 80-90% confluency prior to use for experimentation. We used all primary cell cultures at passage 5 or less.

The cells to be used in toroid experiments were culture to 80% confluence and trypsinized (0.25% Trypsin/EDTA), centrifuged 8 minutes at 800 RPM, and counted. For single cell type experiments, cells were applied in concentrations between 25,000-50,000 cells per gel. Cells were applied 250,000 cells per gel for the hydrogel compression testing due to the larger gels formed in a 24-well plate. Multi-cell toroids were formed with 25,000 cells/cell type/well. The cells in these experiments were gently, but thoroughly, mixed prior to being placed on the gel.

2.32 Hydrogel Preparation

In total, we used 9 different hydrogel matrices including three types of Collagen I (PureCol, Nutrigen, and Fibricol- Type I Bovine, Advanced BioMatrix), Collagen III (Human Placenta, Advanced BioMatrix), Collagen V (Bovine Placenta, Advanced BioMatrix), Rat Tail Collagen, and three types of synthetic matrices (AlphaBioGel, Matrigel, and VitroGel3D). Collagen gels were created in 96 well

culture dishes (Corning Incorporated, Corning, NY, USA) using an 8:1:1 ratio of collagen matrix, 0.2N HEPES pH 9.0 (Fisher Scientific, Hampton, NH, USA), and 10X Minimum Essential Medium (MEM, Sigma-Aldrich, St- Louis, MO, USA). The mixture was added 100 µL per well and stabilized at 37°C overnight. Cells were placed on top of the gels and incubated at 37°C for 30 minutes. Gels were released from the sides of the wells with a thin-tipped probe and incubated at 37°C for an additional 24 hours. For mixed in gels, cells in media were mixed into the matrix prior to being poured and incubated for 24 hours.

Rat tail collagen (RTC) was synthesized from the cartilaginous tendons stripped from the tail of a sacrificed rat, degraded in acetic acid, and dialyzed in 10X MEM until a matrix was formed. To create a usable 3D microenvironment, 1.25 mL rat tail collagen was mixed with 750 µL sterile H_2O, 200 µL M199 media, and 200 µL sterile $NaHCO_3$. With respect to the concentrated RTC (cRTC), all previous steps were the same, however, to create a more concentrated matrix, collagen was centrifuged at 4000 RPM for 20 minutes and the excess water was removed.

Each synthetic matrix was created using the manufacturer-specific protocol. AlphaBioGel (AlphaBioRegen) and Matrigel (Corning Incorporated) were each thawed on ice at 4°C prior to being used. VitroGel3D (TheWell BioScience) protocol called for a dilution of the Vitrogel solution 4:1 in media. 250µL was placed into each well and stabilized for 30 minutes at 37°C. Cells were added to each gel, gels released, and incubated 24 hours at 37°C.

2.33 Collagen Mixture Studies

In our previous studies, both PureCol collagen I and collagen III produced toroids, however, collagen III created smaller, more compact toroids. To generate the various collagen mixtures, a collagen concentration series was performed in triplicate. Hydrogel mixtures followed the 8:1:1 ratio as stated before, however the concentrations of the collagen I was diluted with collagen III. These concentrations were 100% collagen I, 80:20 (collagen I: collagen III), 60:40 (I: III), 40:60 (I: III), and 100% collagen III. NHFs in media were placed on top of the gels, released, and incubated for 24 hours at 37^{o}C. The resulting toroids were imaged, and diameters measured on the Invitrogen EVOS FL Auto microscope. Statistics on the diameter measurements were determined using a student's t-test with significance at $P<0.01$.

2.34 Immunohistochemistry

For fluorescence imaging, hydrogels were fixed with 2% paraformaldehyde (PFA) (pH 7.2) for 20 minutes at room temperature (RT) and rinsed with 1X phosphate buffered saline (PBS) (Thermo Fisher Scientific, Waltham, MA, USA) 3 x 5 minutes. Permeabilization occurred using 0.1% Triton X-100/ 0.01M glycine/ 1X PBS for 30 minutes at RT then washed in 1X PBS. Blocking occurred in 5% BSA/1X PBS for 30 minutes at RT before another PBS wash cycle. Primary antibody (diluted 1:200 in 1X PBS) -either goat polyclonal to CXCR4 or rabbit polyclonal to SDF-1 (Abcam, Cambridge, UK)- was applied overnight at 4^{o}C. Another PBS wash cycle preceded application of secondary antibody (diluted 1:250 in 1X PBS). Alexa Fluor 546 rabbit anti-goat (CXCR4) or Alexa Fluor 546

goat anti-rabbit (SDF-1) (Invitrogen, Carlsbad, CA, USA) were applied for 1 hour at 37^{o}C and washed with PBS. Finally, DAPI (Molecular Probes, Eugene, OR, USA), diluted 1:1000 in 1X PBS, and Alexa Fluor Phalloidin 488 (Invitrogen), diluted 1:250 in PBS, were applied 1 hour at RT. Gels received one final PBS wash and were mounted with DABCO. Images were collected on the Invitrogen EVOS FL Auto Imaging System (Fisher Scientific) and the Zeiss LSM 510 META scanning confocal microscope (Zeiss Microscopy, Jena, Germany).

2.35 Collagen Hybridizing Peptide

The 3Helix peptide (3Helix Incorporated, Salt Lake City, UT, USA), is a collagen hybridizing peptide (CHP) conjugated with 5-FAM (488nm excitation). The peptide was diluted 1:3 in PBS per manufacturer's instructions (20 μM). Fixed hydrogels were blocked as described above for 5 minutes. The 3Helix peptide was heated at 80^{o}C for 5 minutes and then immediately placed on ice to quickly cool. The 3Helix peptide was applied to toroid containing hydrogels, incubated 24 hours at 4^{o}C, and rinsed with PBS. Gels were then counterstained with DAPI and smooth muscle actin (SMA) as described above and imaged with second harmonic generation (SHG) on the Leica SP8 multiphoton confocal microscope. The images were taken in the xyz planes with the depth of the z plane being a total thickness of 150 μm.

2.36 Vybrant Cell Labeling

Cells were stained prior to seeding using a Vybrant multicolor cell labeling kit (Thermo Fisher Scientific) containing three stains: DiO (501 nm), DiL (565 nm), and DiD (665 nm). We chose this kit for two reasons: 1) it can be added directly to

culture media to uniformly label suspended cells, and 2) the subcellular localization of these stains labels the cell membrane and lipids; thus, the entire cell is fluorescent for our toroid studies. Cells were suspended in media, and 5 µL of the chosen dye was added and mixed in by gentle pipetting. The suspension was incubated at 37^{o}C for 15 minutes before being centrifuged at 1500 rpm for 5 minutes. Supernatant was aspirated and cells were gently resuspended in fresh media. This incubation was repeated 3 times before a 10-minute recovery time for the cells. The cells were then placed either in or on top of gels and observed and imaged on the EVOS FL Auto and the Zeiss LSM 510.

2.37 Mechanical Testing

Unconfined uniaxial compression testing was used to determine whether the observed cellular reorganization alters the mechanical properties of the matrix. To facilitate mechanical testing, larger hydrogel samples (1.5 mL) were created in 24-well plates. NHFs were then placed on the surface and incubated for 24 hours at 37^{o}C. Uniaxial compression tests were used to generate force-displacement response data for cylindrical samples formed from the collagen gel variants PureCol Collagen I (PC), RTC, and cRTC, prepared in both the native form and following cell-mediated matrix remodeling. Displacement-controlled compression testing was performed on a commercial system (Bose ElectroForce 3200; Bose Corp., Eden Prairie, MN) equipped with a high-fidelity load cell (max load 22 N; sensitivity ± 0.1N), two flat platens oriented for compression testing, and integrated data acquisition software (Wintest). Cylindrical specimens (n = 4-5; initial sample dimensions: diameter = 5.28 ± 0.1 mm and height = 5 ± 0.1 mm) were subjected

to a constant compression (displacement rate = 0.005 mm/s, max compression = 1 mm) during which the force response and sample dimensions were continuously recorded (data acquisition rate = 25 sec-1).

Acquired response data were transformed into compressive Cauchy stress versus percent sample compression data, wherein the Cauchy stress was computed as the recorded force divided by the cross-sectional area at each deformed state and the percent compression refers to the direction of the applied load. Stress-percent compression data were highly linear and elastic over the examined deformations for all gel variants. Based on the characteristic behavior and to enable comparison among samples, an elastic modulus value was calculated as the slope of a linear regression performed on the stress-compression data for each sample.

2.38 SEM Preparation and Imaging

Initially, hydrogels were fixed with 2% glutaraldehyde (Glut)/2% PFA solution for 30 minutes and rinsed until all fixative was removed (approximately 15 minutes). The hydrogels then went into a cycle of 1% osmium (1 hour at RT), PBS rinse (3 x 5 min), 1% glut/1% tannic acid in PBS (1 hour at RT), and PBS rinse for a total of 3 cycles. After the final rinse, excess moisture was removed using 70% EtOH (2 x 15min), 95% EtOH (2 x 15 min), and 100% EtOH (2 x 30 min), respectively. They were then subjected to critical point drying, mounting, and sputter coating. Those steps were followed as previously described (Nesbitt et al., 2006).

Briefly, samples were placed in an appropriate holder and then into the chamber and dried using a SAMDRI PVT-3B critical point drying system. When finished drying, the sample was removed from the critical point dryer and adhered to a stub with a standard carbon adhesive tab. The stub with the specimen was inserted into the Cressington 108 Auto/SE Sputter Coater. Once completed, the fully prepared specimen was imaged using a JEOL JSM-IT100 Scanning Electron Microscope at a voltage of 10.0kV and a magnification range of 27x-1,600x.

2.4 Results

2.41 Time Series Analysis of Toroids

Our previous studies examined the formation of toroids at 24 hrs when they had fully formed. (Gourdie and Potts, 2014). To begin to understand the process more carefully, we captured the process of toroid formation using time lapse imaging. We used 25,000 of both NHFs and ADSCs cultured to create toroids in a well of a 96 well plate. The NHFs were stained with Vybrant DiD prior to culturing on top or inside the collagen hydrogel. Figure 2.1 shows NHF staining images taken at the 1, 10, 16, and 24-hr marks (A-D respectively). Distinct toroids formed by 10 hrs and toroids continued to form through 24 hrs. We next investigated early times during toroid formation. We examined hydrogels seeded with cells at 1, 2, 3, and 6 hrs. In the first hour, cells appeared to be uniformly dispersed on the surface of the gel. By 3 hrs the cells began to coalesce and organize into the toroid structure, and by 6 hrs a distinct toroid had developed (Figure 2.2). This indicates that the process occurrs rapidly and that cells quickly sense their matrix environment and begin to migrate. By 10 hrs toroids were clearly observed and

by 24 hrs toroids had formed to their usual shape and size. Toroid at 10 hrs was approximately 4,500 μm, whereas by 24 hrs toroids had contracted to approximately 2,250 μm on standard PureCol hydrogels. A similar time frame for toroid formation was also seen using the ADSCs.

2.42 SEM Analysis of Toroid Formation

Our previous confocal analysis clearly demonstrated that during toroid formation cells form a toroid and invade the underlying matrices to form a cylinder-like structure. However, the surface of the gel has not been investigated. In order to accomplish this, we examined the toroid gels using SEM. Due to the immense hydration of the hydrogels, processing of the gels was delicate. The images in Figure 2.3 illustrate the shrinkage that occurred during the processing of the hydrogels. Therefore, no accurate toroid measurement data were obtained from the gels, but morphology of the toroid was analyzed. Even though it was difficult, by using SEM we were able to establish that the toroid showed migration of the cells towards the toroid, and that the toroid itself was raised slightly on the surface of the gel and formed an almost crater-like structure (Figure 2.3 A, B, and D). In comparison, gels with cells mixed in contracted and appeared to have a confluent surface while the gel contracted in on itself (Figure 2.3 C). Lastly, we observed changes to the collagen structure after cells have migrated to the toroid (Figure 2.3 E and F).

2.43 Comparison of Matrices

In 3D cell culture, many different hydrogel matrices have been found to create a suitable *in vivo*-like environment, spanning from natural to synthetic

compositions. To determine if toroid formation was matrix dependent, we created toroids using 9 different matrices, under similar conditions, using the same cell type (ADSCs) and quantity (25,000 cells). ADSCs were placed on top of each matrix, cultured for 24 hrs, and stained with phalloidin conjugated with Alexa-488 and DAPI. Figure 2.4 shows the matrices tested and resulting ability of cells to form toroids when cultured on their surface. Six of nine matrices tested formed toroids while 3 failed to form toroids following multiple attempts. The matrices that produced toroids were, PureCol, Nutrigen, Type III collagen, RTC, AlphaBioGel and Matrigel when cells were cultured on them. In contrast, toroids were not formed when cells were cultured on type V collagen. In this case it appeared that the matrix was degraded by cells. Similarly, the carbohydrate hydrogel made using VitroGel3D produced cell clumps, but no visible toroids. Finally, when cells were cultured on Fibrocol (10% collagen I), cells remained spread over the surface of the gel and no toroids were formed. In contrast, Nutrigen, a 6% collagen I hydrogel, formed the toroids. When we measured the diameter of the forming toroids, Nutrigen had the largest toroid formed (3.67mm average toroid diameter), compared to Matrigel, which formed the smallest toroids (1.70mm average toroid diameter) (Figure 2.4).

2.44 Toroid Analysis in a Multi-Matrix Environment

In vivo cells experience an environment consisting of multiple matrices. In order to try and recapitulate, to some extent, a more *in vivo*-like condition, we created hydrogels containing mixtures of different types of collagen. Both collagen III and collagen I, when used alone, formed toroids. Hydrogels with combinations

of varying percentages of collagen III and I were created and tested. A collagen hydrogel concentration series was performed using concentrations of 100% type I, 80:20 (type I:type III), 60:40, 40:60, and 100% type III. After a 24-hour incubation, toroid formation progressively grew smaller with increasing collagen type III. The toroids created with 100% collagen I produced an average diameter of 2.7mm while the toroids on hydrogels of 100% collagen III had a statistically significant smaller toroid that averaged 1.7mm (Figure 2.5).

2.45 Hydrogel Remodeling During Toroid Formation

It is well known that as cells are placed in a 3D matrix, they attempt to remodel that matrix. The collagen hydrogel model has been used routinely to investigate gel contraction and remodeling by cells (Fix et al, 2011; Potts et al., 1992; Runyan et al., 1990). We sought to determine whether such remodeling was occurring by cells forming toroids. To that end, we took advantage of a novel collagen binding peptide (CHP). This peptide can bind to the triple helix of collagen only when the strands have been opened. The opening of the collagen strands most likely occurred as a result of the cells attempting to remodel the collagen matrix. Using the CHP and second harmonic generation (SHG) capabilities on the Leica SP8 multiphoton confocal microscope, we observed the level of remodeling that occurs during cellular migration through a hydrogel. Figure 2.6 shows the staining of the CHP in relationship to the collagen near the toroid. CHP staining is seen near cells in and around the toroid, but it appears minimal in the outer region of the hydrogel as it appears the majority of the collagen unwinding occurs near, or in, the toroid itself. In addition, we measured the volume of the hydrogel both

with cells embedded and in toroids. We used both 50,000 and 100,000 ADSCs in gels and allowed incubation for 24 hrs.

2.46 Mechanical Testing

To determine whether the cells affected the collagen gel matrix differently when forming a toroid, we performed rheology measurements on toroids created with different matrices. Gels were made using PC, RTC, or cRTC. Mean Cauchy stress–percent compression relations of the PC, RTC, and cRTC specimens indicate an overall softening of the gel matrix with cellular remodeling (Figure 2.7). The cell infused-PC, -RTC, and -cRTC samples all exhibited a significant ($p < 0.05$) decrease in elastic modulus in comparison to the native gels, with reductions of 18.97 ± 4.2 %, 15.80 ± 3.9 % and 19.55 ± 5.0 %, respectively.

2.47 Mixed Cell Interactions

Our model of toroid formation represents an example of how cells react and remodel their matrix environment during migration and differentiation. For this reason, we next set out to recapitulate in vivo like milieus by examining toroid formation with multiple cell types mixed prior to culturing on the surface of the hydrogel. We sought to determine how multiple cell types would react when cultured together to form a toroid. We used numerous combinations with ADSC, BMSC, and NHF cells and each of the combinations formed toroids. When both ADSCs and NHFs, stained with Vybrant DiO (green) and DiD (red) respectively, were combined on a PureCol hydrogel the toroid showed significant cellular intermingling. Using the vibrant dyes, we were able to see clear demarcations between the ADSCs and NHFs. Due to the large number of cells combined on a

small 96-well gel, we expected to observe some overlapping signal (yellow fluorescence) in our images created if the red and green fluorescence were overlapping in any way. However, we did not observe any observable overlap of fluorescent signal (Figure 2.8). This suggests that cells are able to migrate simultaneously and intermingle to form a toroid. In some toroids we observed the formation of cell clusters by the ADSCs when cultured with NHFs (Figure 2.8c). This formation was not observed in any of the other combinations of cells and its significance remains unclear.

2.5 Discussion

This study expands on the findings of toroid formation by modeling cell:cell and cell:ECM interactions through the creation of single- and multi-cellular environments within different hydrogel matrices. Toroids are a self-organizing tissue structure created by cells cultured on top of a hydrogel. In our study, all combinations of cells and matrices produced toroids, except for Collagen V (degraded by cells), Fibricol (cells stayed spread throughout the gel), and synthetic VitroGel3D (produced cell clumps). Likewise, in unpublished studies, our attempted cancer cell lines failed to form toroids but remained viable both on top of and inside collagen matrices. Historically collagen I hydrogels have been the primary acceptable and consistent extracellular matrix environment used for cellular studies due to the replicability of ECM properties (Antoine et al., 2015). In the same respect, we sought to investigate toroid formation with numerous different matrices to determine the optimal, most consistent matrix for the modeling of cell:cell and cell:ECM interactions. In order to do this, many different matrices

had to be tested. PureCol, Nutrigen, and Fibricol are all derived from collagen type I at concentrations of 2%, 6%, and 10%, respectively. Rat Tail Collagen is collagen type I from rat instead of bovine placenta. Collagen types III and V are both members of the fibril-forming collagen family with type I. Matrigel is a matrix synthesized from a mouse sarcoma tumor consisting of type IV collagen with laminins, proteoglycans, and growth factors. Our two synthetic matrices, AlphaBioGel and VitroGel3D, were advertised as a suitable alternative to natural collagen matrices. Intriguing was that AlphaBioGel was able to create a toroid while VitroGel3D did not. In this study we show that numerous matrices appeared to produce consistent toroid sizes. This ability by other matrices suggest that toroid formation is a cellular phenomenon that is inherent in most cells when cultured in this manner. Furthermore, most of these matrices are sufficient for 3D culture experiments and provide the opportunity to explore advancements in the optimization for hydrogel protocols.

To study the initial formation of the toroid, we used time lapse imaging of cell migration over a 24-hour period using fluorescently labeled cells. Cells were shown to originally be spread over the surface of the hydrogel (1 hr) then migrate from the outside of the hydrogel to form the toroid (24 hrs). We also observed how these cells migrated over these hydrogels during toroid formation. Cells appeared to create channels in the gel. They appear to migrate as spokes on a bicycle wheel lined up and following each other until they stop and form a toroid. When a toroid is formed, collagen is remodeled through the unwinding of the triple helix, demonstrated by the binding of the CHP (Figure 2.6). This remodeling was also

demonstrated in the compression of hydrogels. During the formation of the toroid there is an apparent and measurable softening of the hydrogel. This change was observed in all three matrices we tested.

Our data is similar to earlier studies that have suggested that cells align collagen, rather than collagen organizing cells. Smooth muscle cells seeded into a pre-aligned matrix reorganized collagen in response to mechanical loading conditions (Barocas et al., 1998). Likewise, when exposed to a change in uniaxial loading direction, fibroblasts rapidly remodeled the matrix, even after previous mechanical alignment (Lee et al., 2008). Although the reason for alignment in the unconstrained direction is not fully understood, stress generated during gel compaction is likely a primary factor. Measuring strains using fiducial markers or modifying the stiffness of our matrices could provide quantitative data on the role of mechanical load in the alignment of cells in our hydrogels. In fact, that is exactly what we found when we cultured cells on the surface of a very stiff collagen hydrogel, Fibrocol. In this instance, cells remained on the surface of the gel and failed to form toroids.

Generally, most hydrogel studies consist of a single matrix. Although that makes a consistent variable it does not truly reflect the *in vivo* matrix environment most cells will experience. In this study, we created mixed hydrogels of varying percentages of collagen type I and III. We observed that toroid size was smaller with decreasing percentages of collagen. Pure collagen III hydrogels produced smaller toroids that were 37% reduced in size when compared to collagen I, which could suggest a different or enhanced receptor utilization when forming a toroid

(Figure 2.5). Most cells use either α2β1 or α11β1 integrins to bind to collagen III (Gullberg et al., 1992). Type III collagen is the second most abundant collagen of soft tissues and dominates early phases of wound healing and granulation tissue formation. Type III collagen is a homotrimer of three identical polypeptide chains and is located in skin, blood vessel walls, and pleuroperitoneal lining; bone has a minimal amount of type III collagen (Kuivaniemi & Tromp, 2019).

Historically, single cell type experiments are important to understand the response of cells to hydrogels to activators and inhibitors of cellular functions, likewise toroid formation, a more *in vivo*-like environment consists of multiple cell types interacting with each other as they migrate. Thus, we mixed multiple cell types prior to culturing on the surface of the hydrogel and observed their interactions and their ability to form toroids. We chose both undifferentiated and differentiated cell types in our toroid experiments. Adipose-derived stem cells (ADSCs) are undifferentiated mesenchymal stem cells that maintain the ability to differentiate into mesodermal, endodermal, and ectodermal cell-specific lineages. Upon transplantation into a damaged site, they interact with the microenvironment to generate new progenitors and cells. Likewise, they aid in tissue regeneration. Bone-marrow stem cells (BMSCs) have similar capabilities and have become a primary cell source in regenerative medicine due to their ability to differentiate into different lineages such as chondroblasts, adipocytes, fibroblasts, and osteoblasts. In addition, we chose a differentiated control cell, neonatal cardiac fibroblasts (NHFs). Fibroblasts are also the major cell type in the synthesis of the ECM. They are abundantly available in the proliferative phase of wound healing, synthesizing

new ECM and collagen fibers. Of note was the fact that these cells mixed together and combined to create a toroid. Upon closer analysis, cells intermingled when forming the toroid (Figure 2.8). Interestingly, we also observed the unusual formation of cell clusters by the ADSCs in which they appeared to be surrounded by other stem cells or fibroblasts when cultured together. We had not observed this type of structure in any our previous toroid experiments. It is possible that these clusters of cells were not completely dispersed when cultured but more likely they sought out similar cells to migrate together but separate to other cell types.

Ongoing studies are focused on examining multi-cell microenvironments and attempt to understand the formation of ADSC cell clusters. We are also pursuing assays to better understand the full molecular regulation in toroid formation as well as the communication mechanisms utilized between cells. One such pathway that shows preliminary importance is the CXCL12/CXCR4 pathway used in other stem cells (Hu et al., 2013). To reiterate, using this model of cellular interactions and programming, we can examine and explore (1) the understanding of early embryonic development, (2) the optimization of hydrogels for *in vivo* applications and (3) the creation of a model system for future tissue formation and regeneration and disease.

2.6 Conclusion

To summarize, we have created a tunable and adaptable model to examine cellular differentiation that resembles processes found in development and disease. We have created a hydrogel model that mimics the *in vivo* environment and examined the importance of specific matrices on cellular migration and

differentiation. We have successfully co-cultured cells on the same hydrogel to investigate maturation and differentiation of ADSCs and NHFs into toroids. Co-cultured cells were shown to migrate together to form a toroid. We have used this model to demonstrate that there are measurable changes in the hydrogel elastic properties during toroid formation. Furthermore, the stem cells remodel the matrix during toroid formation demonstrated by the binding of a collagen binding peptide demonstrating the unwinding of collagen helices. Finally, we have shown toroid formation begins within 3 hrs of seeding on the hydrogel. This suggests that these cells quickly recognize the matrix they are seeded on and begin to coordinate a coordinated cellular migration that ends with the formation of a toroid. This novel 3D system allows for tunability and reproducibility to investigate cellular interactions, maturation, and differentiation in both healthy and injured cells.

2.7 Acknowledgments

The authors would like to recognize Lorain Junor M.S. for technical support and the Instrumentation Resource Facility at the University of South Carolina School of Medicine for technical assistance.

2.8 Grant Support

This work was supported in part by the NSF and SC EPSCoR Program under award number (NSF Award #OIA-1655740 and EPSCoR GEAR-CRP Award 18-GC04). JDP acknowledges financial support from the University of South Carolina ASPIRE program.

2.9 References

Antoine EE, Vlachos PP, Rylander MN. (2015). Tunable Collagen I Hydrogels for Engineered Physiological Tissue Micro-Environments. *PLoS ONE*. 10(3): e0122500.

Badylak SF, Freytes DO, Gilbert TW. (2009). Extracellular matrix as a biological scaffold material: structure and function. *Acta biomaterialia*. 5(1):1-3.

Barocas VH, Girton TS, Tranquillo RT. (1998). Engineered alignment in media equivalents: magnetic prealignment and mandrel compaction. J Biomech Eng. 120(5):660-6.

Bian, X., Song, Z.L., Qian, Y., Gao, W., Cheng, Z.Q., Chen, L., Liang, H., Ding, D., Nie, X.K., Chen, Z. and Tan, W. (2014). Fabrication of graphene-isolated-Au-nanocrystal nanostructures for multimodal cell imaging and photothermal-enhanced chemotherapy. *Scientific reports*, 4, 1-9.

Cen, L., Liu, W. E. I., Cui, L. E. I., Zhang, W., & Cao, Y. (2008). Collagen tissue engineering: development of novel biomaterials and applications. *Pediatric research*, 63, 492-496.

de Castro Brás LE, Proffitt JL, Bloor S, Sibbons PD. (2010). Effect of crosslinking on the performance of a collagen-derived biomaterial as an implant for soft tissue repair: A rodent model. *Journal of Biomedical Materials Research Part B: Applied Biomaterials*. 95(2):239-49.

Engler AJ, Sen S, Sweeney HL, Discher DE. (2006). Matrix elasticity directs stem cell lineage specification. *Cell*. 126(4):677-89.

Fix C., Bingham K., Carver W. (2011). Effects of interleukin-18 on cardiac fibroblast function and gene expression. *Cytokine*, 53(1):19-28. PMID: 21050772, PMCID: PMC3018826, DOI: 10.1016/j.cyto.2010.10.002

Gaetani, R., Zizzi, E.A., Deriu, M.A.; Morbiducci, U., Pesce, M., & Messina, E. (2020). When Stiffness Matters: Mechanosensing Heart Development and Disease. *Front. in Cell Dev. Biol*, 8, 334.

Glowacki, J., & Mizuno, S. (2008). Collagen scaffolds for tissue engineering. *Biopolymers: Original Research on Biomolecules*, 89, 338-344

Gourdie RG, Potts JD, inventors; MUSC Foundation for Research Development, assignee. Compositions and methods for tissue engineering, tissue regeneration and wound healing. United States patent US 8,815,556. 2014 Aug 26.

Gourdie, R. G., Myers, T. A., McFadden, A., Li, Y.X., & Potts, J. D. (2012). Self-organizing tissue-engineered constructs in collagen hydrogel. *Microsc Microanal*. 18(1), 99-106.

Gullberg D, Gehlsen KR, Turner DC, Ahlén K, Zijenah LS, Barnes MJ, Rubin K. (1992). Analysis of alpha 1 beta 1, alpha 2 beta 1 and alpha 3 beta 1 integrins in cell--collagen interactions: identification of conformation dependent alpha 1 beta 1 binding sites in collagen type I. *EMBO J.* 11(11):3865-73. PMID: 1396580; PMCID: PMC556896.

Hansen, L. K., Wilhelm, J., & Fassett, J. T. (2006). Regulation of hepatocyte cell cycle progression and differentiation by type I collagen structure. *Current topics in developmental biology*, 72, 205-236.

Hu C, Yong X, Li C, Lü M, Liu D, Chen L, Hu J, Teng M, Zhang D, Fan Y, Liang G. (2013). CXCL12/CXCR4 axis promotes mesenchymal stem cell mobilization to burn wounds and contributes to wound repair. *J Surg Res*. 183:427-34. doi: 10.1016/j.jss.2013.01.019. Epub 2013 Feb 1. PMID: 23462453.

Hunt NC, Grover LM. (2010). Cell encapsulation using biopolymer gels for regenerative medicine*. Biotechnology letters*. 32(6):733-42.

Huynh, T., Abraham, G., Murray, J., Brockbank, K., Hagen, P. O., & Sullivan, S. (1999). Remodeling of an acellular collagen graft into a physiologically responsive neovessel. *Nature biotechnology*, 17, 1083-1086.

Kuivaniemi H, Tromp G. (2019). Type III collagen (COL3A1): Gene and protein structure, tissue distribution, and associated diseases. *Gene*. 707:151-171. doi: 10.1016/j.gene.2019.05.003. Epub 2019 May 7. PMID: 31075413; PMCID: PMC6579750.

Lee JH, Kim HE, Im JH, Bae YM, Choi JS, Huh KM, Lee CS. (2008). Preparation of orthogonally functionalized surface using micromolding in capillaries technique for the control of cellular adhesion. Colloids Surf B Biointerfaces. 64(1):126-34.

Li F, Guo WY, Li WJ, Zhang DX, Lv AL, Luan RH, Liu B, Wang HC. (2009). Cyclic stretch upregulates SDF-1α/CXCR4 axis in human saphenous vein smooth muscle cells. *Biochemical and biophysical research communications*. 386:247-51.

Macleod TM, Williams G, Sanders R, Green CJ. (2005). Histological evaluation of Permacol™ as a subcutaneous implant over a 20-week period in the rat model. *British journal of plastic surgery*. 58(4):518-32.

Mercado-Pimentel, M. E., & Runyan, R. B. (2007). Multiple transforming growth factor-β isoforms and receptors function during epithelial-mesenchymal cell transformation in the embryonic heart. *Cells Tissues Organs*, 185, 146-156.

Nesbitt T, Lemley A, Davis J, Yost MJ, Goodwin RL, Potts JD. (2006). Epicardial development in the rat: a new perspective. *Microsc Microanal*. 12(5):390-8. doi: 10.1017/S1431927606060533.PMID: 16984665

Pang, Y., & Greisler, H. P. (2010). Using a type 1 collagen-based system to understand cell-scaffold interactions and to deliver chimeric collagen-binding growth factors for vascular tissue engineering. *Journal of investigative medicine*, 58, 845-848.

Patino, M. G., Neiders, M. E., Andreana, S., Noble, B., & Cohen, R. E. (2002). Collagen as an implantable material in medicine and dentistry. *Journal of Oral Implantology*, 28, 220-225.

Pedraza CE, Marelli B, Chicatun F, McKee MD, Nazhat SN. (2010). An In Vitro assessment of a cell-containing collagenous extracellular matrix–like scaffold for bone tissue engineering*. Tissue engineering Part A*. 16(3):781-93.

Potts JD, Vincent EB, Runyan RB, Weeks DL. (1992). Sense and antisense TGF beta 3 mRNA levels correlate with cardiac valve induction. *Dev Dyn*. 193(4):340-5. doi: 10.1002/aja.1001930407.PMID: 1511174

Rennert, R. C., Sorkin, M., Garg, R. K., & Gurtner, G. C. (2012). Stem cell recruitment after injury: lessons for regenerative medicine. *Regenerative medicine*, 7, 833-850.

Ribeiro, M. C., Tertoolen, L. G., Guadix, J. A., Bellin, M., Kosmidis, G., D'Aniello, C., Monshouwer-Kloots, J., Goumans, M. J., Wang, Y. L., Feinberg, A. W. and Mummery, C. L. (2015). Functional maturation of human pluripotent stem cell derived cardiomyocytes in vitro–correlation between contraction force and electrophysiology. *Biomaterials*, 51, 138-150.

Runyan RB, Potts JD, Sharma RV, Loeber CP, Chiang JJ, Bhalla RC. (1990). Signal transduction of a tissue interaction during embryonic heart development. *Cell Regul.* 1(3):301-13. doi: 10.1091/mbc.1.3.301.PMID: 2129222

Sun Y, Wang Q. (2013). Modeling and simulations of multicellular aggregate self-assembly in biofabrication using kinetic Monte Carlo methods. *Soft Matter*. 9(7):2172-86.

Tonnesen, M. G., Feng, X., Clark, R. A. (2000). Angiogenesis in wound healing. *Journal of Investigative Dermatology Symposium Proceedings*, 5, 40-46.

Vu, L. T., Jain, G., Veres, B. D., Rajagopalan, P. (2015). Cell migration on planar and three-dimensional matrices: a hydrogel-based perspective. *Tissue Engineering Part B: Reviews*, 21, 67-74.

Xing F, Li L, Zhou C, Long C, Wu L, Lei H, Kong Q, Fan Y, Xiang Z, Zhang X. (2019). Regulation and directing stem cell fate by tissue engineering functional microenvironments: scaffold physical and chemical cues. *Stem Cells International*. 2180925. doi: 10.1155/2019/2180925.

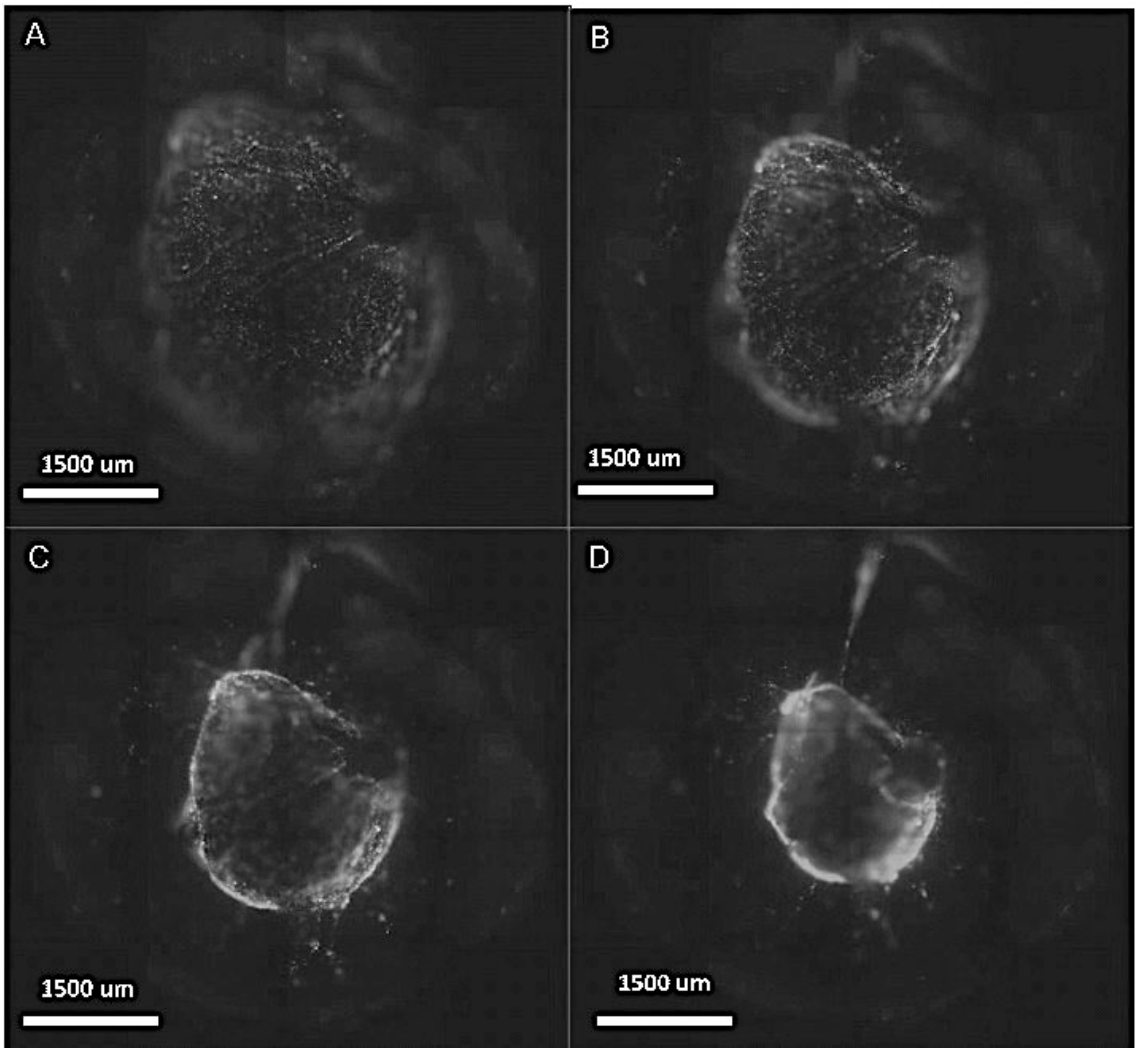

Figure 2.1 Fluorescent time series showing cellular migration. Images from a time series using PureCol collagen I hydrogel in a 96-well plate with 50,000 NHFs show the formation of a toroid over a 24-hr period. Cells were stained with Vybrant Cell Labeling DiD which emits in the far-red spectrum (665 nm). Still-frame images were taken at 1, 10, 16, and 24-hrs (A-D respectively) to analyze the movement seen in the time series. We can see that the cells are migrating from the outer portions of the gel to form a toroid.

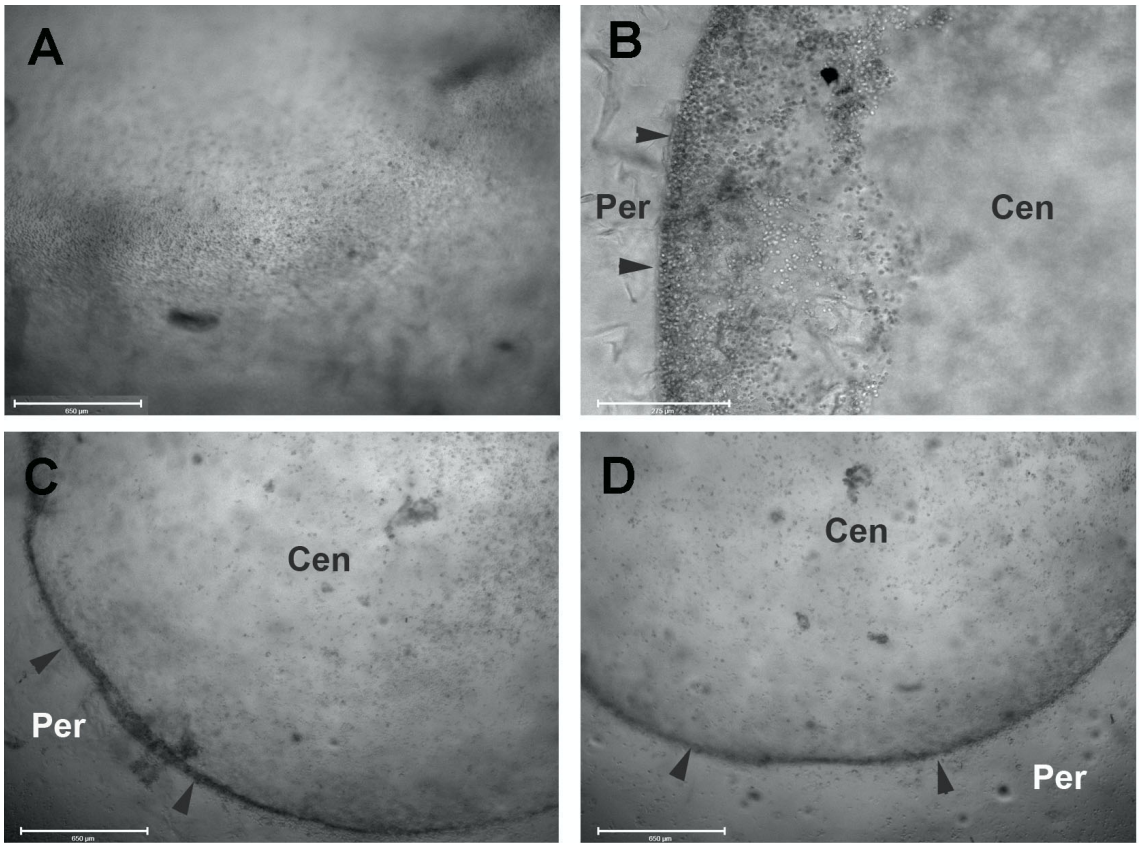

Figure 2.2. Early time series of toroid formation. Bright field images of the hydrogel seeded with cells at 1, 2, 4, 6 hr (A-D) respectively. Notice by 2 hours (B) the cells have begun to migrate and coalesce and by 4 hr (C) there is a clear border to the toroid formed (arrowheads). The center of the toroid is labeled (Cen) as is the periphery of the gel (Per). Scale bars = 650um.

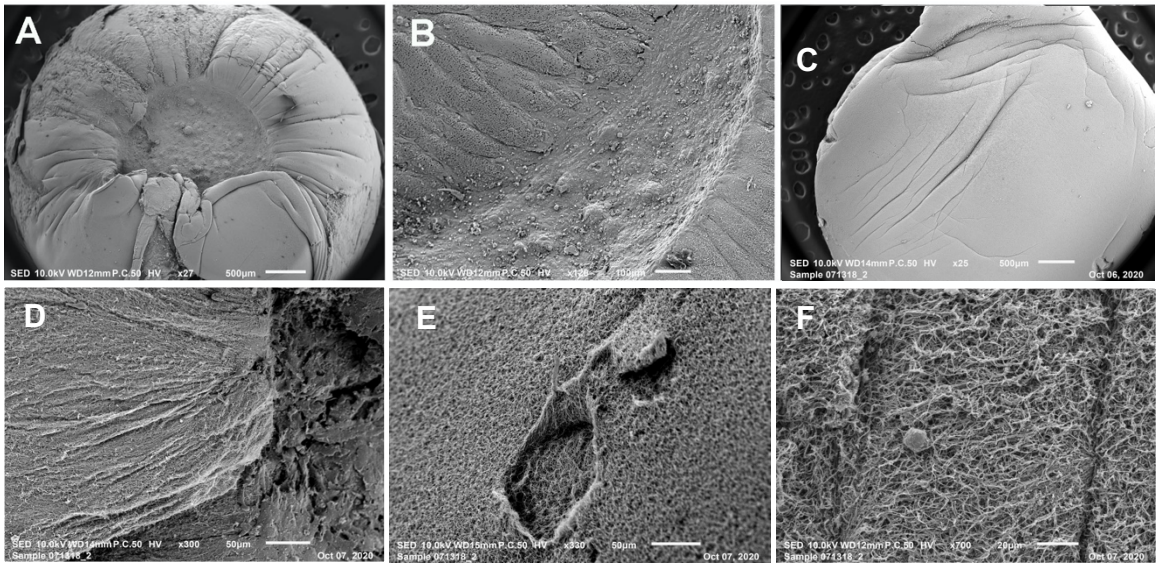

Figure 2.3. Scanning EM images of the toroid and mixed in hydrogels. The toroid appears as a crater on the surface of the hydrogel (A). Image of the collagen gel with toroid. (D) A higher magnification of the rim of the crater shows cells on the surface and down into the crater (B). In comparison, the hydrogels that have cells mixed in contract the entire gel (C). (E) and (F) Images on the outside of the hydrogel showing collagen remodeling. Scale bars for A and C =500 μm. Scale bar for B =100 μm. Scale bars for D, E, and F = 75 μm.

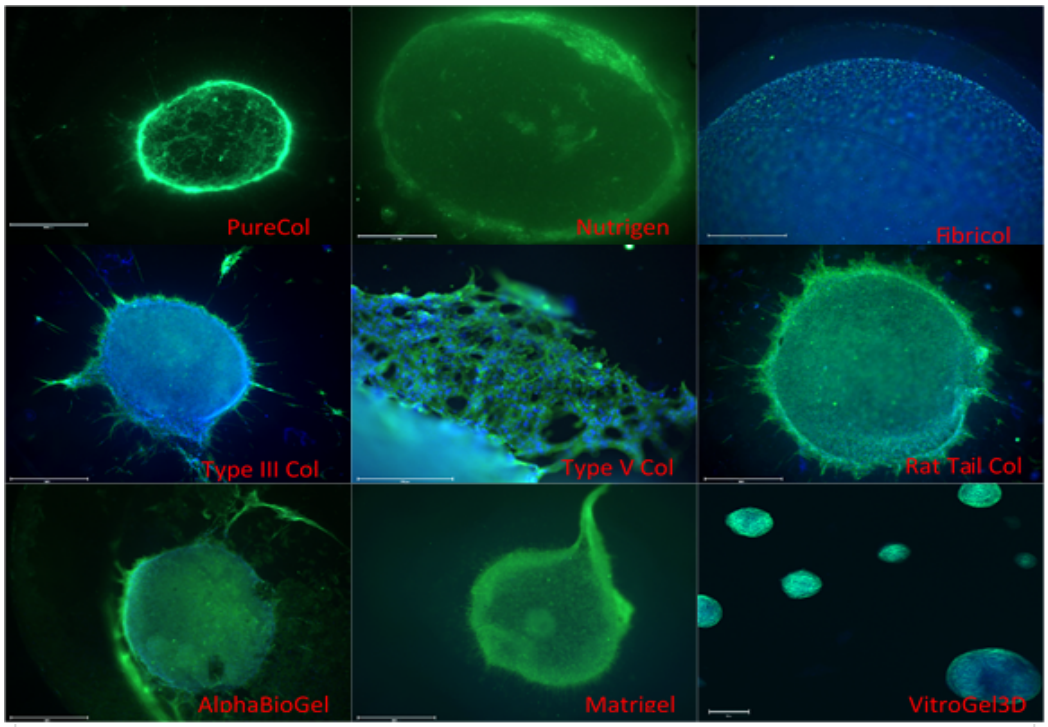

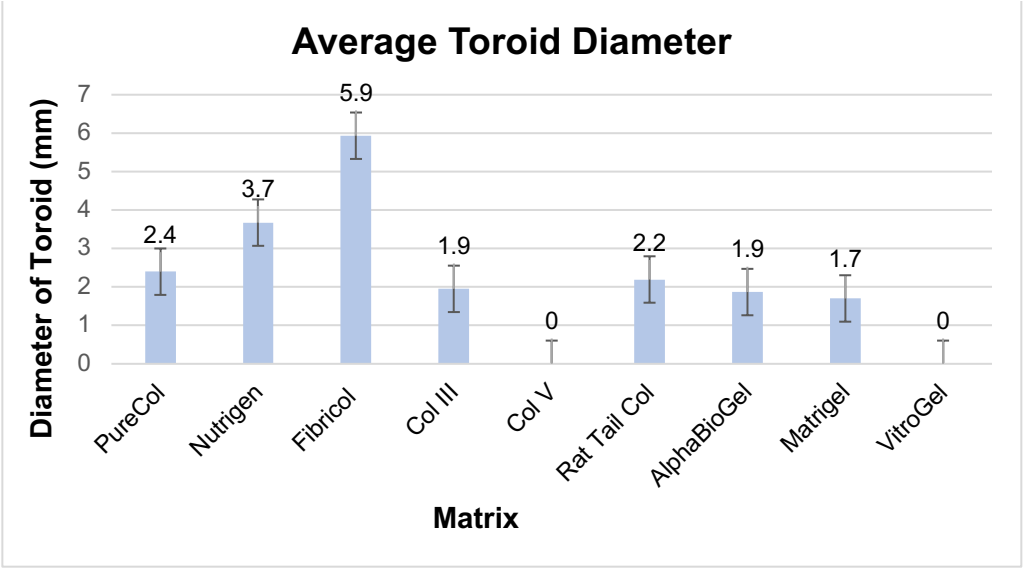

Figure 2.4 Comparison of 3D cell culture matrices. Twenty-five thousand ADSCs were cultured on top of each 100µL gel. Fibricol (cells stayed spread throughout gel, collagen V (degraded by cells), and VitroGel3D (created cell clumps) did not form toroids. All other matrices formed toroids between 1.70 mm and 3.67 mm average diameter. There was no difference in the toroid structure other than size and possibly how the cells migrated through the matrix. Toroid size may provide for better optimization of hydrogel applications. Scale bars=50µm, Green=Phalloidin, Blue=DAPI

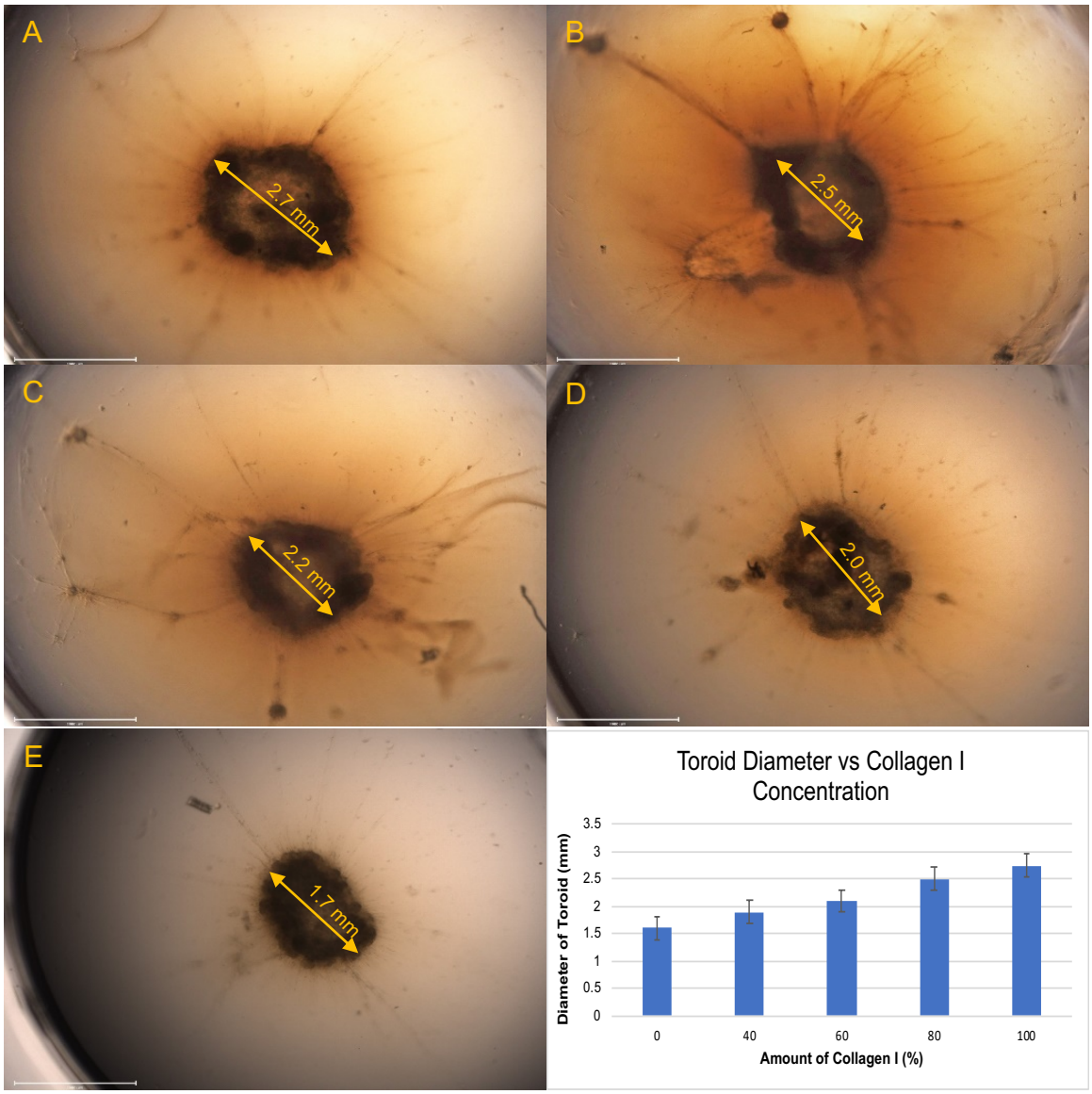

Figure 2.5. Varying collagen type I concentration series. Toroids were created with gels seeded on top with fifty-thousand NHFs on each of the following concentrations of collagen I and collagen III and allowed to incubate for 24-hours: A) 100% collagen I. B) 80% collagen I to 20% collagen III. C) 60% collagen I to 40% collagen III. D) 40% collagen I to 60% collagen III. E) 100% collagen III. N=6. When the diameters of the toroids were measured and averaged, we saw a 1 mm (37.04% difference between 100% collagen I (A) and 100% collagen III (E)). F) Bar graph analysis of the collagen concentration series. There is a correlating decrease in toroid diameter with increased collagen III concentration. The differences were significant at $P < 0.01$. Scale bars=200μm

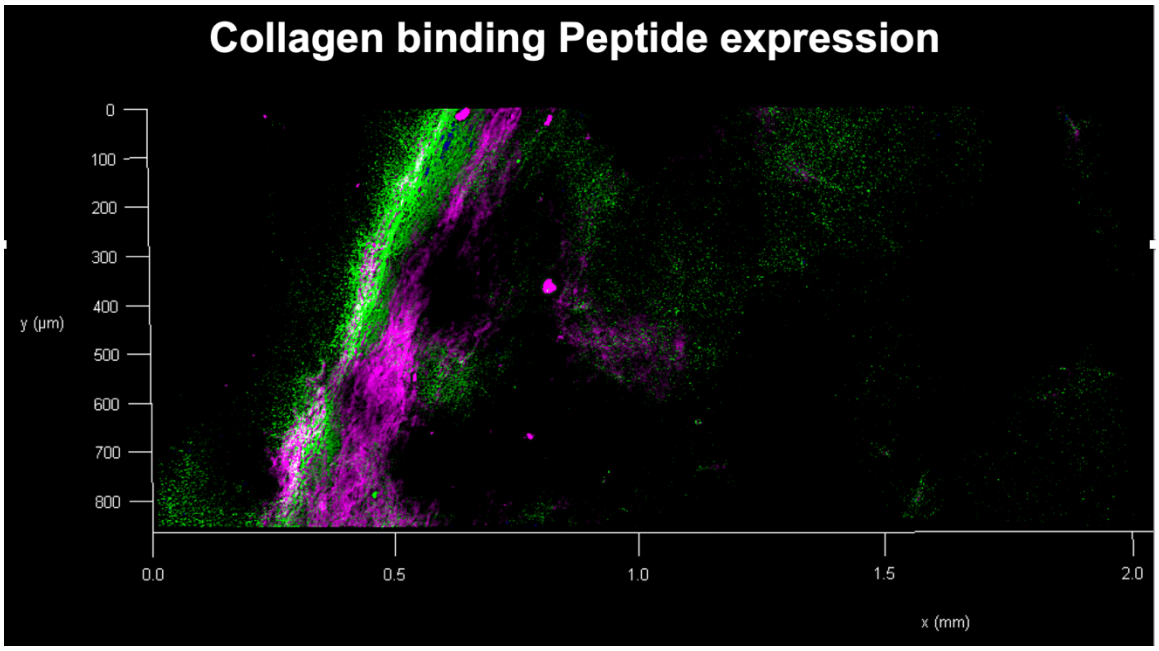

Figure 2.6. Collagen hybridizing peptide showing collagen remodeling. Multiphoton confocal image of a toroid. A 3-D image of the ADSCs migrating towards the toroid (cells=purple). The toroid (top) consists of a group of cells with more migrating towards it. The collagen fibrils are seen as green using CHP. CHP binds to the unwound double-helix during remodeling thus providing evidence of the extent of remodeling that occurs in a hydrogel during cellular migration.

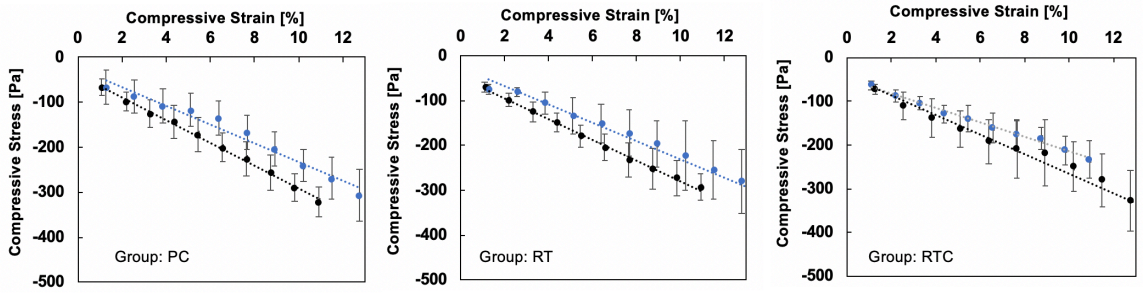

Figure 2.7. Rheology of toroids. Uniaxial compression response of gels pre- (•) and post- (•) cell-mediated remodeling. Solid circles are mean experimental measurements ± standard deviation; dashed lines are linear regressions of the group mean data. Gels were created using either PureCol (PC), Rat tail collagen (RTC) or Concentrated Rat tail collagen (cRTC).

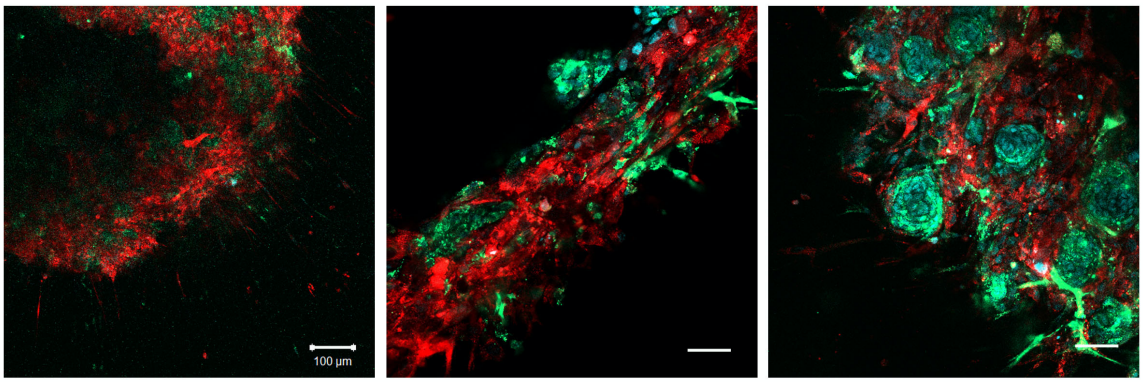

Figure 2.8. Mixed cell toroids showing cellular integration. Twenty-five thousand NHFs and ADSCs were seeded on top of a PureCol collagen I hydrogel. Confocal images show that while the cells appear to be intermingling, there is no overlapping signal. These results suggest that mixed cells will interact, migrate, and form a toroid. We also observed a cell clustering phenomenon in certain toroids (C). Scale bars=100µm A, 50µm B-C, Red=NHF, Green= ADSC, Blue=DAPI

CHAPTER 3

CXCL12-CXCR4 AS A POTENTIAL REGULATOR OF ADSC MIGRATION DURING TOROID FORMATION[2]

[2] Worden A, Stern M, and Potts JD. To be submitted to *Biomaterials*.

3.1 Abstract

The use of three-dimensional (3D) culture systems (hydrogels) and adipose-derived stem cells (ADSCs) in regenerative medicine has allowed for early-stage investigation and modeling of the mechanisms in diseases, treatments, targets, etc. without having to involve an animal model. ADSCs, specifically, are utilized due to their ability to differentiate into mesodermal, endodermal, and ectodermal cell-specific lineages. The innate programming of stem cells during embryonic development that drive them to a specific location for structural differentiation can be replicated during a process, termed toroid formation, where the cells are cultured on top of a hydrogel. Toroid formation appears to be a near universal process with the exception being cancer cell lines we have tried (<4). Interestingly, when cells are cultured inside the hydrogel rather than on the surface, there is contraction of the gel, but no toroid is formed. Our lab discovered that the CXCL12-CXCR4/7 pathway, the pathway implicated in numerous diseases including cancer and HIV, is upregulated during toroid formation and downregulated for mixed-in gels. By thoroughly dissecting this signaling pathway, our data pinpointed four key targets that significantly delayed, but did not eliminate, toroid formation. This work will define the underlying signaling pathways that regulate ADSC directed migration used during embryonic development and establish toroid formation as a novel 3D model for high throughout investigation of diverse *in vivo* molecular mechanisms.

3.2 Introduction

Complex organisms are composed of tissues in which most cells are embedded within a fibrous extracellular matrix (ECM). To study the intricate, three-dimensional (3D) organization of cells and ECM *ex* vivo, regenerative medicine has turned to collagen hydrogels due to their significant ease of use and versatility. Hydrogels can be used in a wide variety of ways including tissue repair and engineering, coated wells for cell culture, drug delivery, and 3D matrices for modeling and imaging (Xing et al, 2019; Provenzano, 2017; Pedraza et al, 2010; Greenbaum et al, 2013; Tamamura et al, 1998). Due to their biocompatibility and widely tunable structure, they have been shown to simulate the ECM in physical structure to a point that promotes cell proliferation and regeneration of tissues (Li et al, 2009). Of importance is that they are well-tolerated immunologically when implanted *in vivo* (Hunt and Grover, 2010; Badylak et al 2009; deCastro et al, 2010). Moreover, these hydrogels are remodeled and degraded by living tissues over time through enzymes such as metalloproteases (MMP)s, thus enhancing the potential for integration of implants with surrounding tissue. We have utilized collagen hydrogels in numerous studies (Worden et al, 2022).

While the study of cellular organization is limited due to lack of experimental approaches, matrix mechanics have been identified as a driving factor for cellular behavior. Matrix stiffness and mechanical properties of the ECM not only allow tissues to withstand physical stress, but are also regulatory for cellular functions including spreading, migration, proliferation, and stem cell differentiation (Xing et al, 2019; Engler et al, 2006), thus impacting many fundamental biological

processes including embryonic development, adult tissue homeostasis, and the pathogenesis of diseases such as fibrosis and cancer (Provenzano, 2017; Trappmann and Chen, 2013). The understanding of these inherently coded processes has expanded over the last several decades, however, the interconnected network between cells that responds to external stimuli is still largely uncharted and the current models make it difficult to advance these studies. Thus, it is important to create an *in vivo*-like, non-animal model that allows for the exploration of cell-cell and cell-ECM relationships.

Since the ultimate goal of regenerative medicine is to create functional tissues and organs, studies have been focused on utilizing stem cells with the hydrogel. Stem cells are affected by the chemical milieu of the matrix that they are being cultured in (Xu et al, 2017; Sinha et al, 2017). To date, there have been several advances in stem cell therapy leading to improved wound healing and tissue regeneration (Hassan et al, 2014; Li et al, 2013). Specifically, adipose-derived stem cells (ADSCs) are mesenchymal stem cells that maintain the ability to differentiate into mesodermic, endodermic, and ectodermic cell-specific lineages (Vermette et al, 2007). Upon transplantation into a damaged site, they interact with the microenvironment to generate new progenitor cells. Likewise, they aid in tissue regeneration and function by secreting exosomes filled with growth factors, cytokines, chemokines, and micro-RNA (Othmani et al, 2019), thus suggesting an innate programming that leads to these molecular mechanisms such as angiogenesis, immunomodulation, and cell proliferation and differentiation.

Our laboratory observed a unique morphological response when studying the self-organization of cells with collagen hydrogels. By culturing adipose-derived stem cells (ADSCs) on the surface of matrices, a toroid ring of cells was formed. These self-organizing tissue structures, or toroids, initially take the shape of the well-plates in which they are formed, and the cells appear long and thin during migration from the outer to inner regions of the hydrogel (Gourdie et al, 2012). In contrast, cells that were mixed inside of the hydrogel did not form toroids. Those studies provide the basis for ongoing studies, but there remains insufficient understanding as to the molecular regulation of cellular migration and toroid formation (Worden et al, 2022).

The current study expands our understanding of this physiological response by linking toroid formation to the CXCL12-CXCR4 signaling pathway. CXCL12 (or SDF-1) is a chemokine protein expressed in several tissues including the brain, heart, and bone marrow. When CXCL12 binds to its cognate receptor, CXCR4, a chemical signaling cascade leads to a number of physiologic responses such as proliferation, migration, and survival (Wang et al, 2017; Wang et al, 2019). This pathway is known for playing a role in neural and cardiac development during embryogenesis as well as regulating adult stem cells during processes involved with wound healing, tissue repair, and angiogenesis (Bleul et al, 1996, Ji et al, 2004). Likewise, it has been implicated in several diseases such as HIV cardiovascular disease, and cancer (Greenbaum et al 2013, Ara et al, 2003, Cojoc et al, 2013, Teicher and Fricker, 2010). Of fundamental importance to this study is that a gene targeted array performed to determine the signaling pathways

responsible for ADSC toroid formation identified this multifunctional chemokine as a likely candidate. These studies seek to define the underlying signaling pathways that regulate ADSC toroid formation in a changing microenvironment.

3.3 Methods

3.31 Cell Culture

Adipose-derived Stem Cells (ADSCs) and 4T1 murine breast cancer cells were extracted from mice and cultured in Dulbecco's Modified Eagle Medium (DMEM) supplemented with 10% Fetal Bovine Serum (FBS), Penicillin-Streptomycin (10mL/L), and Amphotericin B (2.5mg/L). 4T1s were additionally supplemented with RPMI-1640 Medium (ATCC, Manassas, VA, USA). We used all primary cell cultures at passage 5 or less. Cells were grown until 80-90% confluency prior to use for experimentation. The cells used in toroid experiments were then trypsinized (0.25% Trypsin/EDTA), centrifuged 8 minutes at 800 RPM, and counted. For single-celled experiments, cells were applied at a concentration of 25,000 cells per gel. For multi-cell experiments, toroids were formed with 25,000 cells/cell type/gel.

3.32 Hydrogel Preparation

For all studies, we used an 8:1:1 ratio of PureCol Bovine Type I Collagen matrix (Advanced BioMatrix), 0.2N HEPES pH 9.0 (Fisher Scientific, Hampton, NH, USA), and 10X Minimum Essential Medium (MEM, Sigma-Aldrich, St- Louis, MO, USA) formed in a 96 well culture dish (Corning Incorporated, Corning, NY, USA). The mixture was added at 100 µL per well and stabilized at 37^{o}C overnight. Cells were placed on top of the gels and incubated at 37^{o}C for 30 minutes. Gels were

released from the sides of the wells with a thin-tipped probe and incubated at 37°C for an additional 24 hours. For mixed in gels, cells in media were mixed into the matrix prior to being poured and incubated for 24 hours.

3.33 Real Time PCR Analysis of CXCL12 and CXCR4

RNA was isolated from previously formed toroid and mixed-in cultures using Cetyltrimethylammonium Bromide (CTAB) and alcohol precipitation-based methods. Spheroids are another common 3D culture system. ADSC spheroids were generated using Elplasia spheroid generator culture plates at a density of 3,000 cells per spheroid. RNA was isolated from 2D (70-90% confluence) and spheroid cultures using the Qiagen RNeasy Plus Micro kit. Reverse transcription was carried out using Bio-Rad iScript RT Supermix (Bio-Rad Laboratories, Hercules, CA, USA). Real-time PCR was performed using Bio-Rad Sso Advanced Universal SYBR Green Supermix with transcript-specific primers for CXCL12 and CXCR4 and compared to an internal reference gene (Mrpl19) on a Bio-Rad CX96 Real-time PCR system. Data analysis was performed in CFX Manager.

3.34 CXCL12 Inhibition

Different molecules within the CXCL12/CXCR4 signaling cascade were targeted following the same procedure. ADSCs were incubated with the respective treatment for 1 hr prior in media at RT with agitation. Cells were then centrifuged at 800RPM for 8 minutes and resuspended in fresh media. ADSCs were seeded on top of the hydrogels at a concentration of 25,000 cells/gel. Concentrations for the targeted molecules can be found in Table 3.1. Gels were released and allowed to incubate at 37°C for their respective times.

3.35 Immunohistochemistry

For fluorescence imaging, hydrogels were fixed with 2% paraformaldehyde (PFA) (pH 7.2) for 20 minutes at room temperature (RT) and rinsed with 1X phosphate buffered saline (PBS) (Thermo Fisher Scientific, Waltham, MA, USA) 3 x 5 minutes. Permeabilization occurred using 0.1% Triton X-100/ 0.01M glycine/ 1X PBS for 30 minutes at RT then washed in 1X PBS. Blocking occurred in 5% BSA/1X PBS for 30 minutes at RT before another PBS wash cycle. If no primary antibody was used then DAPI (Molecular Probes, Eugene, OR, USA), diluted 1:1000 in 1X PBS, and phalloidin conjugated to Alexa Fluor 488 (Invitrogen), diluted 1:250 in PBS, were applied for 1 hr at RT. Gels received one final PBS wash and were mounted with DABCO. Images were collected on the Invitrogen EVOS FL Auto Imaging System (Fisher Scientific) and the Zeiss LSM 510 scanning confocal microscope (Zeiss Microscopy, Jena, Germany).

If a primary antibody was used, either goat polyclonal to CXCR4 or rabbit polyclonal to SDF-1 (Abcam, Cambridge, UK) diluted 1:200 in 1X PBS was applied overnight at 4^{o}C. Another PBS wash cycle preceded application of secondary antibody (diluted 1:250 in 1X PBS). Alexa Fluor 546 rabbit anti-goat (CXCR4) or Alexa Fluor 546 goat anti-rabbit (SDF-1) (Invitrogen, Carlsbad, CA, USA) were applied for 1 hour at 37^{o}C and washed with PBS. Finally, the application of DAPI and phalloidin conjugated to Alexa Fluor 488 were applied as stated before.

3.36 Protein Extraction

A mixture of 1ml Tissue Protein Extraction Reagent (T-PER, ThermoFisher Scientific) and 10 µL Halt protease inhibitor cocktail (ThermoFisher Scientific) was

created. 200 µL of this mixture was added to the protein sample in a 1.5ml tube. The sample was incubated at RT for 5 minutes then homogenized with a sterile pestle. Once homogenized, the sample was spun at 10,000g for 5 minutes. The supernatant was collected in a new tube.

3.371 Protein Quantification

The Pierce BCA Protein Assay Kit (ThermoFisher Scientific) was used to quantify the protein concentration. A standard curve was made by diluting BSA in the lysis buffer as in Table 3.2. Working reagent was created by combining 50parts of BCA reagent A with 1 part BCA reagent B. 200 µL of this working reagent was in each well of a 96-well plate. 25 µL of each standard and unknown sample was pipetted into their respective wells and immediately mixed with the working reagent by swirling with a pipette tip. Toroid samples were performed in triplicate while standards and blanks were performed in duplicates. The well plate was covered and incubated at 37^{o}C for 30 min. Absorbance was measured at 595nm on the BioRad iMark Microplate Absorbance Reader. Four-parameter (quadratic) was used to analyze the standard curve.

3.37 Denaturing SDS-PAGE

Protein and standards were thawed on ice. Fresh loading buffer was made with 950 µL of Laemmli buffer (Bio-Rad, Hercules, CA, USA) and 50 µL of beta-mercaptoethanol (BME). 30µg/ml was used as the protein concentration. 15µL of both the sample and loading buffer were mixed in a tube and heated to 70^{o}C for 10 min. A BioRad TGX 12+2 gel (Cat # 567-1083) was placed inside the tank filled with 1X running buffer (BioRad Cat # 161-0732). The comb was removed from the

gel and the wells were flushed with running buffer. Once the standards and samples were added, SDS-PAGE was run at 200V for 40-45 min until the bands were separated. The gel was then stained in Commassie blue and rinsed in de-stain. Results were observed using the BioRad GelDoc XR+ System.

3.38 Western/Immunoblotting

Once SDS-PAGE was carried out under denaturing conditions, the gel "sandwich" was assembled in the following order: sponge-filter paper-gel-membrane-filter paper-sponge. Proteins were transferred from the gel to the membrane at 80V for 45 min using 4^{o}C Tris/glycine buffer supplemented with 20% methanol as the transfer buffer. After transfer, the membrane was rinsed with PBS for 3 min. It was then blocked in 5% milk/PBS for 1 hr at RT with gentle agitation. The membrane was rinsed with PBS-T 6 x 5 min. Primary antibody was added overnight at 4^{o}C with gentle agitation (Table 3.3) and the membrane rinsed in PBS-T as before. Secondary antibody (IRDye 800 CW goat anti-rabbit; Li-Cor, Lincoln, NE, USA) was added for 1 hour at RT before another PBS-T rinse. The final membrane rinse was with PBS 2 x 10 min. Membranes were imaged on the LiCor Odyssey CLX System.

3.39 Statistical Analysis

Toroid circumference was measured using the Invitrogen EVOS FL Auto Imaging System where N=6. A 2-tailed, type-3 T-test was utilized in Microsoft Excel to determine significance at P=0.05.

3.4 Results

3.41 CXCL12-CXCR4 Expression in Toroid Formation.

To determine the molecular regulation of toroid formation a targeted gene array was performed using ADSC RNA extracted toroid forming and non-forming gels. CXCL12-CXCR4 was the only pathway that was upregulated in toroids but was downregulated when ADSCs were mixed into the hydrogel. In fact, there was a 2.49-fold increase in CXCL12 expression when cells were forming a toroid versus when they were not.

To validate this finding, toroid and mixed-in-gel cultures were stained with antibodies to CXCL12. Abundant staining of CXCL12 was observed in the toroid cultures but was virtually absent in the cells in mixed-in-gel cultures (Figure 3.1) To determine the onset of CXCL12 expression during toroid formation, ADSC gels were cultured, fixed, and stained. Figure 3.2 shows the time course of toroid formation by ADSCs. There was little to no CXCL12 expression in the first 3 hours of culture (Figure 3.2 A-B). However, by 4 hrs of formation, CXCL12 expression is apparent, becoming stronger by 6 hrs of culture (Figure 3.2 C-D).

3.42 Real Time PCR analysis of CXCL12 and CXCR4

The identification of CXCL12 in toroid formation was confirmed using real-time PCR (RT-PCR) which showed an upregulation in *Cxcl12* transcript in ADSC toroids compared to mixed in and 2D cultures which do not support toroid formation (Figure 3.3). We observed that CXCL12 and CXCR4 were differentially expressed in 2D planar cultures at 70% and 90% confluence and in toroids and spheroid cultures. When using RT-PCR, CXCL12 transcript level compared between

standard 2D 70% cell confluence, showed a minimal fold increase when compared to 2D 90% confluency (1.6), mixed in gels (1.2), and toroids (1.3) while there was a decrease of 2.6 in spheroids (Figure 3.3A). We saw a decrease of 1.1 and 3.3-fold respectively when CXCL12 levels from mixed in gels and spheroids were compared to toroids (Figure 3.3c). We next looked at the changes in transcript levels for the main cognate CXCL12 receptor CXCR4 (Figure 3.3 b and d). We found a dramatic increase in fold change in mixed in gels (128.2) and toroid (41.8) when compared to 2D 70% confluency. Similarly, we observed a 3.1 fold increase (mixed in) and -33.3 decrease (spheroids) when compared to toroids. Furthermore, *Cxcr4* transcripts show a significant increase in level compared to planar culture but significantly less than the level in mixed in gels (Figure 3.3). This suggests that the presence of CXCL12 is crucial to toroid formation. However, CXCR4 showed sparse staining during toroid formation (Figure 3.1). Interestingly, *Cxcl12*/*Cxcr4* transcripts were significantly reduced in a 3D spheroid culture system suggesting that our toroid model system is a unique 3D system.

3.43 Dissecting the Signaling Pathway

Our preliminary studies focused on the downregulation of the entire pathway through the inhibition of the CXCL12 cognate receptors, CXCR4 and CXCR7. Figure 3.4 shows standard toroid formation after 24 hrs, suggesting a more specific regulatory method within the pathway. To delve deeper into the pathway, we targeted each major molecule with the inhibitors listed in Table 3.1.

We targeted downstream molecules that are integral parts of cellular motility and adhesion such as the integrin receptors, focal adhesion kinase (FAK), Akt,

Rho/Cdc42, and p160 ROCK. However, we found that not even one of these delayed or prevented cellular migration or toroid formation. *For risk of redundancy, we did not include images of every inhibitor as they all formed toroids*. Figure 3.5 A and B shows the outer edge of the toroid created by cells inhibited against Akt and FAK. Likewise, we see ample CXCL12 expression (red). Figure 3.5C includes all inhibitors which appear to follow the change in circumference observed in the uninhibited toroid. Data was insignificant at P=0.05.

We then moved on to the remaining four targets including PI3K, N-Cadherin, Ras/Raf, and ERK1/2. While PI3K and N-Cadherin are also important in the adhesion and migration of cells, all four of these are key regulators of signal transduction from the ECM to the cell (Guo et al, 2016; Tilton et al, 2000; Wojcechowsky et al, 2011). When these were inhibited, we observed a change in ADSC behavior. Within 24 hrs, PI3K showed a significant ~16 hr delayed migration (Figure 3.6A) while N-Cadherin, Ras/Raf, and ERK 1/2 showed little to no migration (Figure 3.6 B-D).

To understand the extent of the inhibition observed in Figure 3.6, we examined the migration inhibiting molecules over 72 hrs. In Figure 3.6E, we graphed the circumference of the outer migration wall over 72 hrs. What we observed was that, at T=24h, PI3K, Ras/Raf, N-Cadherin, and ERK1/2 inhibited cells only migrated to 21.1%, 14.4%, 8.2%, and 3.2% of their initial distribution throughout the well, respectively. To give a comparison, the uninhibited toroid shows an average migration of 80.2% from T=0 to T=24 hrs. However, once the ADSCs move past T=24 hrs and on to T=72 hrs, PI3K, Ras/Raf, and ERK1/2

inhibited cells have all migrated to 75.8%, 62.2%, and 56.7%, respectively. Interestingly, N-Cadherin inhibition appeared to be most effective as inhibited ADSCs only migrated to 12.8% between T=0 and T=72 hrs. Significance was determined for N-Cadherin, PI3K, ERK1/2, and Ras/Raf at P=0.05 when compared to an uninhibited toroid. At T=24 hrs, we calculated $3.02e^{-10}$, $3.51e^{-9}$, $1.34e^{-9}$, and $4.49e^{-9}$, respectively. At T=48 hrs, we calculated $7.09e^{-7}$, $5.37e^{-5}$, $1.49e^{-8}$, and $3.16e^{-7}$, respectively. At T=72 hrs, we calculated $3.08e^{-10}$, 0.13, $2.23e^{-7}$, and $2.44e^{-6}$, respectively.

3.44 Co-cultured ADSCs with 4T1s

Our model of toroid formation represents a recapitulation of how cells interact with a changing microenvironment. While we have previously shown that different cells can be co-cultured on the same hydrogel (Worden et al, 2022), we next sought to investigate the reaction of ADSCs with a diseased cell line that does not typically form toroids (4T1 breast cancer cell line). Likewise, how would CXCL12 expression change during this interaction. When ADSCs and 4T1s, stained with Vybrant DiO (green) and DiD (red) respectively, were combined on a PureCol hydrogel there was significant cellular intermingling (Figure 3.7 A-B). In addition to this, a co-cultured toroid was observed (Figure 3.7A). We chose this kit for two reasons: 1) it can be added directly to culture media to uniformly label suspended cells, and 2) the subcellular localization of these stains labels the cell membrane and lipids; thus, the entire cell is fluorescent for our toroid studies. Just as in previous results, we were able to see clear cellular demarcation with no overlapping signals. Figure 3.7C shows a cluster of co-cultured cells stained for

CXCL12 expression (white). Interestingly, we observed the majority of the expression located in 4T1 cells during the migratory process.

3.5 Discussion

The universality of toroid formation was striking. We have tested 12 different cell types which all form toroids under the proper conditions. This led us to do two things, first was the targeted gene approach of toroids vs non toroid gels and the other was looking at various cancer cell lines to determine if they also formed toroids. To begin to tease out the molecular basis for toroid formation, a targeted multiplex gene expression analysis was performed on toroid formation. It was found that the CXCL12-CXCR4 pathway was upregulated during toroid formation, but downregulated when cells were mixed into the hydrogel. In fact, there was a 2.49-fold increase of CXCL12 expression in toroid forming cells. The CXCL12/CXCR4 pathway (Figure 1.4) is crucial for numerous developmental processes such as blood vessel and heart development (Li et al, 2009; Greenbaum et al, 2013; Ji et al, 2004). Furthermore, this axis is also key for the regulation of many cancers including from breast, lung and prostate and has been found to be involved in tumor cell growth, survival, and metastasis (Cojoc et al, 2013, Teicher and Fricker, 2010). What we found was striking in that no cancer cell line tested formed toroids. We found that, when ADSCs were labeled with antibodies against CXCL12 and CXCR4, expression was observed in toroids while not in mixed in gels. We observed at the 6-hour time point, an upregulation of CXCL12 expression suggesting that this pathway is activated in the early stages of cellular migration and toroid formation. Similarly, we found CXCL12 transcripts are more abundant

in toroid gels vs non toroid gels but interestingly, CXCR4 transcripts are upregulated in mixed in gels vs toroids. However, it is not known why there is a large fold change in mixed in (128.2) compared to toroids (41.8) when compared to standard 2D culture.

When inhibiting the pathway, we found that targeting the cognate receptors individually did not hinder toroid development thus suggesting a more specific means of regulation from one or more of its downstream signaling molecules. While a number of these target molecules produces little to no inhibition, we did uncover four candidates for short to long-term inhibition of migration (Figure 3.8). PI3K offered a delayed migration of ~16 hrs, but the treatment quickly vanished allowing for an uninhibited migration after that point. Ras/Raf and ERK1/2 treatments lasted ~10 hrs longer than PI3K, but in the end still wore away and allowed for cellular migration. Lastly, treatment with N-Cadherin, a key regulator for myofibril anchorage and cell-cell contact, appeared to affect the cells in a long-term capacity. Not only was there little movement of cells at 24 hrs, but this was also consistent over 72 hrs as well with only a 12% migration. We also found that at T=24 and 48 hrs, all four inhibitors were significant at P=0.05 when compared to an uninhibited toroid. At T=72 hrs, only PI3K was not significant. This could suggest that toroid formation is less about migration regulation and more about the chemotactic signaling occurring between cells that causes them to make decisions.

Regenerative medicine has been focused on utilizing stem cells by injecting them into diseased or damaged tissues. The model we created has proven

successful in the investigation of co-cultured cells. We sought to further our understanding by observing ADSCs co-cultured with a diseased cell type (4T1 breast cancer cells). From previous results, we knew that 4T1s failed to create toroids when cultured under toroid forming conditions. With this knowledge in hand, we believed one of two outcomes would occur. First, the ADSCs would be unchanged and would create a toroid, leaving the 4T1s spread throughout the well. Second, the 4T1s would signal ADSC differentiation causing them to have no migration. The results from this study provided an unforeseen outcome (Figure 3.7). When co-cultured on the same hydrogel, ADSCs and 4T1s mix and migrate to form a toroid consisting of both cell types. We then sought to observe CXCL12 expression which appeared primarily in the regions surrounding the 4T1 cells and not the ADSCs (Figure 3.7 C). While we know that the CXCL12 pathway also regulates the pathogenesis of cancer, it was very interesting that little to no pathway expression was observed in the ADSCs.

We are currently performing western blot and densitometric analysis on our 72 hr experiment using the N-Cadherin, PI3K, Ras/Raf, and ERK1/2 treatments. This analysis will allow us to understand the extent of inhibition and the different levels of expression over the 72 hr period. Likewise, we are also performing western blot analysis on toroids from hours 1-6 to better investigate when CXCL12 is upregulated during the migratory process.

Future studies are focused on pursuing more gene assays to understand the full molecular regulation in toroid formation as well as the communication mechanisms utilized between cells. We will also focus heavily on the unforeseen

results from the co-cultured ADSCs and 4T1s. The CXCL12-CXCR4 pathway will be studied when these cells are co-cultured. Using this model of cellular interactions and programming, we can examine and explore (1) the understanding of early embryonic development, (2) the optimization of hydrogels for *in vivo* applications and (3) the creation of a model system for future tissue formation and regeneration and disease.

3.6 Conclusion

To summarize, we have advanced our understanding of the novel model we created which simulates cellular processes observed during development and disease. Using a gene targeted approach, we identified a single pathway that was upregulated during toroid formation and downregulated when cells were mixed into the hydrogel. After our initial studies of silencing the CXCL12 cognate receptors key to driving the signaling cascade, we dissected the pathway into its key elements, finding four targets that changed ADSC behavior. While PI3K, N-Cadherin, Ras/Raf, and ERK ½ all appeared effective at delaying migration for 24 hrs, N-Cadherin inhibited ADSCs withstood migration for up to 72 hrs. Finally, we have shown a surprising result when 4T1 cancer cells defied our previous understanding and formed a co-cultured toroid with ADSCs. This 3D system will continue to provide a tunable and reproducible model for the investigation of cellular interactions and the molecular mechanisms that drive their innate behaviors.

3.7 References

Ara T, Nakamura Y, Egawa T, Sugiyama T, Abe K, Kishimoto T, Matsui Y, Nagasawa T. (2003). Impaired colonization of the gonads by primordial germ cells in mice lacking a chemokine, stromal cell-derived factor-1 (SDF-1). Proceedings of the National Academy of Sciences. 100(9):5319-23.

Badylak SF, Freytes DO, Gilbert TW. Extracellular matrix as a biological scaffold material: structure and function. Acta biomaterialia. 2009 Jan 1;5(1):1-3.

Bleul CC, Fuhlbrigge RC, Casasnovas JM, Aiuti A, Springer TA. (1996). A highly efficacious lymphocyte chemoattractant, stromal cell-derived factor 1 (SDF-1). The Journal of Experimental Medicine. 184(3):1101–9.

Cojoc M, Peitzsch C, Trautmann F, Polishchuk L, Telegeev GD, Dubrovska A. (2013). Emerging targets in cancer management: role of the CXCL12/CXCR4 axis. OncoTargets and therapy. 6:1347.

de Castro Brás LE, Proffitt JL, Bloor S, Sibbons PD. (2010). Effect of crosslinking on the performance of a collagen-derived biomaterial as an implant for soft tissue repair: A rodent model. Journal of Biomedical Materials Research Part B: Applied Biomaterials. 95(2):239-49.

Engler AJ, Sen S, Sweeney HL, Discher DE. Matrix elasticity directs stem cell lineage specification. Cell. 2006 Aug 25;126(4):677-89.

Gourdie, R. G., Myers, T. A., McFadden, A., Li, Y.X., & Potts, J. D. (2012). Self-organizing tissue-engineered constructs in collagen hydrogel. *Microsc Microanal*. **18**(1), 99-106.

Greenbaum A, Hsu YM, Day RB, Schuettpelz LG, Christopher MJ, Borgerding JN, Nagasawa T, Link DC. CXCL12 in early mesenchymal progenitors is required for haematopoietic stem-cell maintenance. Nature. 2013 Mar;495(7440):227-30.

Hassan WU, Greiser U, Wang W. (2014). Role of adipose-derived stem cells in wound healing. *Wound Repair Regen.* 22:313-325.

Hunt NC, Grover LM. Cell encapsulation using biopolymer gels for regenerative medicine. Biotechnology letters. 2010 Jun 1;32(6):733-42.

Ji JF, He BP, Dheen ST, Tay SSW. (2004). Interactions of chemokines and chemokine receptors mediate the migration of mesenchymal stem cells to the impaired site in the brain after hypoglossal nerve injury. Stem Cells. 22:415.

Li F, Guo WY, Li WJ, Zhang DX, Lv AL, Luan RH, Liu B, Wang HC. Cyclic stretch upregulates SDF-1α/CXCR4 axis in human saphenous vein smooth muscle cells. Biochemical and biophysical research communications. 2009 Aug 14;386(1):247-51.

Li L, He Y, Zhao M, Jiang J. (2013). Collective cell migration: implications for wound healing and cancer invasion. Burns Trauma. 1:21–6

Macleod TM, Williams G, Sanders R, Green CJ. Histological evaluation of Permacol™ as a subcutaneous implant over a 20-week period in the rat model. British journal of plastic surgery. 2005 Jun 1;58(4):518-32.

Othmani AE, Rouam S, Abbad A, Erraoui C, Harriba S, Boukind H, et al. Cryopreservation Impacts Cell Functionality of Long Term Expanded Adipose-Derived Stem Cells. J Stem Cell Res Ther. 2019;09(01)

Pedraza CE, Marelli B, Chicatun F, McKee MD, Nazhat SN. An In Vitro assessment of a cell-containing collagenous extracellular matrix–like scaffold for bone tissue engineering. Tissue engineering Part A. 2010 Mar 1;16(3):781-93.

Provenzano PP. Tug of War at the Cell-Matrix Interface. Biophysical journal. 2017 May 9;112(9):1739-41.

Sinha R, Verdonschot N, Koopman B, Rouwkema J. Tuning Cell and Tissue Development by Combining Multiple Mechanical Signals. (2017). Tissue Eng Part B Rev. 23(5):494-504.

Tamamura H, Xu Y, Hattori T, Zhang X, Arakaki R, Kanbara K, Omagari A, Otaka A, Ibuka T, Yamamoto N, Nakashima H. A low-molecular-weight inhibitor against the chemokine receptor CXCR4: a strong anti-HIV peptide T140. Biochemical and biophysical research communications. 1998 Dec 30;253(3):877-82.

Teicher BA, Fricker SP. CXCL12 (SDF-1)/CXCR4 pathway in cancer. Clinical cancer research. 2010 Jun 1;16(11):2927-31.

Trappmann B, Chen CS. How cells sense extracellular matrix stiffness: a material's perspective. Current opinion in biotechnology. 2013 Oct 1;24(5):948-53.

Vermette M, Trottier V, Ménard V, Saint-Pierre L, Roy A, Fradette J. Production of a new tissue-engineered adipose substitute from human adipose-derived stromal cells. Biomaterials. 2007;28(18):2850–60.

Wang X, Cao Y, Zhang S, Chen Z, Fan L, Shen X, Zhou S, Chen D. (2017). Stem cell autocrine CXCL12/CXCR4 stimulates invasion and metastasis of esophageal cancer. Oncotarget. 8(22): 36149-36160.

Wang X, Jiang B, Sun H, Zheng D, Zhang Z, Yan L, Li E, Wu Y, Xu R. (2019). Noninvasive application of mesenchymal stem cell spheres derived from hESC accelerates wound healing in a CXCL12-CXCR4 axis-dependent manner. Theranostics. 9(21): 6112-6128.

Worden A, Uline MJ, Shazley T, Stern M, Potts JD. (2022). Self-Assembling Toroidal Cell Constructs for Tissue Engineering Applications. *Microscopy & Microanalysis*.

Xing F, Li L, Zhou C, Long C, Wu L, Lei H, Kong Q, Fan Y, Xiang Z, Zhang X. Regulation and directing stem cell fate by tissue engineering functional microenvironments: scaffold physical and chemical cues. Stem Cells International. 2019 Dec 27;2019.

Xu, Ruodan & Besenbacher, Flemming & Chen, Menglin. (2017). The 3D mechanical environment and chemical milieu influence the hMSC fibrogenesis and fibroblast-to-myofibroblast transition. RSC Adv.. 7. 20-25. 10.1039/C6RA25422E.

Table 3.1: List of CXCL12-CXCR4/7 targets for inhibition.

Target	Name	Concentration	Company
Cdc42/Rac1	ML141	50uM	Tocris
P160 ROCK	Y-27632	50uM	Tocris
Ras/Rac	SCH 51344	500nM	Sigma Aldrich
ERK 1 and 2	CAS 1049738-54-6	500nM	Sigma Aldrich
PI3K	LY294002	50uM	Fisher Scientific
AKT	GSK690693	5nM	Fisher Scientific
N-Cadherin	ADH-1	0.2 mg/mL	Fisher Scientific
FAK	GSK2256098	10uM	Fisher Scientific
CXCR4 (antagonist)	AMD3100	50nM	ChemCruz
CXCR4 (agonist)	NUCC-390	10nM	MedChemExpress
CXCR7 (agonist)	TC14012	350nM	Tocris
CXCR7 (agonist)	VUF11207	50nM	Tocris
Integrin α2β1	TC-I 15	500nM	Tocris
Integrin α2β1	BTT 3033	130nM	Tocris

Table 3.2: Standard curve for protein quantification.

Vial	Volume of Diluent, ul (T-PER)	Volume of Protein Stock 2mg/ml	Final BSA concentration ug/ml
A	0	300 of stock	200
B	125	375 of stock	1500
C	325	325 of stock	100
D	175	175 of vial B	750
E	325	325 of vial C	500
F	325	325 of vial E	250
G	325	325 of vial F	125
H	400	100 of vial G	25
I	400	0	0

Table 3.3: List of primary antibodies for western blot analysis.

Target	Name	Company
CXCL	Rabbit Polyclonal to SDF-1	Abcam
Ras/Raf	Phospho-A-Raf	Fisher Scientific
PI3K	Phospho-PI3K	Fisher Scientific
ERK ½	Phospho-ERK1/ERK2	Fisher Scientific
N-Cadherin	N-Cadherin Clone 3B9	Fisher Scientific

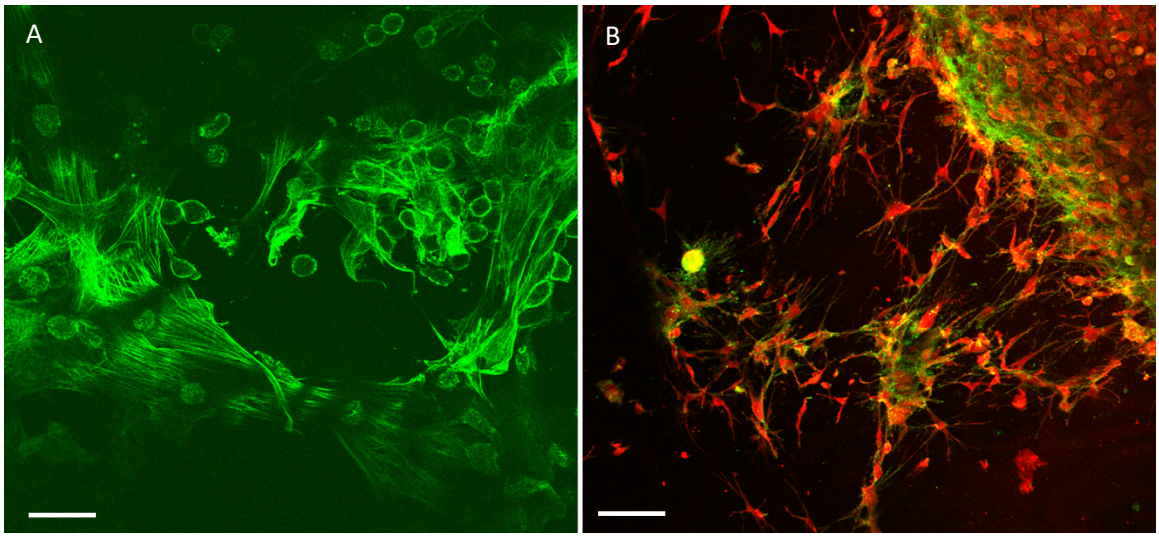

Figure 3.1. CXCL12 presence in toroids. ADSCs mixed in and placed on top of PureCol collagen I hydrogels, labeled with CXCL12 antibody (red), counterstained with phalloidin conjugated to Alexa Fluor 488 (green) and imaged with the Zeiss LSM 510. A) No CXCL12 seen when cells are mixed into a hydrogel. B) CXCL12 activity when cells form a toroid. Scale bars= 100 μm.

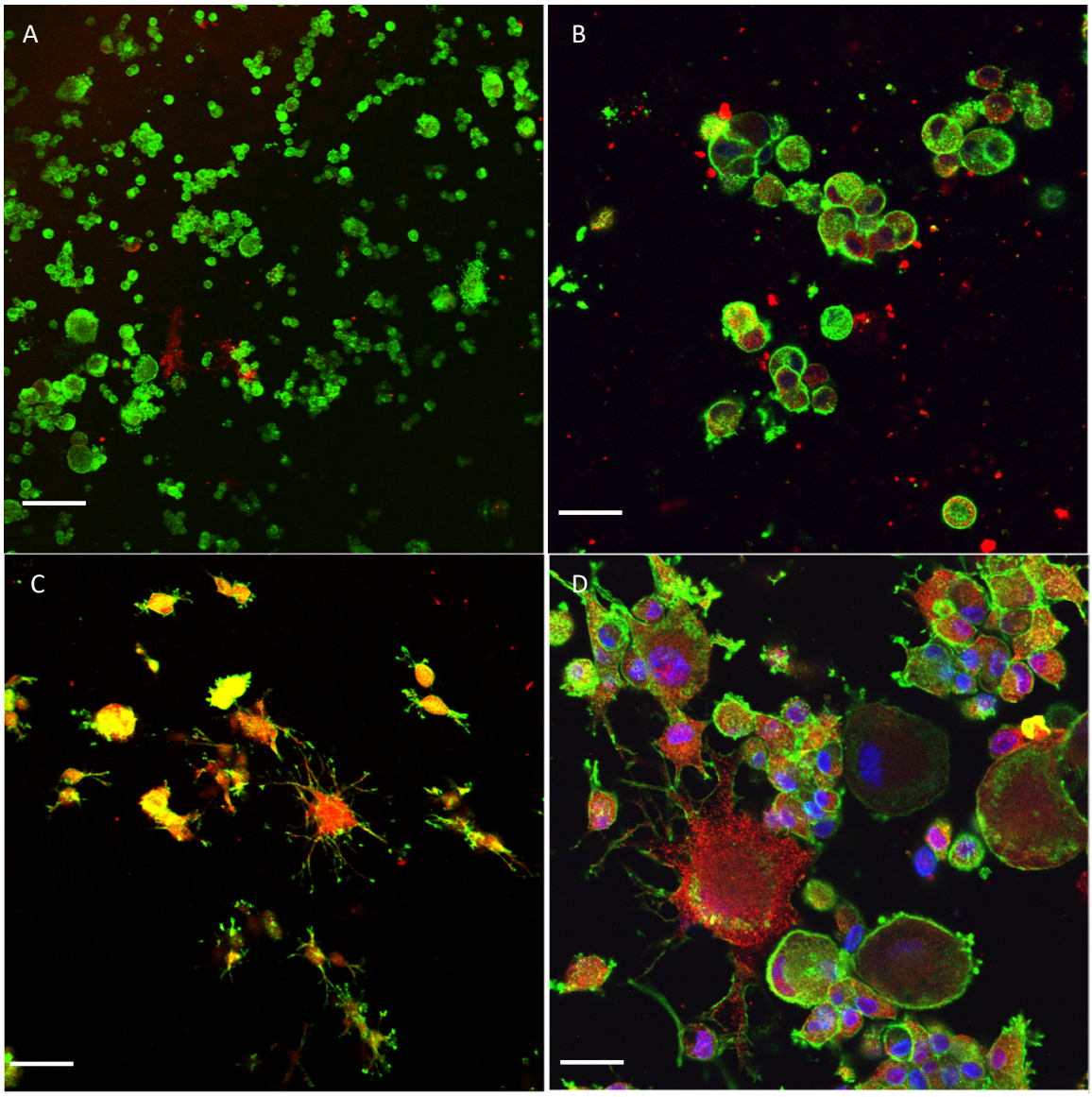

Figure 3.2. Early-stage toroid forming ADSCs stained with CXCL12. Toroid formation at 2 and 3 hrs show little CXCL12 staining (A, B). Considerable expression is seen at 4 and 6 hrs (C, D) as cells begin to open from their "balled-up" state to begin migration. Scale bars= 100 μm, Red= CXCL12, Green= phalloidin, Blue= DAPI.

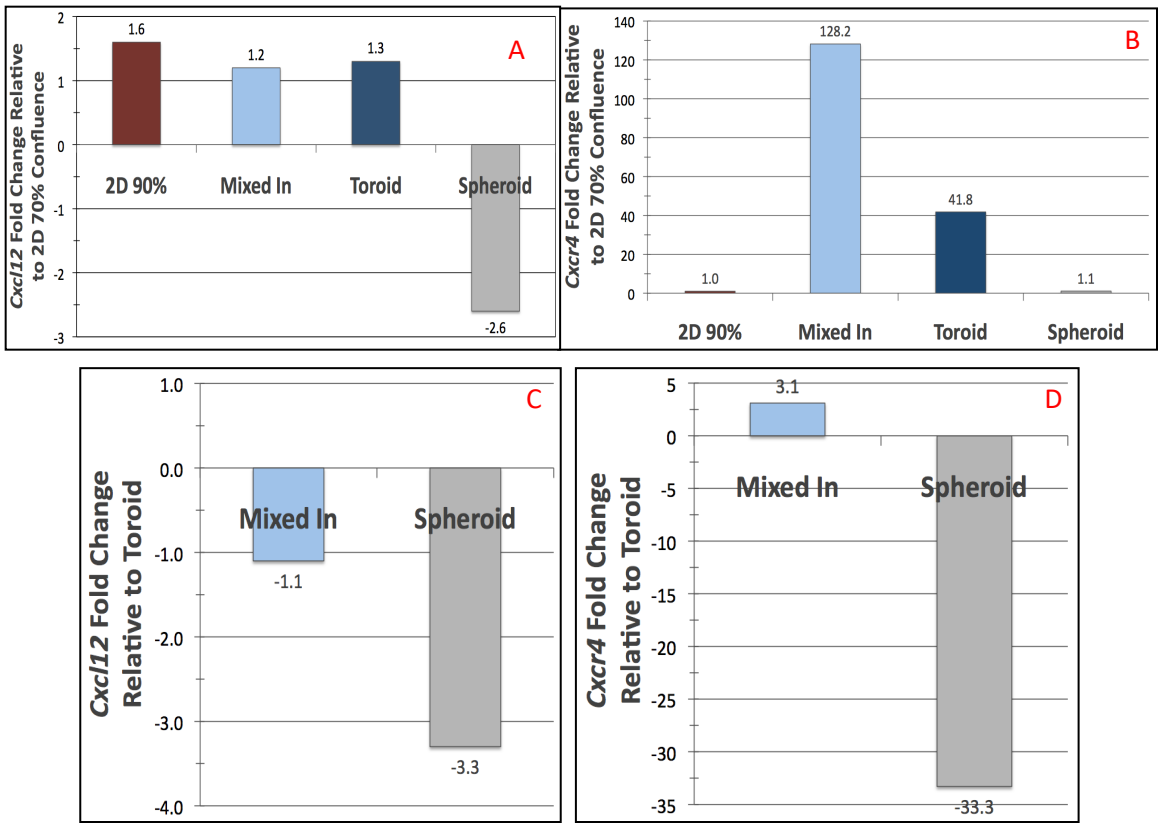

Figure 3.3. CXCL12 and CXCR4 are differentially expressed in 2D and 3D culture platforms. RNA was extracted from either 70 or 90% confluency 2D cultures, mixed in hydrogels, toroids, or spheroids. We see a slight differentiation in CXCL12 between the different cultures (a and c). Interestingly, we see a major differentiation in CXCR4 in mixed in gels (128.2 fold change) and in toroids (41.8) (b). We are unsure as to the reason behind the mixed in differentiation since we previously showed no activity in mixed in gels, however, one explanation for the jump in CXCR4 could be the higher chemokine reactivity in cellular interactions.

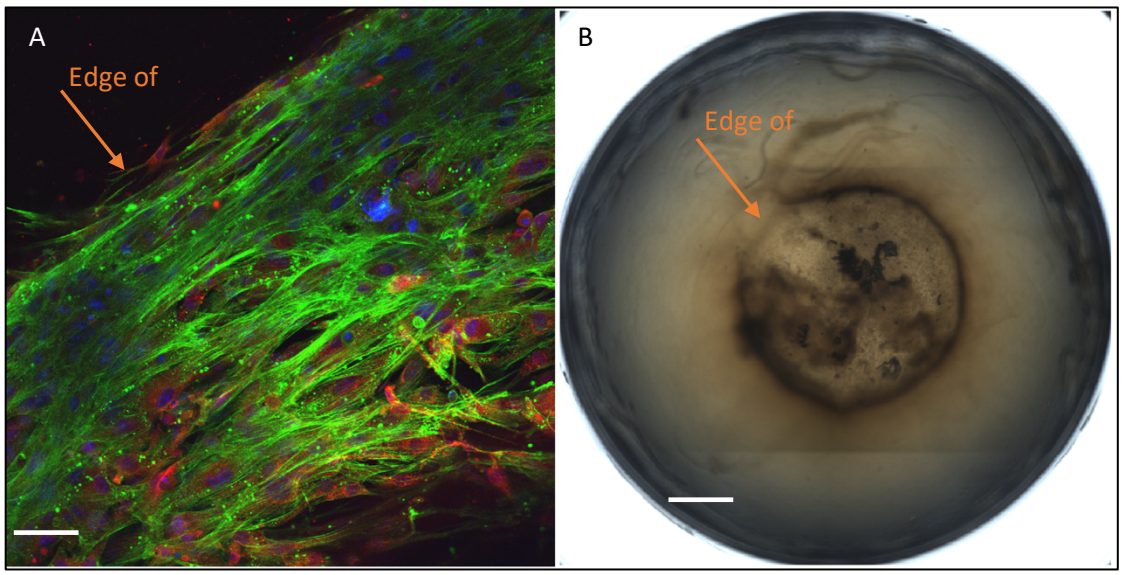

Figure 3.4. Inhibition of CXCL12 cognate receptors CXCR4 and CXCR7. Toroid formation was observed when inhibiting both CXCR4 and CXCR7, suggesting downstream molecules as the regulators of ADSC migration. A) Fluorescence imaging of the toroid ring. B) Brightfield imaging of the toroid scale. Scale bars= A) 100 μm B) 5 μm; Red= CXCL12 antibody, Green= phalloidin, Blue= DAPI

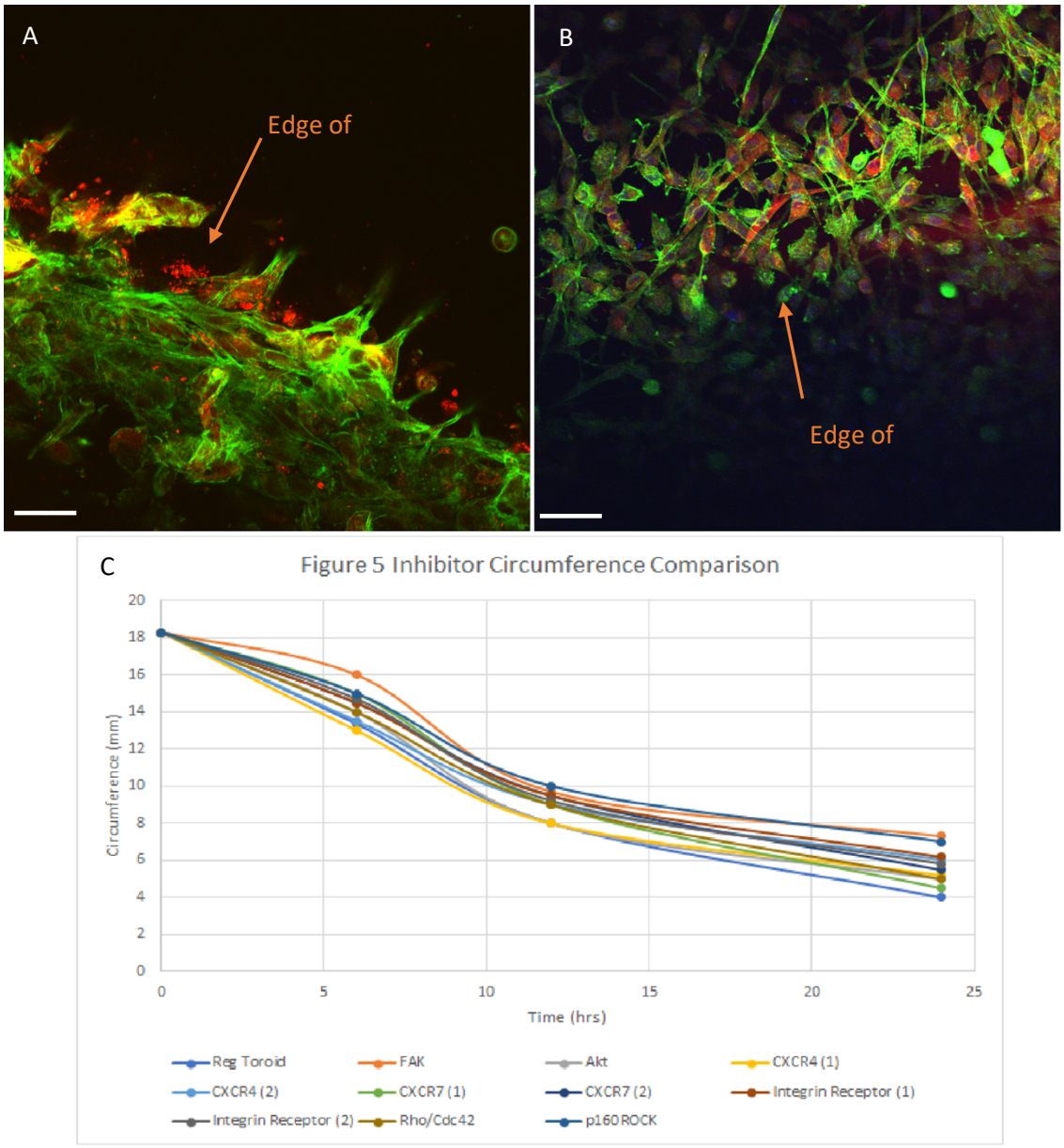

Figure 3.5. Dissecting the CXCL12-CXCR4 pathway. Toroid formation was still observed when inhibitors were used to block activity in ADSCs. A) Akt inhibited ADSCs. B) FAK inhibited cells. In each, we see ample CXCL12 expression (red). C) Scatter plot showing migration of the cells at T= 0, 6, 12, and 24 hrs. Uninhibited toroid shown for comparison. To note, only images of two inhibitors were shown for redundancy reasons. Scale bars= 100μm. Red= CXCL12 antibody, Green= phalloidin.

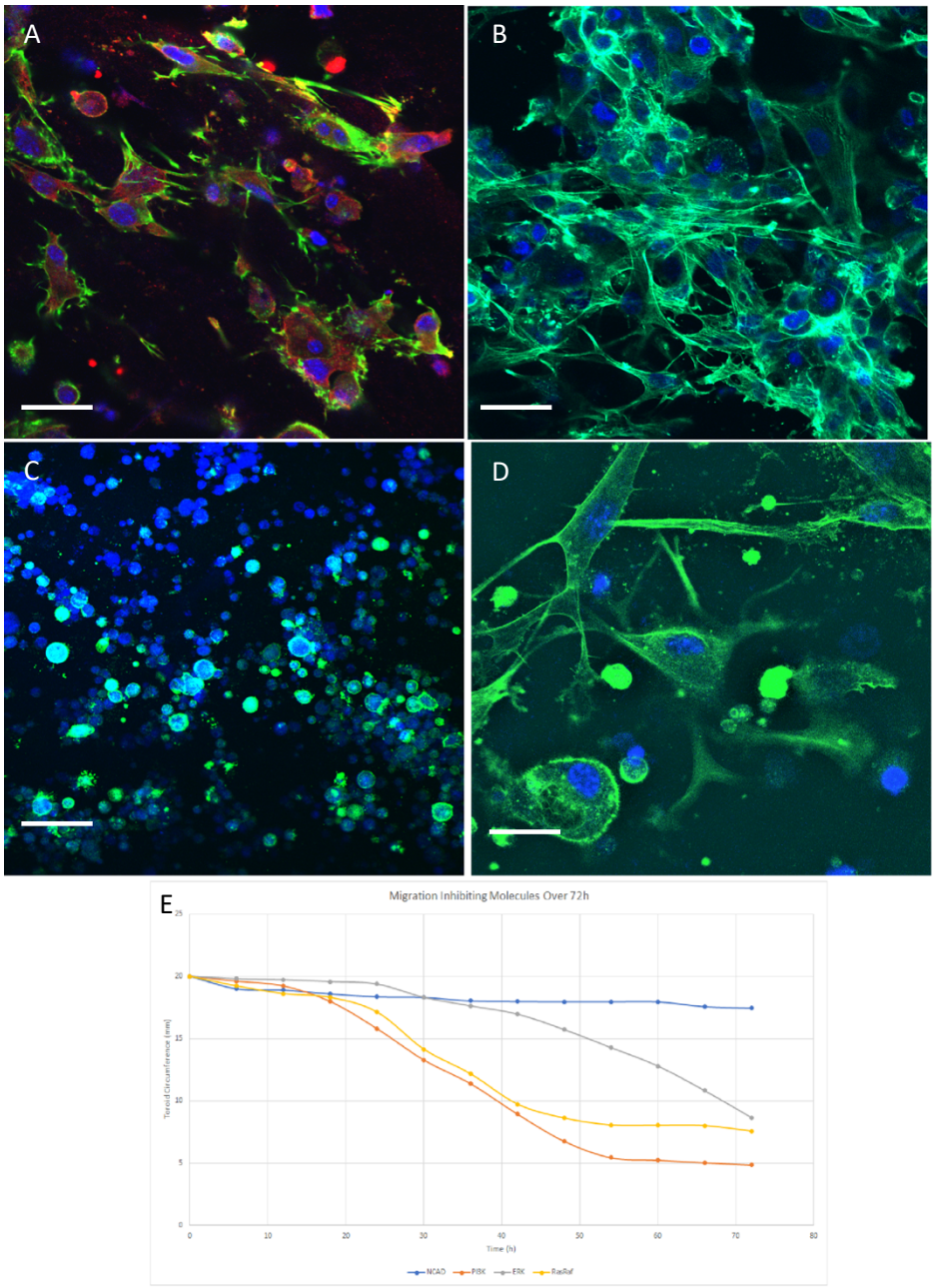

Figure 3.6. Inhibiting toroid formation. Inhibition of cellular migration at 24 hrs with A) PI3K, B) N-Cadherin, C) Ras/Raf, and D) ERK1/2. Notice the lack of CXCL12 expression (red) in non-migrating cells (B-D). PI3K inhibited ADSCs appeared to be delayed for ~16h before beginning their migration. These cells show CXCL12 expression. E) Scatter plot of these four inhibitors over 72 hrs. N-Cadherin inhibition appears to be most continuous during this period. Scale bars= 100μm. Red= CXCL12 antibody, Green= phalloidin, Blue= DAPI.

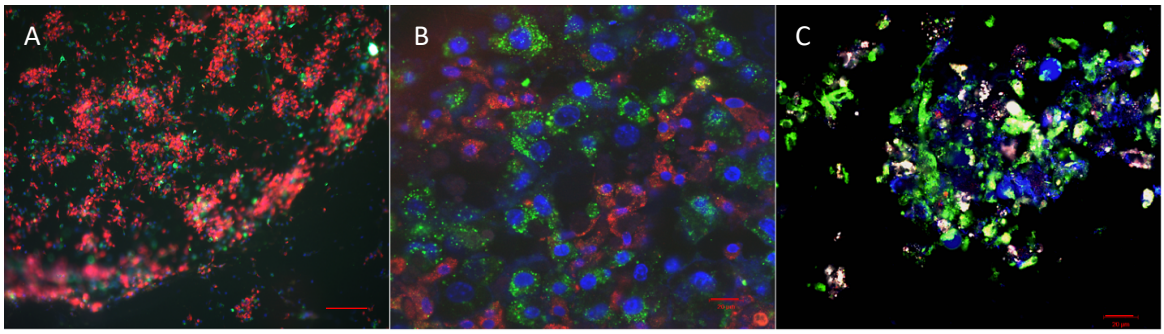

Figure 3.7 ADSCs co-cultured with 4T1 breast cancer cells. A) and B) show ADSCS (green) and 4T1 breast cancer cells (red) co-cultured on the same hydrogel. Cells appear to mix and migrate to form a toroid. C) A cluster of ADSC and 4T1 cells with CXCL12 expression (white). Interestingly, it appears that the majority of CXCL12 expression is fluorescent in the migrating 4T1 cells. Scale bars= 10μm (A) and 100μm. Red= 4T1 breast cancer cells, Green= ADSCs, Blue= DAPI, White= CXCL12 antibody.

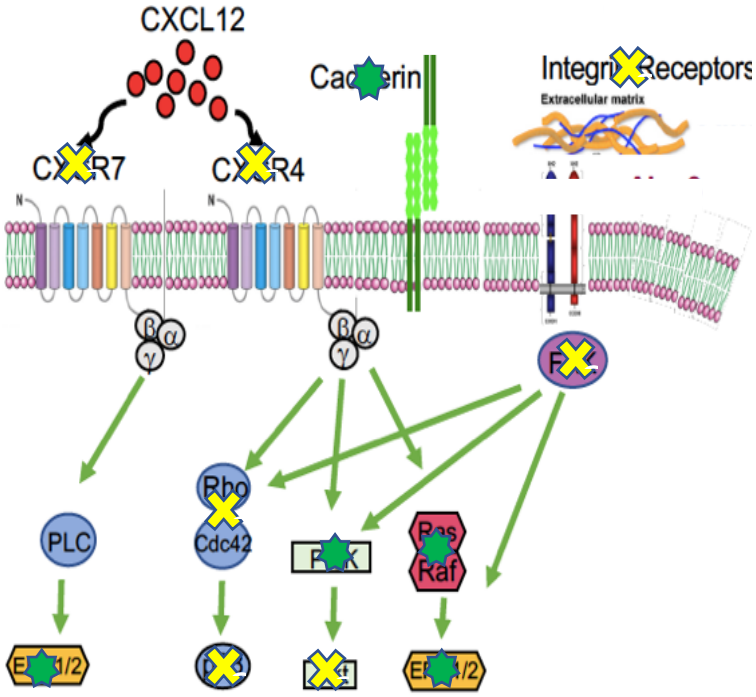

Figure 3.8. Dissected CXCL12-CXCR4 pathway. We have inhibited the key downstream molecules of the CXCL12-CXCR4 pathway. The X denotes inhibitors that did not hinder toroid formation. The star denotes inhibitors that delayed ADSC toroid formation.

CHAPTER 4

ADDITIONAL WORK

4.1 Background

The additional experiments that are presented in this section are either advancements of previous work (i.e. three-collagen hydrogels) or were investigated based on questions we received during talks based on previous results.

4.11 Three Collagen Hydrogels

We sought to further investigate the *in vivo*-like, tunable nature of the collagen hydrogel through the addition of collagen type II to our previous collagen concentration studies utilizing collagen types I and III. Collagen is the most widely used biopolymer, and in mammals, is the most abundant protein in major structural components for almost all organs and tissues thus providing a ubiquitous framework for cell attachment and growth (Badylak et al, 2009). Collagen types I (skin, tendons, and bones), II (cartilage), and III (reticulate) are the most prevalent, making up approximately 80-90% of the human body's total collagen (Karsdal et al, 2016). Based on our previous work in chapter 2, there was a physiological response to the changing concentrations of collagens I and III (Figure 2.5). This data also resulted in toroids being formed in 100% collagen I and III. However, when ADSCs were added on top of a collagen II hydrogel, no toroid was formed,

and the majority of cells did not survive suggesting an inhospitable environment. It was unknown what would occur when adding collagen II to the mixture of collagen I and III. This novel study could lead to a more accurate simulation of the environment through which cells are migrating during embryogenesis, would healing, etc.

4.12 Hydrogels with Cells Mixed-in and On-top

Preliminary studies proved that toroids are formed when cells are placed on top of the hydrogel, whereas mixing cells into a hydrogel only shows a contraction of the scaffold with no migration and no toroid formation (Figure 1.1). There is evidence that cellular migration begins with chemotactic signaling leading to remodeling of the surrounding matrix to form migratory channels. It is theorized that the spatial and planar differences observed, when cells are mixed into the hydrogel, could prevent cells from receiving and processing such signals (Bluel et al, 1996). Thus, if cells were cultured on top of a hydrogel as well as mixed in, would the additional signaling from the on top cells penetrate the hydrogel during its remodeling to change the behavior of the mixed-in cells.

4.13 CXCR4 Agonist Mixed-in into a Hydrogel

Many questions were received regarding the inactivity of the mixed-in cells. Previous work suggested that the CXLC12-CXCR4 pathway, the signaling cascade supposedly driving cellular migration, is downregulated when ADSCs are cultured inside of a hydrogel but upregulated while the cells are actively migrating to form a toroid (Figure 3.1). While it makes sense that there would be no evident pathway activity when cells are not migrating, would upregulating this pathway in

the microenvironment change the inactivity. We investigated this potential solution by 1) mixing a CXCR4 agonist into the hydrogel and 2) treating ADSCs with the agonist prior to placement in the hydrogel.

4.2 Methods

4.21 Three Collagen Hydrogel

We used three different hydrogel matrices including PureCol type I bovine collagen (Advanced Biomatrix), bovine collagen type II (Advanced Biomatrix), and human type III collagen (Advance Biomatrix). Collagen gels were created in 96 well culture dishes (Corning Incorporated, Corning, NY, USA) using an 8:1:1 ratio of collagen matrix, 0.2N HEPES pH 9.0 (Fisher Scientific, Hampton, NH, USA), and 10X Minimum Essential Medium (MEM, Sigma-Aldrich, St- Louis, MO, USA). The mixture was added 100 µL per well and stabilized at 37^{o}C overnight. Cells were placed on top of the gels and incubated at 37^{o}C for 30 minutes. Gels were released from the sides of the wells with a thin-tipped probe and incubated at 37^{o}C for an additional 24 hrs.

In our previous studies, PureCol collagen I and collagen III were proven successful at producing toroids both singularly and in a mixture. Collagen II, however, proved to be an inhospitable environment when cells were cultured on the hydrogel as no toroid was formed from lack of cellular sustainability. To generate the collagen mixtures, hydrogel mixtures followed the 8:1:1 ratio as stated before, however collagen types I, II, and III, were combined prior to the addition of HEPES and MEM. The attempted concentrations were a 1:1:1 (types I:II:III) and a 7:3:1 (I:III:II) ratio that would be characteristic of the dermis (McGrath,

2020; Sorushanova et al, 2017). ADSCs in media were placed on top of the gels, released, and incubated for 24 hrs at 37^{o}C. The resulting toroids were imaged with the Zeiss LSM 510 META confocal microscope and diameters measured on the Invitrogen EVOS FL Auto.

4.22 Hydrogels with Cells Mixed-in and On-top

Prior to seeding, ADSCs were trypsinized, centrifuged, and resuspended in fresh media. They were then stained with either the DiO (501nm) or DiD (665nm) stains from the Vybrant multicolor cell labeling kit (Thermo Fisher Scientific). 5 µL of the chosen dye was added directly to cells in media and mixed in by gentle pipetting. The suspension was incubated at 37^{o}C for 15 minutes before being centrifuged at 1500 rpm for 5 minutes. Supernatant was aspirated and cells were gently resuspended in fresh media. The centrifugation and aspiration steps were repeated 3 times before a 10-minute recovery period for the cells.

ADSCs (25k cells/gel) were mixed into the 8:1:1 PureCol hydrogel mixture. The hydrogel was then poured and stabilized in a 96-well plate prior to an additional 25k ADSCs placed on top of the hydrogel. The gel was then released and incubated as before. Gels were imaged on the EVOS FL Auto and the Zeiss LSM 510 META.

4.23 CXCR4 Agonist Mixed-in into a Hydrogel

The PureCol collagen I hydrogel and ADSCs were prepared as before. Prior to placement, the CXCR4 agonist, NUCC-290 (10 µM, MedChemExpress), was used to treat either the matrix or the cells. For the matrix, the agonist was mixed into the hydrogel prior to addition of the cells. For the cell treatment, the agonist

was added to ADSCs in media and incubated for 30 minutes, 2 hrs, and 24 hrs, per the MedChemExpress protocol. After treatment, ADSCs were centrifuged at 1500rpm for 5 minutes. The supernatant was removed, and cells were resuspended at 25,000 cells/gel in the matrix. The gels were incubated for 24h at 37^{o}C before they were fixed with 2% PFA, stained using immunohistochemistry, and imaged on the Zeiss LSM 510 META.

4.24 Immunohistochemistry

For fluorescent imaging, hydrogels were fixed with 2% paraformaldehyde (PFA) (pH 7.2) for 20 minutes at room temperature (RT) and rinsed with 1X phosphate buffered saline (PBS) (Thermo Fisher Scientific, Waltham, MA, USA) 3 x 5 minutes. Permeabilization occurred using 0.1% Triton X-100/ 0.01M glycine/ 1X PBS for 30 minutes at RT then washed in 1X PBS. Blocking occurred in 5% BSA/1X PBS for 30 minutes at RT before another PBS wash cycle. Primary antibody (rabbit polyclonal to SDF-1, Abcam, Cambridge, UK), diluted 1:200 in 1X PBS, was applied overnight at 4^{o}C. Another PBS wash cycle preceded application of secondary antibody (diluted 1:250 in 1X PBS). Alexa Fluor 546 rabbit anti-goat (CXCR4) or Alexa Fluor 546 goat anti-rabbit (SDF-1) (Invitrogen, Carlsbad, CA, USA) were applied for 1 hr at 37^{o}C and washed with PBS. Finally, DAPI (Molecular Probes, Eugene, OR, USA), diluted 1:1000 in 1X PBS, and phalloidin conjugated to Alexa Fluor 488 (Invitrogen), diluted 1:250 in PBS, were applied 1 hr at RT. Gels received one final PBS wash and were mounted with DABCO. Images were collected on the Invitrogen EVOS FL Auto Imaging System (Fisher Scientific) and the Zeiss LSM 510 META (Zeiss Microscopy, Jena, Germany).

4.3 Results

4.31 ADSC Response to a 3-Collagen Microenvironment

We observed an intriguing physiological response when ADSCs were cultured on top of the 3-collagen hydrogels. In Figure 4.1A, we observe ADSCs cultured on the 1:1:1 collagen hydrogel still in their balled-up form 24h after placement. There has been no migration and no toroid formation. In Figure 4.1 B, the 7:3:1 hydrogel, we observe the presence of a toroid with a novel physiological response from the ADSCs. It appears that the cells have formed clumps upon forming the toroid, giving the ring-like structure an almost broken characteristic (Figure 4.1B). When viewing the toroid at a higher magnification, we can clearly see that there are holes in the cellular network that we have not observed in other studies (Figure 4.1 C-D). We also measured the diameter of the toroids. On average (N=8), the diameter of the three-collagen toroid was 3.2mm. As a comparison, the average diameter of a PureCol collagen I toroid 2.7mm with the diameter decreasing with the addition of collagen III.

4.32 A Mixture of Mixed-in and On-top Hydrogels

We conducted an experiment where ADSCs were seeded inside and on top of a hydrogel to investigate whether the additional signaling and remodeling of toroid forming cells would induce a novel behavior for cells cultured inside the gel. We found in Figure 4.2 that, even though the ADSCs were remodeling the collagen, their chemical signals still did not change the behavior of the mixed in cells. The ADSCs placed on top of the hydrogel (red) have migrated to form a

toroid while the cells mixed in (green) have contracted the edge of the collagen hydrogel, but they are still spread throughout the gel.

4.33 CXCR4 Agonist Treatments

We sought to investigate the notion that upregulation of the CXCL12-CXCR4 pathway within the hydrogel microenvironment could enable cellular migration and potential toroid formation from mixed-in cells. We found that the CXCR4 agonist treatment did little to change the outcome. In Figure 4.3A, we see ADSCs that are in a CXCR4-treated hydrogel. In Figure 4.3B, we see a hydrogel with treated ADSCs. Interestingly, the cells have formed clumps which is less common in the untreated microenvironment. However. this was not a novel response for mixed-in cells. There is also no CXCL12 expression (red) observed in these gels. To note, the time of the cellular treatment made no difference to their migration (comparison data not shown).

4.4 Discussion

The goal of this additional work was to aid in our understanding of the ADSCs response to a changing microenvironment. We clearly observed a novel physiological response to the addition of collagen II to the mixed collagen hydrogels. While the cells still formed a toroid, the cells clumped together to form what looks like sheets (Figure 4.1 B-D). One potential explanation for this is that this is a more accurate form of migration that would be seen during embryonic development. It takes a lot of cells to form different appendages or organs which could exhibit cell clumps. On the other hand, it was evident that concentration plays a major factor in ADSC behavior as the cells remained balled-up when the collagen

types were of equal concentrations (Figure 4.1A). This could be a result of an inhospitable environment where the chemical signals are either not being produced by the cells or transduced throughout the matrix. We did observe, however, a larger toroid diameter on average compared to our previous work. With the wide tunability of hydrogels, this study brings us closer to being able to replicate the *in vivo* environment *ex vivo*, thus aiding in the usability as a model to study diseases in throughout the body.

We then wanted to understand how cells suspended on different planes in the hydrogel would react to new stimuli. First, we cultured ADSCs both in and on a collagen hydrogel. With the cells placed on top in a typically collagen-remodeling role, those that were embedded within the hydrogel remained unchanged and did not form toroids, suggesting a measure of the limitations of chemotactic signaling. There was a slight contraction of the outer gel, but the mixed-in cells remained spread throughout the hydrogel while the on-top cells migrated to form a toroid (Figure 4.2). Another possibility is that, when cells are mixed into a hydrogel, the matrix stabilizes around the cell creating an environment that could prevent the cell from spreading its processes.

Next, we utilized a CXCR4 agonist in the hope that it would upregulate the CXCL12-CXCR4 pathway, giving a novel response from mixed-in cells. We saw, in both treatment categories, that the cells still did not form toroids. Just as with untreated cells, the treated ADSCs proved that the spatial distribution between individual cells is key to their signaling. To further this study, we need to focus on the molecular regulation of mixed-in cells. Western blot analysis should be

performed to understand if there was a change in expression of the CXCL12-CXCR4 pathway after the CXCR4 agonist was introduced. Likewise, different agonist could be attempted such as CXCR7, N-Cadherin, or PI3K.

In conclusion, we found that it is possible to combine more than two hydrogel matrices together and still observe cellular migration characteristic of embryogenesis. In fact, we may be observing a more *in vivo*-like representation of the migration process. We also found that the spatial difference of mixed-in cells outweighs the cell signaling transduction. Even with the regulatory pathway upregulated, the cells mixed into a hydrogel showed no change in behavior. This suggests two potential reasons: 1) the migratory signaling is regulated by a more specific molecules that is not being stimulated in these cells or 2) the properties of the hydrogel, when stabilized, physically encases the cells where they are unable to spread their processes to migrate. These studies provide important answers to the different questions uncovered during the process of the overall study.

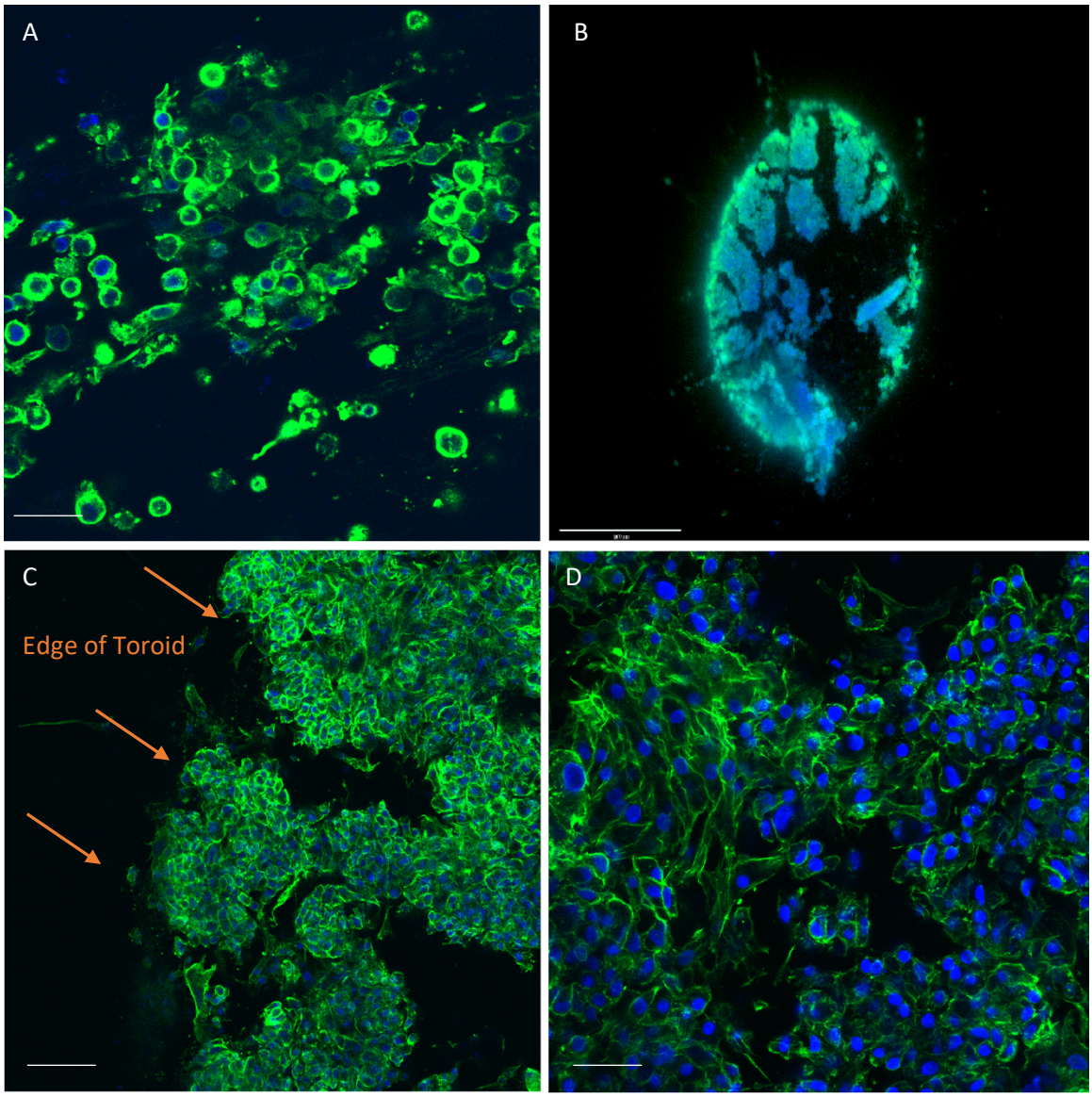

Figure 4.1 ADSC response to a 3-collagen hydrogel. A) The response of ADSCs to an equal concentration of all three collagens. B) View of the shape of the toroid made by cells in the unequal collagen concentrations. C and D) Higher magnification view of cell clumps formed in the toroid. Scale bars A and D=50μm, B=1000μm, C= 100μm, Green=Phalloidin, Blue=DAPI.

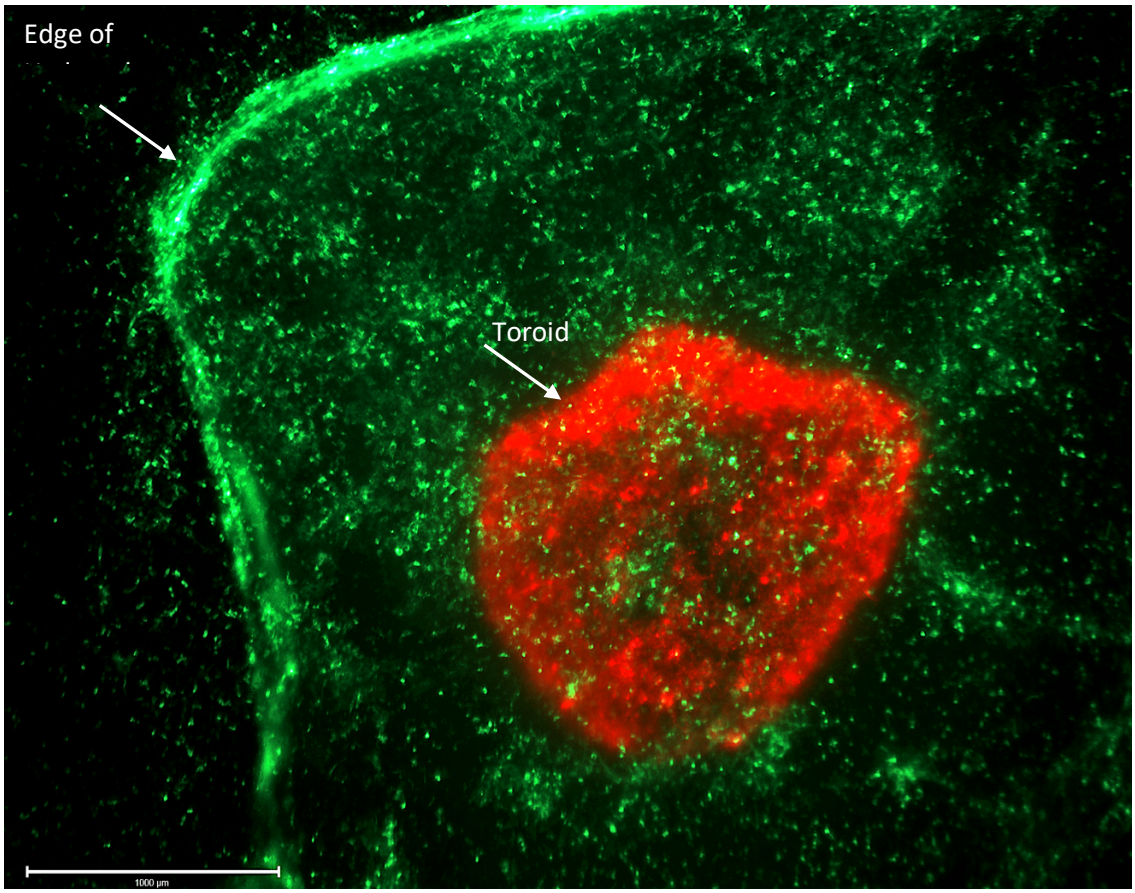

Figure 4.2 ADSCs placed inside and on top of the same hydrogel. Image provides a clear view of the toroid formed from cells cultured on top of the hydrogel (red) while also showing the spatial distribution of the mixed-in cells (green). Note that there is still a slight contraction of the hydrogel by the mixed-in cells. Scale bar=1000µm, Green= Vybrant DiO, Red= Vybrant DiD.

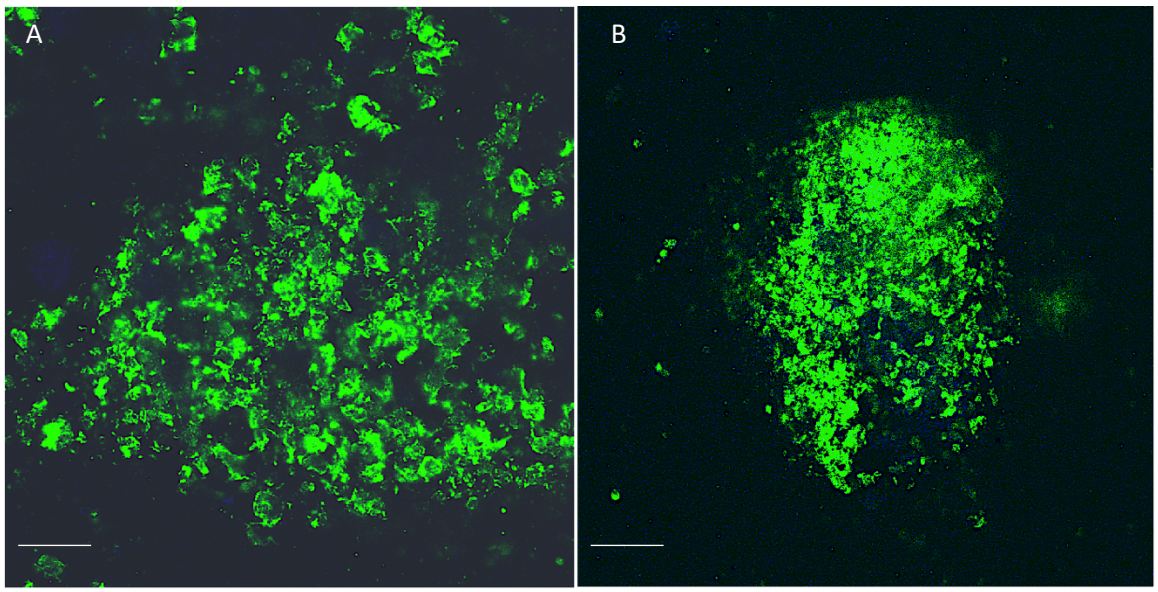

Figure 4.3 ADSCs do not respond to upregulation of CXCR4 within a hydrogel. CXCR4 agonist was mixed into the hydrogel (A) or used to treat ADSCs (B). In each case, mixed-in ADSCs did not have a change in their behavior. Note that there is no CXCL12 expression (red) even though CXCR4 was upregulated. Scale bars=50μm, Green=Phalloidin, Blue=DAPI, Red= CXCL12 antibody.

CHAPTER 5

FUTURE DIRECTIONS

While many of the studies presented have been finished, there are numerous paths and unanswered questions remaining that could allow for this project to progress further. We have shown the impact of a changing microenvironment on cellular behavior. While there are ongoing studies focused on the examination of multi-cell and multi-collagen microenvironments, other biomaterials that have shown an impact on regenerative medicine should be investigated including Polyethylene Glycol (PEG) and Poly-Lactic-co-Glycolic Acid (PLGA). The novel ADSC cell clusters observed in several of our fabricated microenvironments needs to be further studied to understand this behavior. The 3-collagen study needs to be expanded to include more ratios that would be seen in different parts of the body as well as expanding to add more types of collagen to the mixture. Likewise, the multi-cell and multi-matrix microenvironments need to be combined to study the response of multiple cells both to each other and to the different matrices. Lastly, a question arose in a previous talk regarding what would happen if the different types of collagen were layered in a well instead of being homogenous.

An expanded study of how healthy cells react to co-cultured diseased cells should be conducted. We saw that, when ADSCs were co-cultured with 4T1s, there was an unprecedented response of the cancer cells forming toroids and

expressing the majority of CXCL12. Additional cancer cells and stem cells as well as different diseased or injured cells need to be studied. For instance, a study could be focused on the response of stem cells to injured cardiomyocytes. This would simulate the response of stem cells injected into the heart of an individual with heart disease. This would also be steps towards the creation of a universal model that can be tuned to study different diseases without having to involve a live specimen.

The structural remodeling of hydrogels is another aspect that could be advanced. First, the studies utilizing second harmonic generation and collagen hybridizing peptide should be repeated with different cell types. It would be interesting to view this with the mixed-in cells as well as the cancer cell types that are not forming toroids.

We are also pursuing assays to better understand the full molecular regulation in toroid formation as well as the communication mechanisms utilized between cells. While the CXCL12-CXCR4 pathway has shown promise in being the regulatory body of toroid formation, it is imperative to look at additional pathways (i.e. signal transduction pathways) involved in cell-cell signaling. Additional pathways could include the Wnt signaling pathway key to proliferation, VEGF signaling pathway involved in embryonic cellular migration, and TGF-β signaling pathway involved in proliferation and migration.

REFERENCES

Abbott A. (2003). Cell culture: biology's new dimension. Nature. 424:870–2.

Ahmed EM. (2015). Hydrogel: Preparation, characterization, and applications: A review. Journal of Advanced Research. 6: 105-121.

Amann PM, Eichmüller SB, Schmidt J, Bazhin AV. (2011). Regulation of gene expression by retinoids. Curr Med Chem. 18:1405–12.

American Cancer Society. Cancer Facts and Figures 2021. Atlanta, Ga: American Cancer Society; 2021.

Angers S, Moon RT. (2009). Proximal events in Wnt signal transduction. Nat Rev Mol Cell Biol. 10:468–77.

Anseth EK, Sims D, McIntosh W, Randolph M, Langer R. (1996). Transdermal photopolymerization for minimally invasive implantation. Proc Natl Acad Sci USA. 96(6):3104-3107.

Antoine EE, Vlachos PP, Rylander MN. (2015). Tunable Collagen I Hydrogels for Engineered Physiological Tissue Micro-Environments*. PLoS ONE*. 10(3): e0122500.

Ara T, Nakamura Y, Egawa T, Sugiyama T, Abe K, Kishimoto T, Matsui Y, Nagasawa T. (2003). Impaired colonization of the gonads by primordial germ cells in mice lacking a chemokine, stromal cell-derived factor-1 (SDF-1). Proceedings of the National Academy of Sciences. 100(9):5319-23.

Askari AT, Unzek S, Popovic ZB, Goldman CK, Forudi F, Kiedrowski M, Rovner A, Ellis SG, Thomas JD, DiCorleto PE, Topol EJ, Penn MS. (2003). Effect of stromal-cell-derived factor 1 on stem-cell homing and tissue regeneration in ischaemic cardiomyopathy. Lancet. 362(9385):697–703.

Atala A, Lanza R. (2012). Handbook of Stem Cells. Academic Press. p. 452.

Badylak SF, Freytes DO, Gilbert TW. (2009). Extracellular matrix as a biological scaffold material: structure and function. Acta biomaterialia. 5(1):1-3.

Bahram M, Mohseni N, Moghtader M. (2016). An Introduction to Hydrogels and Some Recent Applications. In (Ed.), Emerging Concepts in Analysis and Applications of Hydrogels. IntechOpen. https://doi.org/10.5772/64301

Bajaj P, Schweller RM, Khademhosseini A, West JL, Bashir R. (2014). 3D biofabrication strategies for tissue engineering and regenerative medicine. Annu. Rev. Biomed. Eng. 16:247–276.

Balkwill F. (2004). Cancer and the chemokine network. Nat Rev Cancer. 4:540–50.

Barocas VH, Girton TS, Tranquillo RT. (1998). Engineered alignment in media equivalents: magnetic prealignment and mandrel compaction. J Biomech Eng. 120(5):660-6.

Behonick DJ, Werb Z. (2003). A bit of give and take: the relationship between the extracellular matrix and the developing chondrocyte. Mech Dev. 120:1327–36.

Belay E, Matrai J, Acosta-Sanchez A, Ma L, Quattrocelli M, Mates L, et al. (2010). Novel hyperactive transposons for genetic modification of induced pluripotent and adult stem cells: a nonviral paradigm for coaxed differentiation. Stem Cells. 28:1760–71.

Benoit DS, Dumey AR, Anseth KS. (2007). The effect of heparin-functionalized PEG hydrogels on three-dimensional human mesenchymal stem cell osteogenic differentiation. Biomaterials. 28:66–77.

Bertassoni LE, Cecconi M, Manoharan V, Nikkhah M, Hjortnaes J, Cristino AL, Barabaschi G, Demarchi D, Dokmeci MR, Yang Y, Khademhosseini A. (2014). Hydrogel bioprinted microchannel networks for vascularization of tissue engineering constructs. Lab Chip 14:2202–2211.

Bian, X., Song, Z.L., Qian, Y., Gao, W., Cheng, Z.Q., Chen, L., Liang, H., Ding, D., Nie, X.K., Chen, Z. and Tan, W. (2014). Fabrication of graphene-isolated-Au-nanocrystal nanostructures for multimodal cell imaging and photothermal-enhanced chemotherapy. *Scientific reports*, 4, 1-9.

Binder KW, Zhao W, Aboushwareb T, Dice D, Atala A, Yoo JJ. (2010). In situ bioprinting of the skin for burns. J. Am. Coll. Surg. 211:S76.

Bleul CC, Fuhlbrigge RC, Casasnovas JM, Aiuti A, Springer TA. (1996). A highly efficacious lymphocyte chemoattractant, stromal cell-derived factor 1 (SDF-1). The Journal of Experimental Medicine. 184(3):1101–9.

Caplan AI (1991). Mesenchymal Stem Cells. Journal of Orthopaedic Research. 9(5): 641–50.

Carlesso N, Cardoso AA. (2010). Stem cell regulatory niches and their role in normal and malignant hematopoiesis. Curr Opin Hematol. 17:281–6.

Cen, L., Liu, W. E. I., Cui, L. E. I., Zhang, W., & Cao, Y. (2008). Collagen tissue engineering: development of novel biomaterials and applications. *Pediatric research*, 63, 492-496.

Chambers A, Groom A, MacDonald I. (2002). Dissemination and growth of cancer cells in metastatic sites. Nat. Rev. Cancer. 2:563–572.

Chang CW, Seibel AJ, Avendano A, Cortes-Medina MG, Song JW. (2020). Distinguishing Specific CXCL12 Isoforms on Their Angiogenesis and Vascular Permeability Promoting Properties. Advanced Healthcare Materials. 9(4):1901399.

Chang L and Karin M. (2001). Mammalian MAP kinase signaling cascades. Nature. 410:37–40.

Cojoc M, Peitzsch C, Trautmann F, Polishchuk L, Telegeev GD, Dubrovska A. (2013). Emerging targets in cancer management: role of the CXCL12/CXCR4 axis. OncoTargets and therapy. 6:1347.

Cossu G, Bianco P. (2003). Mesoangioblasts vascular progenitors for extravascular mesodermal tissues. Curr Opin Genet Dev. 13:537–42.

Coughlin RP, Oldweiler A, Mickelson DT, Moorman CT. (2017). Adipose_Derived Stem Cell Transplant Technique for Degerative Joint Disease. Arthroscopy Techniques. 6(5):1761–1766.

Cui X, Gao G, Yonezawa T, Dai G. (2014). Human cartilage tissue fabrication using three-dimensional inkjet printing technology. J. Vis. Exp. 88:e51294.

Curnock A, Sotsios Y, Wright K, Ward S. (2003). Optimal chemotactic responses of leukemic T cells to stromal cellderived factor-1 requires the activation of both class IA and IB phosphoinositide 3-kinases. J. Immunol. 170:4021–4030.

Curtis AS, Casey B, Gallagher JO, Pasqui D, Wood MA, Wilkinson CD. (2001). Substratum nanotopography and the adhesion of biological cells. Are symmetry or regularity of nanotopography important? Biophys Chem. 94:275–83.

Darash-Yahana M, Pikarsky E, Abramovitch R, Zeira E, Pal B, Karplus R, et al. (2004). Role of high expression levels of CXCR4 in tumor growth, vascularization, and metastasis. Fed. Am. Soc. Exp. Biol. J.

de Castro Brás LE, Proffitt JL, Bloor S, Sibbons PD. (2010). Effect of crosslinking on the performance of a collagen-derived biomaterial as an implant for soft

tissue repair: A rodent model. Journal of Biomedical Materials Research Part B: Applied Biomaterials. 95(2):239-49.

De Felici M, Farini D, Dolci S. (2009). In or out stemness: comparing growth factor signalling in mouse embryonic stem cells and primordial germ cells. Curr Stem Cell Res Ther. 4:87–97.

De Francesco F, Ricci G, D'Andrea F, Nicoletti GF, Ferraro GA, (2015). Human adipose stem cells: from bench to bedside. *Tissue Eng Part B Rev*. 21:572-584.

den Braber ET, de Ruijter JE, Smits HT, Ginsel LA, von Recum AF, Jansen JA. (1996). Quantitative analysis of cell proliferation and orientation on substrata with uniform parallel surface micro-grooves. Biomaterials. 17:1093–9.

Discher DE, Janmey P, Wang YL. (2005). Tissue cells feel and respond to the stiffness of their substrate. Science. 310:1139–43

Doring Y, Pawig L, Weber C, Noels H. (2014). The CXCL12/CXCR4 chemokine ligand/receptor axis in cardiovascular disease. Front. Physiol. 5:212.

Duan B, Kapetanovic E, Hockaday LA, Butcher JT. (2014) Three-dimensional printed trileaflet valve conduits using biological hydrogels and human valve interstitial cells. Acta Biomater. 10:1836–1846.

Engler AJ, Sen S, Sweeney HL, Discher DE. (2006). Matrix elasticity directs stem cell lineage specification. *Cell*. 126(4):677-89.

Fix C., Bingham K., Carver W. (2011). Effects of interleukin-18 on cardiac fibroblast function and gene expression. *Cytokine*, 53(1):19-28. PMID: 21050772, PMCID: PMC3018826, DOI: 10.1016/j.cyto.2010.10.002

Flemming RG, Murphy CJ, Abrams GA, Goodman SL, Nealey PF. (1999). Effects of synthetic micro- and nano-structured surfaces on cell behavior. Biomaterials. 20:573–88.

Folkman J. (2002). Role of angiogenesis in tumor growth and metastasis. Semin. Oncol. 29:15–18.

Franz CM, Jones GE, Ridley AJ. (2002). Cell migration in development and disease. Dev. Cell 2:153–8

Fresno Vara J, Casado E, de Castro J, Cejas P, Belda-Iniesta C, Gonzalez-Baron M. (2004). PI3K/Akt signalling pathway and cancer. Cancer Treat. Rev. 30:193–204.

Friedl F, Locker J, Sahai E, Segall JE. (2012). Classifying collective cancer cell invasion. Nat. Cell Biol. 14:777–83

Gaetani R, Doevendans PA, Metz CH, Alblas J, Messina E, Giacomello A, Sluijter JP. (2012). Cardiac tissue engineering using tissue printing technology and human cardiac progenitor cells. Biomaterials 33:1782–1790.

Gaetani, R., Zizzi, E.A., Deriu, M.A.; Morbiducci, U., Pesce, M., & Messina, E. (2020). When Stiffness Matters: Mechanosensing Heart Development and Disease. *Front. in Cell Dev. Biol*, 8, 334.

Gao G, Schilling AF, Yonezawa T, Wang J, Dai G, Cui X. (2014). Bioactive nanoparticles stimulate bone tissue formation in bioprinted three-dimensional scaffold and human mesenchymal stem cells. Biotechnol. J. 9:1304–1311.

Ghanem I, Riveiro ME, Paradis V, Faivre S, de Parga PM, Raymond E. (2014). Insights on the CXCL12-CXCR4 axis in hepatocellular carcinoma carcinogenesis. Am J Transl Res 6:340–352

Gilbert PM, Havenstrite KL, Magnusson KE, Sacco A, Leonardi NA, Kraft P, et al. (2010). Substrate elasticity regulates skeletal muscle stem cell self-renewal in culture. Science. 329:1078–81.

Glowacki, J., & Mizuno, S. (2008). Collagen scaffolds for tissue engineering. *Biopolymers: Original Research on Biomolecules*, 89, 338-344

Gourdie RG, Myers TA, McFadden A, Li YX, Potts JD. (2012). Self-organizing tissue-engineered constructs in collagen hydrogel. *Microsc Microanal*. 18(1), 99-106.

Gourdie RG, Potts JD, inventors; MUSC Foundation for Research Development, assignee. Compositions and methods for tissue engineering, tissue regeneration and wound healing. United States patent US 8,815,556. 2014 Aug 26.

Greenbaum A, Hsu YM, Day RB, Schuettpelz LG, Christopher MJ, Borgerding JN, Nagasawa T, Link DC. (2013). CXCL12 in early mesenchymal progenitors is required for haematopoietic stem-cell maintenance. Nature. 495(7440):227-30.

Guillemot F, Mironov V, Nakamura M. (2010). Bioprinting is coming of age: Report from the International Conference on Bioprinting and Biofabrication in Bordeaux (3B'09). Biofabrication 2:010201.

Gullberg D, Gehlsen KR, Turner DC, Ahlén K, Zijenah LS, Barnes MJ, Rubin K. (1992). Analysis of alpha 1 beta 1, alpha 2 beta 1 and alpha 3 beta 1 integrins in cell--collagen interactions: identification of conformation

dependent alpha 1 beta 1 binding sites in collagen type I. *EMBO J.* 11(11):3865-73. PMID: 1396580; PMCID: PMC556896.

Guo F, Wang Y, Mok SC, Xue F, Zhang W. (2016). CXCL12/CXCR4: a symbiotic bridge linking cancer cells and thwir stromal neighbors in oncogenic communication networks. *Oncogene*. 35:816-826.

Guo L, Zhao RC, Wu Y. (2011). The role of microRNAs in self-renewal and differentiation of mesenchymal stem cells. Exp Hematol. 39:608–16.

Han S, Sun HM, Hwang KC, Kim SW. (2015). Adipose-derived stromal vascular fraction cells: update on clinical utility and efficacy. *Crit Rev Eukaryot Gene Expr.* 25:145-152.

Hansen LK, Wilhelm J, Fassett JT. (2006). Regulation of hepatocyte cell cycle progression and differentiation by type I collagen structure. *Current topics in developmental biology*, 72, 205-236.

Hassan WU, Greiser U, Wang W. (2014). Role of adipose-derived stem cells in wound healing. *Wound Repair Regen.* 22:313-325.

Hatten ME. (1993). The role of migration in central nervous system neuronal development. Curr. Opin. Neurobiol. 3:38–44

Hill-West JL, Chowdhury SM, Sawhney AS, Pathak CP, Dunn RC, Hubbell JA. (1994). Prevention of postoperative adhesions in the rat by in situ photopolymerization of bioresorbable hydrogel barriers. Obstet Gyneco., 83(1):59-64

Hill-West JL, Chowdhury SM, Slepian MJ, Hubbell JA. (1994). Inhibition of thrombosis and intimal thickening by in situ photopolymerization of thin hydrogel barriers. Proc Natl Acad Sci USA. 91(13):5967-5971.

Hockemeyer D, Jaenisch R. (2016). Induced Pluripotent Stem Cells Meet Genome Editing. Cell Stem Cell. 18(5):573–86.

Hoffman MD, Van Hove AH, Benoit DS. (2014). Degradable hydrogels for spatiotemporal control of mesenchymal stem cells localized at decellularized bone allografts. Acta biomaterialia. 10:3431–3441.

Hu C, Yong X, Li C, Lü M, Liu D, Chen L, Hu J, Teng M, Zhang D, Fan Y, Liang G. (2013). CXCL12/CXCR4 axis promotes mesenchymal stem cell mobilization to burn wounds and contributes to wound repair. *J Surg Res*. 183:427-34. doi: 10.1016/j.jss.2013.01.019. Epub 2013 Feb 1. PMID: 23462453.

Hunt NC, Grover LM. (2010). Cell encapsulation using biopolymer gels for regenerative medicine. *Biotechnology letters*. 32(6):733-42.

Huynh, T., Abraham, G., Murray, J., Brockbank, K., Hagen, P. O., & Sullivan, S. (1999). Remodeling of an acellular collagen graft into a physiologically responsive neovessel. *Nature biotechnology*, 17, 1083-1086.

Imai H, Sunaga N, Shimizu Y, Kakegawa S, Shimizu K, Sano T, et al. (2010). Clinicopathological and therapeutic significance of CXCL12 expression in lung cancer. Int. J. Immunopathol. Pharmacol. 23:153–164.

Ishigami S, Natsugoe S, Okumura H, Matsumoto M, Nakajo A, Uenosono Y, et al. (2007). Clinical implication of CXCL12 expression in gastric cancer. Ann. Surg Oncol. 14:3154-3158.

Jeong B, Bae YH, Lee DS, Kim SW. (1997). Biodegradable block copolymers as injectable drug-delivery systems. Nature. 388:860–862.

Ji JF, He BP, Dheen ST, Tay SSW. (2004). Interactions of chemokines and chemokine receptors mediate the migration of mesenchymal stem cells to the impaired site in the brain after hypoglossal nerve injury. Stem Cells. 22:415.

Jiang Y, Jahagirdar BN, Reinhardt RL, Schwartz RE, Keene CD, Ortiz-Gonzalez XR, Reyes M, Lenvik T, Lund T, Blackstad M, Du J, Aldrich S, Lisberg A, Low WC, Largaespada DA, Verfaillie CM. (2002). Pluripotency of mesenchymal stem cells derived from adult marrow. Nature. 418(6893): 41–9.

Kang H, Mansel R, Jiang W. (2005). Genetic manipulation of stromal cell-derived factor-1 attests the pivotal role of the autocrine SDF-1-CXCR4 pathway in the aggressiveness of breast cancer cells. Int. J. Oncol. 26:1429–1434.

Kang H, Watkins G, Parr C, Douglas-Jones A, Mansel RE, Jiang WG. (2005). Stromal cell derived factor-1: its influence on invasiveness and migration of breast cancer cells in vitro, and its association with prognosis and survival in human breast cancer. Breast Cancer Res. 7:R402.

Karastergiou K, Mohamed Ali V. (2010). The autocrine and paracrine roles of adipokines. *Mol Cell Endocrinol.* 318:69-78.

Karsdal MA, Leeming DJ, Henriksen K, Bay-Jensen AC. (2016). Biochemistry of Collagens, Laminins and Elastin: Structure, Function and Biomarkers.

Kayali A, Van Gunst K, Campbell I, Stotland A, Krittzik M, Liu G, et al. (2003). The stromal cell-derived factor-1alpha/CXCR4 ligand–receptor axis is critical for progenitor survival and migration in the pancreas. J. Cell Biol. 163:859–869.

Killat, J, Reimers K, Choi CY, Jahn S, Vogt PM, Radtke C. (2013). Cultivation of keratinocytes and fibroblasts in a three-dimensional bovine collagen-

elastin matrix (Matriderm) and application for full thickness wound coverage in vivo. Int. J. Mol. Sci. 14:14460–14474.

Kuivaniemi H, Tromp G. (2019). Type III collagen (COL3A1): Gene and protein structure, tissue distribution, and associated diseases. *Gene*. 707:151-171. doi: 10.1016/j.gene.2019.05.003. Epub 2019 May 7. PMID: 31075413; PMCID: PMC6579750.

Kumari A, Kumar Yadav S, Yadav SC. (2010). Biodegradable polymeric nanoparticles based drug delivery systems. Review. Colloids Surf B Biointerfaces. 75:1–18.

Lagerstrom MC, Schioth HB. (2008). Structural diversity of G protein coupled receptors and significance for drug discovery. Nat Rev Drug Discov. 7:339–57.

Lee JH, Kim HE, Im JH, Bae YM, Choi JS, Huh KM, Lee CS. (2008). Preparation of orthogonally functionalized surface using micromolding in capillaries technique for the control of cellular adhesion. Colloids Surf B Biointerfaces. 64(1):126-34.

Lee PH, Park HJ. (2009). Bone marrow-derived mesenchymal stem cell therapy as a candidate disease-modifying strategy in Parkinson's disease and multiple system atrophy. J Clin Neurol. 5:1–10.

Lee VK and Dai G (2016). Printing of Three-Dimensional Tissue Analogs for Regenerative Medicine. Annals of Biomedical Engineering. 45(1), 1–11.

Lee VK, Kim DY, Ngo H, Lee Y, Seo L, Yoo SS, Vincent PA, Dai G. (2014). Creating perfused functional vascular channels using 3D bio-printing technology. Biomaterials 35:8092–8102.

Lee W, Debasitis JC, Lee VK, Lee JH, Fischer K, Edminster K, Park JK, Yoo SS. (2009). Multi-layered culture of human skin fibroblasts and keratinocytes through three-dimensional freeform fabrication. Biomaterials 30:1587–1595.

Lee W, Lee V, Polio S, Keegan P, Lee JH, Fischer K, Park JK, Yoo SS. (2010). On-demand three-dimensional freeform fabrication of multi-layered hydrogel scaffold with fluidic channels. Biotechnol. Bioeng. 105:1178–1186.

Li F, Guo WY, Li WJ, Zhang DX, Lv AL, Luan RH, Liu B, Wang HC. (2009). Cyclic stretch upregulates SDF-1α/CXCR4 axis in human saphenous vein smooth muscle cells. *Biochemical and biophysical research communications*. 386:247-51.

Li J, He L, Zhou C, Zhou Y, Bai YY, Lee FY, Mao JJ. (2015). 3D printing for regenerative medicine: from bench to bedside. MRS Bull. 40:145–153.

Li L, He Y, Zhao M, Jiang J. (2013). Collective cell migration: implications for wound healing and cancer invasion. Burns Trauma. 1:21–6

Li SM, Rashkov I, Espartero JL, Manolova N, Vert M. (1996). Synthesis, characterization, and hydrolytic degradation of PLA/PEO/PLA triblock copolymers with long poly(L-lactic acid) block. Macromolecules. 29(1):57-62

Liang Z, Yoon Y, Votaw J, Goodman M, Williams L, Shim H. (2005). Silencing of CXCR4 blocks breast cancer metastasis. Cancer Res. 65:967–971.

Lin CC and Anseth KS. (2009). PEG hydrogels for the controlled release of biomolecules in regenerative medicine. Pharmaceutical research. 26:631–643.

Luker KE and Luker GD. (2005). Functions of CXCL12 and CXCR4 in breast cancer. Cancer Lett. 238(1):30-41.

Ma Q, Jones D, Borghesani PR, Segal RA, Nagasawa T, Kishimoto T, Bronson RT, Springer TA. (1998). Impaired B-lymphopoiesis, myelopoiesis, and derailed cerebellar neuron migration in CXCR4- and SDF-1-deficient mice. Proc. Natl. Acad. Sci. USA. 95:9448–9453.

Macleod TM, Williams G, Sanders R, Green CJ. (2005). Histological evaluation of Permacol™ as a subcutaneous implant over a 20-week period in the rat model. *British journal of plastic surgery*. 58(4):518-32.

Mahla RS. (2016). Stem Cell Applications in Regenerative Medicine and Disease Therapeutics. International Journal of Cell Biology. e6940283.

Marión RM, Strati K, Li H, Murga M, Blanco R, Ortega S, et al. (2009). A p53-mediated DNA damage response limits reprogramming to ensure iPS cell genomic integrity. Nature. 460(7259):1149–53.

McGrath JA. (2020). McKee's Pathology of the Skin. Elsevier. Chapter 1: The structure and function of skin; p. 1-34.

McNamara LE, McMurray RJ, Biggs MJ, Kantawong F, Oreffo RO, Dalby MJ. (2010). Nanotopographical control of stem cell differentiation. J Tissue Eng. 2010:120623.

Mercado-Pimentel, M. E., & Runyan, R. B. (2007). Multiple transforming growth factor-β isoforms and receptors function during epithelial-mesenchymal cell transformation in the embryonic heart. *Cells Tissues Organs*, 185, 146-156.

Metters AT, Anseth KS, Bowman CN. (2000). Fundamental studies of a novel, biodegradable PEG-b-PLA hydrogel. Polymer 41:3993–4004.

Michel F, L vesque TN, Rezak M. (2009). Therapeutic microinjection of autologous adult human neural stem cells and differentiated neurons for Parkinson's disease: five-year postoperative outcome. Open Stem Cell J. 1:20–9.

Mir TA and Nakamura M. (2017). Three-Dimensional Bioprinting: Toward the Era of Manufacturing Human Organs as Spare Parts for Healthcare and Medicine. Tissue Engineering B. 23(3): 245-256.

Muller A, Homey B, Soto H, Ge N, Catron D, Buchanon M, et al. (2001). Involvement of chemokine receptors in breast cancer metastasis. Nature. 410:50–56.

Nagasawa T, Tachibana K, Kishimoto T. (1998). A novel CXC chemokine PBSF/SDF-1 and its receptor CXCR4: their functions in development, hematopoiesis and HIV infection. Seminars Immunol. 10:179–185.

Nesbitt T, Lemley A, Davis J, Yost MJ, Goodwin RL, Potts JD. (2006). Epicardial development in the rat: a new perspective. *Microsc Microanal*. 12(5):390-8. doi: 10.1017/S1431927606060533.PMID: 16984665

Nili N, Cheema AN, Giordano FJ, Barolet AW, Babaei S, Hickey R, et al. (2003). Decorin inhibition of PDGF-stimulated vascular smooth muscle cell function: potential mechanism for inhibition of intimal hyperplasia after balloon angioplasty. Am J Pathol. 163:869–78.

Nuttelman C, Benoit DS, Tripodi MC, Anseth KS. (2006). The effect of ethylene glycol methacrylate phosphate in PEG hydrogels on mineralization and viability of encapsulated hMSCs. Biomaterials. 27:1377–1386.

Othmani AE, Rouam S, Abbad A, Erraoui C, Harriba S, Boukind H, et al. (2019). Cryopreservation Impacts Cell Functionality of Long Term Expanded Adipose-Derived Stem Cells. J Stem Cell Res Ther. 09(01)

Ozbolat, I. T. (2015). Bioprinting scale-up tissue and organ constructs for transplantation. Trends Biotechnol. 33:395–400.

Pang, Y., & Greisler, H. P. (2010). Using a type 1 collagen-based system to understand cell-scaffold interactions and to deliver chimeric collagen-binding growth factors for vascular tissue engineering. *Journal of investigative medicine*, 58, 845-848.

Pashuck ET, and Stevens MM. (2012). Designing regenerative biomaterial therapies for the clinic. Sci Transl Med 4:160sr164.

Patino, M. G., Neiders, M. E., Andreana, S., Noble, B., & Cohen, R. E. (2002). Collagen as an implantable material in medicine and dentistry. *Journal of Oral Implantology*, 28, 220-225.

Paulos SP, Hausman DB, Hausman GJ. (2010). The development and endocrine functions of adipose tissue. *Mol Cell Endocrinol*. 323:20-34.

Pedraza CE, Marelli B, Chicatun F, McKee MD, Nazhat SN. (2010). An In Vitro assessment of a cell-containing collagenous extracellular matrix–like scaffold for bone tissue engineering*. Tissue engineering Part A*. 16(3):781-93.

Peng S, Peek V, Zhai Y, Paul D, Lou Q, Xia X, et al. (2005). Akt activation, but not extracellular signal-regulated kinase activation, is required for SDF-1alpha/CXCR4-mediated migration of epitheloid carcinoma cells. Mol. Cancer Res. 3:227–236.

Potts JD, Vincent EB, Runyan RB, Weeks DL. (1992). Sense and antisense TGF beta 3 mRNA levels correlate with cardiac valve induction. *Dev Dyn*. 193(4):340-5. doi: 10.1002/aja.1001930407.PMID: 1511174

Pedraza CE, Marelli B, Chicatun F, McKee MD, Nazhat SN. An In Vitro assessment of a cell-containing collagenous extracellular matrix–like scaffold for bone tissue engineering. Tissue engineering Part A. 2010 Mar 1;16(3):781-93.

Rennert, R. C., Sorkin, M., Garg, R. K., & Gurtner, G. C. (2012). Stem cell recruitment after injury: lessons for regenerative medicine. *Regenerative medicine*, 7, 833-850.

Ribeiro, M. C., Tertoolen, L. G., Guadix, J. A., Bellin, M., Kosmidis, G., D'Aniello, C., Monshouwer-Kloots, J., Goumans, M. J., Wang, Y. L., Feinberg, A. W. and Mummery, C. L. (2015). Functional maturation of human pluripotent stem cell derived cardiomyocytes in vitro–correlation between contraction force and electrophysiology. *Biomaterials*, 51, 138-150.

Richards M, Tan SP, Tan JH, Chan WK, Bongso A. (2004). The transcriptome profile of human embryonic stem cells as defined by SAGE. Stem Cells. 22:51–64.

Rubin J, Kung A, Klein R, Chan J, Sun Y, Schmidt K, et al. (2003). A small-molecule antagonist of CXCR4 inhibits intracranial growth of primary brain tumors. Proc. Natl Acad. Sci. USA 100:13513–13518.

Runyan RB, Potts JD, Sharma RV, Loeber CP, Chiang JJ, Bhalla RC. (1990). Signal transduction of a tissue interaction during embryonic heart development. *Cell Regul.* 1(3):301-13. doi: 10.1091/mbc.1.3.301.PMID: 2129222

Rutz AL, Hyland KE, Jakus AE, Burghardt WR, Shah RN. (2015). A multimaterial bioink method for 3D printing tunable, cell-compatible hydrogels. Adv. Mater. 27:1607–1614.

Sakai N, Yoshidome H, Shida T, Kimura F, Shimizu H, Ohtsuka M, et al. (2012). CXCR4/CXCL12 expression profile is associated with tumor microenvironment and clinical outcome of liver metastases of colorectal cancer. Clin. Exp. Metastasis 29:101–110.

Santra M, Reed CC, Iozzo RV. (2002). Decorin binds to a narrow region of the epidermal growth factor (EGF) receptor, partially overlapping but distinct fromthe EGF-binding epitope. J Biol Chem. 277:35671–81.

Sanz-Pamplona R, Garcia-Garcia J, Franco S, Messeguer X, Driouch K, Oliva B et al. (2012). A taxonomy of organ-specific breast cancer metastases based on a protein-protein interaction network. Mol Biosyst. 8: 2085–2096.

Satoshi K, Kashina A. (2008). Cell biology of embryonic migration. Birth Defects Res. C. 84:102–22

Sawhney AS, Pathak CP, Hubbell JA. (1993). Bioerodible hydrogels based on photopolymerized poly(ethylene glycol)-co-poly(.alpha.-hydroxy acid) diacrylate macromers. Macromolecules. 26(4):581-587.

Scarpa E, Mayor R. (2016) Collective cell migration in development J. Cell Biol. 212:143–55.

Schrader AJ, Lechner O, Templin M, Dittmar KE, Machtens S, Mengel M, Probst-Kepper M, Franzke A, Wollensak T, Gatzlaff P, Atzpodien J, Buer J, Lauber J. (2002). CXCR4/CXCL12 expression and signaling in kidney cancer. British Journal of Cancer. 86(8):1250–6.

Selvaraj V, Plane JM, Williams AJ, Deng W. (2010). Switching cell fate: the remarkable rise of induced pluripotent stem cells and lineage reprogramming technologies. Trends in Biotechnology. 28(4):214–23.

Seol YJ, Kang HW, Lee SJ, Atala A, Yoo JJ. (2014). Bioprinting technology and its applications. Eur. J. Cardiothorac. Surg. 46:342–348, 2014.

Shu L, Zhang H, Boyce BF, Xing L. (2013). Ubiquitin E3 ligase Wwpl negatively regulates osteoblast function by inhibiting osteoblast differentiation and migration. Journal of bone and mineral research. 28:1925–1935.

Sinha R, Verdonschot N, Koopman B, Rouwkema J. Tuning Cell and Tissue Development by Combining Multiple Mechanical Signals. (2017). Tissue Eng Part B Rev. 23(5):494-504.

Smela E. (2003). Conjugated polymer actuators for biomedical applications. Adv Mater. 15:481–94.

Smith M, Luker K, Garbow J, Prior J, Jackson E, Piwnica-Worms D, et al. (2004). CXCR4 regulates growth of both primary and metastatic breast cancer, Cancer Res. 64: 8604–8612.

Soriano S, Serrano A, Hernanz-Falcon P, Martin De Ana A, Monterrubio M, Martinez-A C, et al. (2003). Chemokines integrate JAK/STAT and G-protein pathways during chemotaxis and calcium flux responses. Eur. J. Immunol. 33:1328–1333.

Sorushanova A, Coentro JQ, Pandit A, Zeugolis DI, Raghunath M. (2017). Comprehensive Biomaterials II. Elsevier. 2.15 Collagen: Materials Analysis and Implant Uses; p. 332-350.

Strobel LA, Rath SN, Maier AK, Beier JP, Arkudas A, Greil P, Horch RE, Kneser U. (2014). Induction of bone formation in biphasic calcium phosphate scaffolds by bone morphogenetic protein-2 and primary osteoblasts. J. Tissue Eng. Regen. Med. 8:176–185.

Subbaiah R, Thomas B. (2011). Efficacy of a bioactive alloplast, in the treatment of human periodontal osseous defects-a clinical study. Med Oral Patol Oral Cir Bucal. 16:239–44.

Sun Y, Wang Q. (2013). Modeling and simulations of multicellular aggregate self-assembly in biofabrication using kinetic Monte Carlo methods. *Soft Matter*. 9(7):2172-86.

Tachibana K, Hirota S, Iizasa H, Yoshida H, Kawabata K, Kataoka Y, Kitamura Y, Matsushima K, Yoshida N, Nishikawa S. (1998). The chemokine receptor CXCR4 is essential for vascularization of the gastrointestinal tract. Nature. 39:591–594.

Takahashi K, Yamanaka S. (2006). Induction of pluripotent stem cells from mouse embryonic and adult fibroblast cultures by defined factors. Cell. 126:663–76.

Takano T, Li YJ, Kukita A, Yamaza T, Ayukawa Y, Moriyama K, Uehara N, Nomiyama H, Koyano K, Kukita T. (2014). Mesenchymal stem cells markedly suppress inflammatory bone destruction in rats with adjuvant-induced arthritis. Laboratory Investigation. 94(3):286–96.

Tamamura H, Xu Y, Hattori T, Zhang X, Arakaki R, Kanbara K, Omagari A, Otaka A, Ibuka T, Yamamoto N, Nakashima H. A low-molecular-weight inhibitor against the chemokine receptor CXCR4: a strong anti-HIV peptide T140. Biochemical and biophysical research communications. 1998 Dec 30;253(3):877-82.

Teicher BA, Fricker SP. CXCL12 (SDF-1)/CXCR4 pathway in cancer. Clinical cancer research. 2010 Jun 1;16(11):2927-31.

Teng F, Tian WY, Wang YM, Zhang YF, Guo F, Zhao J, et al. (2016). Cancer-associated fibroblasts promote the progression of endometrial cancer via the SDF-1/CXCR4 axis. J. Hematol. Oncol. 9:8.

Thomson JA, Itskovitz-Eldor J, Shapiro SS, Waknitz MA, Swiergiel JJ, Marshall VS, Jones JM. (1998). Embryonic Stem cell lines derived from human blastocysts. Science. 282(5391):1145–7.

Tilton B, Ho L, Oberlin E, Loetscher P, Baleux F, Clark-Lewis I, Thele M. (2000). Signal transduction by CXC chemokine receptor 4. Stromal cell-derived factor 1 stimulates prolonged protein kinase B and extracellular signal-regulated kinase 2 activation in T lymphocytes. J Exp Med. 193(3): 313-324.

Tonnesen, M. G., Feng, X., & Clark, R. A. (2000). Angiogenesis in wound healing. *Journal of Investigative Dermatology Symposium Proceedings*, 5, 40-46.

Trappmann B, Chen CS. How cells sense extracellular matrix stiffness: a material's perspective. Current opinion in biotechnology. 2013 Oct 1;24(5):948-53.

Trounson A. (2006). The production and directed differentiation of human embryonic stem cells. Endocr Rev. 27:208–19.

Van Duinen V, Trietsch SJ, Joore J, Vulto P, Hankemeier T. (2015). Microfluidic 3D cell culture: from tools to tissue models. Current Opinion in Biotechnology. 35: 118-126.

Vermette M, Trottier V, Ménard V, Saint-Pierre L, Roy A, Fradette J. (2007). Production of a new tissue-engineered adipose substitute from human adipose-derived stromal cells. Biomaterials. 28(18):2850–60.

Viola A, Luster AD. (2008). Chemokines and their receptors: drug targets in immunity and inflammation. Annu Rev Pharmacol Toxicol. 48:171–97.

Vu, L. T., Jain, G., Veres, B. D., & Rajagopalan, P. (2015). Cell migration on planar and three-dimensional matrices: a hydrogel-based perspective. *Tissue Engineering Part B: Reviews*, 21, 67-74.

Wang E, Zhao M, Forrester JV, McCaig CD. (2003). Bi-directional migration of lens epithelial cells in a physiological electrical field. Exp Eye Res.76:29–37.

Wang X, Cao Y, Zhang S, Chen Z, Fan L, Shen X, Zhou S, Chen D. (2017). Stem cell autocrine CXCL12/CXCR4 stimulates invasion and metastasis of esophageal cancer. Oncotarget. 8(22): 36149-36160.

Wang X, Jiang B, Sun H, Zheng D, Zhang Z, Yan L, Li E, Wu Y, Xu R. (2019). Noninvasive application of mesenchymal stem cell spheres derived from hESC accelerates wound healing in a CXCL12-CXCR4 axis-dependent manner. Theranostics. 9(21): 6112-6128.

Weigelt B, Peterse J, van't Veer L. (2005). Breast cancer metastasis: markers and models. Nat Rev Cancer. 5: 591–602.

Weinand C, Gupta R, Weinberg E, Madisch I, Neville CM, Jupiter JB, Vacanti JP. (2009). Toward regenerating a human thumb in situ. Tissue Eng. Part A 15:2605–2615.

Worden A, Uline MJ, Shazley T, Stern M, Potts JD. (2022). Self-Assembling Toroidal Cell Constructs for Tissue Engineering Applications. *Microscopy & Microanalysis*.

Wojcechowsky JA, Lee JY, Seeholzer SH, Doms RW. (2011). Quantitative Phosphoproteomics of CXCL12 (SDF-1) Signaling. PLoS One. 6(9): e24918.

Xing F, Li L, Zhou C, Long C, Wu L, Lei H, Kong Q, Fan Y, Xiang Z, Zhang X. (2019). Regulation and directing stem cell fate by tissue engineering functional microenvironments: scaffold physical and chemical cues. *Stem Cells International*. 2180925. doi: 10.1155/2019/2180925.

Xu, Ruodan & Besenbacher, Flemming & Chen, Menglin. (2017). The 3D mechanical environment and chemical milieu influence the hMSC fibrogenesis and fibroblast-to-myofibroblast transition. RSC Adv.. 7. 20-25. 10.1039/C6RA25422E.

Yang D, Xin M, Wang J, Xu H, Huo Q, Tang Z, et al. (2015a). Chemokine receptor CXCR4 and its ligand CXCL12 expressions and clinical significance in bladder cancer. Genet. Mol. Res. 14:17699–17707. doi:10.

Yi R, Fuchs E. (2011). MicroRNAs and their roles in mammalian stem cells. J Cell Sci. 124:1775–83.

Yuan HP, Kurashina K, de Bruijn JD, Li YB, de Groot K, Zhang XD. (1999). Preliminary study on osteoinduction of two kinds of calcium phosphate ceramics. Biomaterials. 20:1799–806.

Zhang S, Qi L, Li M, Zhang D, Xu S, Wang N, et al. (2008). Chemokine CXCL12 and its receptor CXCR4 expression are associated with perineural invasion of prostate cancer. J. Exp. Clin. Canc. Res. 27:62.

Zhao XY, Li W, Lv Z, Liu L, Tong M, Hai T, et al. (2009). iPS cells produce viable mice through tetraploid complementation. Nature. 461(7260):86–90.

Zhao Y, Yao R, Ouyang L, Ding H, Zhang T, Zhang K, Cheng S, Sun W. (2014). Three-dimensional printing of Hela cells for cervical tumor model in vitro. Biofabrication 6:035001.

Zheng H, Fu G, Dai T, Huang H. (2007). Migration of endothelial progenitor cells mediated by stromal cell-derived factor-1 alpha/CXCR4 via PI3K/Akt/eNOS signal transduction pathway. Journal of Cardiovascular Pharmacology. 50(3):274–80.

Zomer HD, Vidane AS, Gonçalves NN, Ambrósio CE. (2015). Mesenchymal and induced pluripotent stem cells: general insights and clinical perspectives. Stem Cells and Cloning: Advances and Applications. 8:125–34.

APPENDIX A: Permission to Reprint

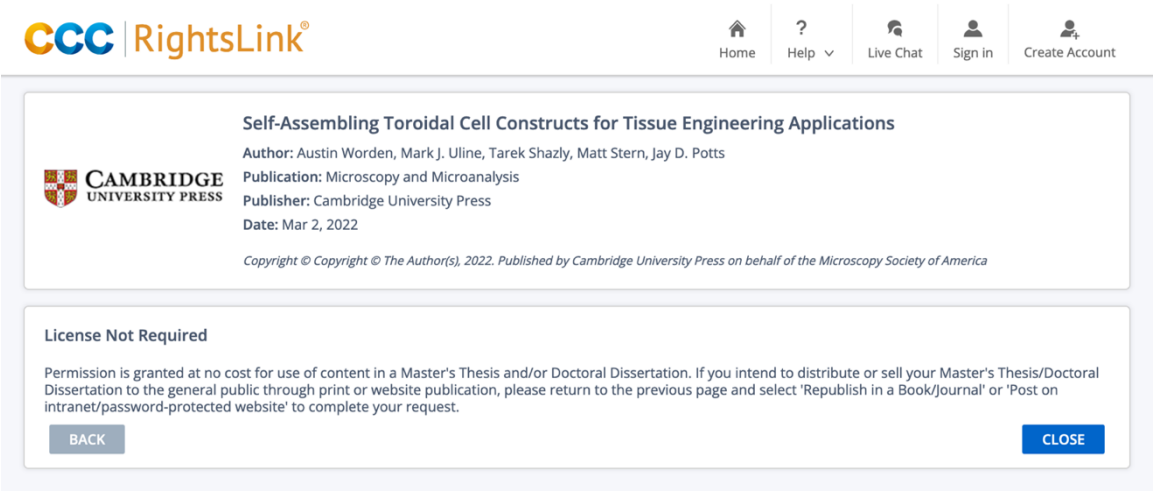

Figure A.1 Microscopy and Microanalysis permission to reprint. Chapter 2 has been reprinted in this paper with the permission of the journal.